CHARACTERIZATION AND MODIFICATION OF THERMAL RESPONSE THROUGH INTENTIONAL DESIGN OF PHASE CHANGE MATERIAL COMPOSITES

A Dissertation

by

ALISON REBA HOE

Submitted to the Graduate and Professional School of
Texas A&M University
in partial fulfillment of the requirements for the degree of

DOCTOR OF PHILOSOPHY

Chair of Committee,	Patrick Shamberger
Committee Members,	Raymundo Arróyave
	Alaa Elwany
	Jonathan Felts
Head of Department,	Ibrahim Karaman

May 2022

Major Subject: Materials Science and Engineering

ABSTRACT

Phase change materials (PCMs) can act as highly efficient cooling components within thermal energy storage systems when effectively applied, accounting for the objectives of a given thermal management application. To compensate for the typically low power density of PCMs, high thermal conductivity elements are often used to increase the effective power density of the resulting composite while also benefitting from the high thermal capacity of the PCMs. In the absence of design guidelines for the internal design of these composites, produced systems are highly unlikely to achieve full utilization of the melting process and available volume, leading to underperforming thermal management systems. By tuning the composition and spacing of the material components within the composite system a given thermal response can be selected to best suit the desired application. Translation of fundamental heat transfer principles into design implications requires exhaustive exploration of the effects of design aspects with relation to well defined design objectives which is pursued analytically, numerically, and experimentally. These pursuits culminate in an increased tractability of the descriptions of thermal transport within these composites and a high degree of control over the thermal behavior of intentionally designed systems.

ACKNOWLEDGEMENTS

I would like to thank those who have supported me on my path to completing my PhD. Especially, Dr. Shamberger of Texas A&M University, my PhD advisor who has supported and guided me throughout this journey. Additional thanks go out to Dr. Pyrak-Nolte of Purdue University, my undergraduate advisor, who gave me the confidence to take the first steps; Dr. Michael Barako of Northrop Grumman, my special appointment committee member and industry mentor, who has inspired me to pursue my passions and; Dr. Jonathan Felts, my committee member who has been an irreplaceable resource in my academic development. I also would also like to thank my other committee members, Dr. Alaa Elwany, and Dr. Raymundo Arróyave who have always shown dedication to the success of their students and a high standard of research. Lastly, I have worked with a suite of amazing undergraduate students over the years who have each helped me greatly in different ways.

On a more personal note, I would like to acknowledge: My parents, sister and brother who have had to put up with me rushing from deadline to deadline through nine years of college and; My lab mates who made long hours in the lab much less painful and taught me so much, especially Adelaide Bradicich, Rebeca Gurrola, and Heidi Clarke. Lastly, to Wade Emmons, Alexa Easley, and the two incomparable Tims (including Tim Brown) thank you so much for helping keep me mostly sane along the way.

CONTRIBUTORS AND FUNDING SOURCES

Contributors

This work was supervised by a dissertation committee consisting of Professor Shamberger of the Department of Materials Science and Engineering, corresponding PhD advisor, Dr. Michael Barako of Northrop Grumman Corporation, Dr. Jonathan Felts of the Department of Mechanical Engineering, Dr. Alaa Elwany of the Department of Industrial and Systems Engineering, and Dr. Raymundo Arróyave of the Department of Materials Science and Engineering.

Experimental results shown in Figure 3.4 c of Chapter 3 and Figure 4.11a of Chapter 4 are provided by Achutha Tamraparni with the support of Dr. Jonathan Felts. The corresponding necessary physical aluminum structures (Figure 3.4 b, Figure 4.11b-e) and additive manufacturing development, as well as 3D models for Figure 4.1, are provided by Chen Zhang with the support of Dr. Alaa Elwany. The foundational analytical work for the material presented in Chapter 4 and the development of the fin approximation in Chapter 2 was established by Dr. Jonathan Felts of the Department of Mechanical Engineering. Portions of this research were conducted with the advanced computing resources provided by Texas A&M High Performance Research Computing.

Funding Sources

Graduate study was supported in part by the Merit Fellowship from Texas A&M University with additional support from The National Science Foundation Research Traineeship Program grant 1545403. The material contained in this work is based upon

research supported by, or in part by, the U. S. Office of Naval Research under award number N00014-17-1-2802.

TABLE OF CONTENTS

Page

LIST OF FIGURES

Page

LIST OF TABLES

Page

1. INTRODUCTION

1.1. Phase Change Materials for Thermal Energy Storage Systems

The general purpose of thermal management systems is to regulate the operational temperature levels of a system/device through the transport and/or storage of thermal energy. Thermal energy storage (TES) systems accomplish this goal through the capture or release of thermal energy using sensible heating, latent heating, physio-chemical, or various types of energy conversion. Through their energy storage ability, TES systems have widespread applications including, but not limited to, building environmental control, battery thermal management, server cluster temperature controls, among others. [1, 2] Phase change materials (PCMs) are common components in TES systems for thermal management due to their associated high latent heat allowing for high levels of heat storage. [3-5] These materials are especially of interest for applications in pulsed or high-power thermal management systems due to their ability to buffer transient thermal loads.

Cooling for various applications currently represent a significant portion of thermal management efforts with the need for more efficient systems consistently increasing through technological and energy-based development demands. Traditional thermal management systems for cooling applications can largely be classified as active and passive cooling systems, where active systems require external power or controls and passive systems do not. Many applications necessitate the utilization of a thermal management system to prevent from system overheating or decreases in efficiency with temperature rise. Thermal loads can be dealt with by using passive elements, such as

heatsinks, active components, such as fans or pumps, or any combination thereof. Pulsed or transient thermal loads can often add high levels of complexity to the thermal management system, through the inclusion of sensors or externally activated elements. When these elements are not included there is often a failure to reflect the transient nature of the thermal problem, where cooling is applied at a higher level than typically necessary at all times, inefficiently using the available energy and space. Transient thermal applications provide an opportunity for the application of PCMs to mitigate transient thermal loads. Many studies have shown systems incorporating PCMs efficiently act as passive elements which can manage spikes of thermal energy for a certain period of time while cooling the heat dissipating device or component. [6-8]

Phase change materials can be found in many different categories of materials including, but not limited to, paraffins, sugar alcohols, low melting point alloys, inorganic salts, and salt hydrates, each with their benefits and challenges. [3, 9] When these materials undergo a phase transition, they are able to quasi-isothermally and reversibly absorb or release heat. The high associated latent heat of these materials corresponds to a large amount of energy that can be stored within a relatively small volume during this phase transition. Throughout this work we will be investigating the phase transition as a melting problem, i.e. from solid to liquid, as that is the most common phase change of interest in high latent heat PCMs. Other condensed phase transitions including solid-gel [10] or solid-solid [11] are also possible and utilization can be informed by this work. Additional non-condensed phase transitions such as solid-vapor and liquid-vapor also have many applications in thermal management systems such as oscillating heat pipes or vapor

chambers. However this class of transitions represent a fundamental departure from dynamics of condensed phase transitions and are not explored within this work.

1.2. Phase Change Materials Composites

Despite the advantages of their high associated latent heat, PCMs are often limited in application by their thermal conductivity, limiting their ability to rapidly transport energy away from a heat source. As such, many practical engineering applications of phase change materials (PCMs) require a PCM component to be combined with a thermally conductive component (e.g., fibers [12, 13], flakes [14, 15], macroscopic fins [16, 17]), for the purpose of increasing heat transfer into the PCM volume. Previous investigations of melting and solidification of phase change material (PCM) systems containing additional elements have largely focused on either 1) micro- or nano-scale conductive particles introduced into and suspended within a PCM matrix, or 2) macroscopic thermally conductive foams or finned structures. On the micro- and nano-scale, a diverse range of nano-scale conductive additives and fillers have been investigated with the primary goal of increasing thermal conductivity, including metallic nanoparticles,[18-21] carbon based additives,[12, 22-24] and oxide nanoparticles. [25, 26] In general, systems consisting of discrete micro- and nano-sized conductive particles are limited both by the small volume fraction of conductive material that is able to be accommodated without agglomerating or segregating, and by the non-negligible role of thermal interfacial resistances in these systems. [21, 27, 28]

In contrast to micro- and nano- scale composites, macro-scale multi-component systems (e.g., open foams and finned structures) can span a much wider range of volume

fraction of constituent components than accessible in PCM materials containing conductive particles in suspension and are relatively easy to manufacture. While many of these structures have been explored extensively as single component heatsinks, their counterparts containing PCMs lack the same history and development. Consequently, it may be useful to take techniques used to describe and analyze traditional heatsinks and translate them to PCM composite systems. Within PCM composite systems, 3D foams and finned structures have been assessed both numerically and experimentally to investigate the physical nature of the phase change process in these complicated structures,[29-31] and to identify some optimal configurations of the conductive components within the overall volume. [29, 32-34]

1.3. Scope of Dissertation

1.3.1. Generalized Scope of Study

The primary purpose of this dissertation is to characterize thermal transport within phase change material composites and translate this knowledge into direct guidance for the application of these composites. Therefore, this work begins by developing numerical and analytical tools that are then used to for the design of PCM composites, around different design objectives. Finally, this work addresses the appropriate application of these materials and describes ongoing work related to the discussion contained herein.

1.3.2. Dissertation Objectives

The first objective of the work contained herein is to develop methodologies for the description of the melting process within lamellar phase change material composites. The purpose of this development is, primarily, to allow for analysis of the characteristic

behavior of these materials. Second, once descriptive methodologies are established, further analysis and development becomes much more tractable. Characterization of standard PCM composite behavior is established in Chapter 2 using numerical methods to simulate the melting process. This is accomplished through the development of a finite element analysis model which allows for direct simulation of melting dynamics within a composite heatsink (Figure 1.1a,b,c). Using this numerical model allows for the general characterization of a PCM or PCM composite system's response to a constant temperature or heat flux thermal load. This characterization involves the identification of response regimes, and the attributes of the critical times associated the regime boundaries. The relationship between geometry and characteristic response is examined through variation of parameters for composition and length scales which directly determines critical times and regime breakdown (Figure 1.1a,b). Using the previously stated observations and numerical results the applicability of two approximate analytical solutions for the melting problem: the fin-based approximation (Figure 1.1d) and the homogeneous composite approximation (Figure 1.1e).

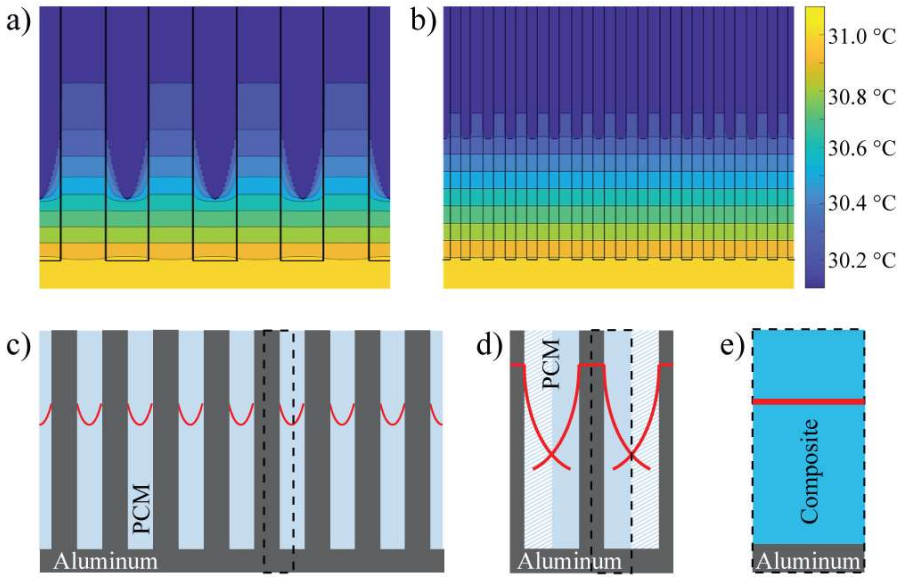

Figure 1.1 Examples of a) an incoherent temperature profile as a result of a relatively large (repeated unit spacing, 3.2 mm) pitch and b) a coherent temperature profile as a result of a relatively small (repeated unit spacing, 0.8 mm) pitch with a constant 1° C temperature difference boundary condition (Boundary is 1 °C over the melting temperature) for an Aluminum-LNH composite system. Fin structured composite heatsink c) modeled by FDA. Approximated by the d) "fin equation" model and e) the homogeneous composite model.

Chapter 3 expands upon the concepts laid out by Chapter 2 by translating fundamental principles into design guidelines. Utilization of the homogeneous composite approximation makes possible the simplified analytical expressions of performance from the perspective of different performance metrics as a function of volume fraction (Figure

1.2a,b). Characteristic behavior is established for both a constant heat flux (Figure 1.2c) and constant temperature (Figure 1.2d) boundary condition with an emphasis on the point of melting completion as a critical pivot where performance rapidly decreases. With the fundamental basis and characteristic behavior established, distinct design regimes can be identified, each with an individual solution for volume fraction leading to optimal performance. The first of these design regimes is identified as the rate limited regime, where the optimization yields the absolute best performance for the design space with no geometric boundaries accounted for. The second design regime is identified as the volume limited regime, where the edge effects from melting of the system cause a new optimal composition to arise allowing for full utilization of the allotted space while preventing post-melt completion performance drops. The solutions for both regimes are provided across Cartesian and Cylindrical coordinate bases, constant temperature and constant heat flux boundary conditions and for temporal and thermal magnitude optimization-based design problems. These analytical solutions are verified using numerical methods where a large number of volume fraction tests can be rapidly executed to determine the true optimum and observe the effects of deviating from this composition. Additional experimental results and examples from the existing body of literature are also provided to further support the framework created here.

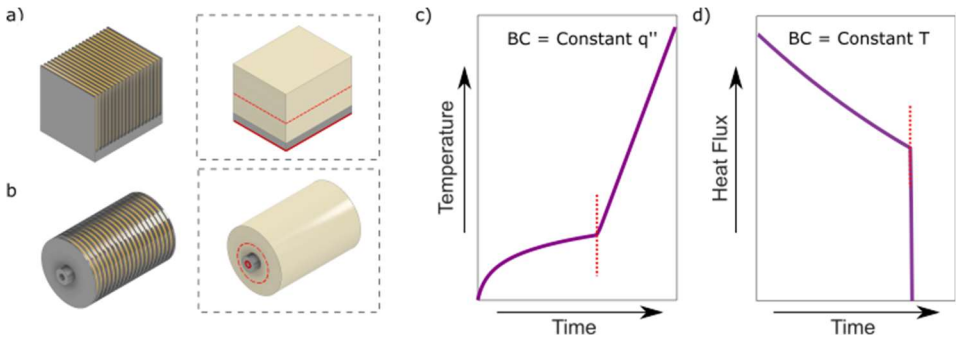

Figure 1.2 Schematic of a) Cartesian and b) cylindrical finned composite system translated to a homogeneous composite c) Characteristic responses of PCM volumes to an applied a) heat flux (q") or b) temperature (T) boundary condition with the melting completion time indicated with a red dashed line.

While Chapter 3 provides solutions for optimized volume fraction selections for a homogeneous composite design, there remains opportunities for expansion within this line of exploration through the consideration of non-uniform optimal designs. To this end, analytical optimization techniques are employed in Chapter 4 for the generation of radially variant optimal system designs within cylindrical PCM composite heatsinks. Within this work we consider a radial volume fraction distribution with a polynomial form where the prefactors serve as fitting parameters, allowing for optimization of the profile. These generated analytical profiles are compared against discrete numerically optimized profiles as a verification of the general form of the problem and the application of our methods. When comparing radially variant and constant composition profiles it is found that variant composites are best utilized in highly cylindrical systems under thermal loading with

longer time scales or larger magnitudes. Furthermore, these systems are explored across performance objectives of temperature minimization, effective heat capacity maximization and effective volumetric heat capacity maximization. Lastly a hybrid optimization method is established and demonstrated, allowing for the successful optimization of a primary performance metric while allowing for a secondary factor to be accounted for.

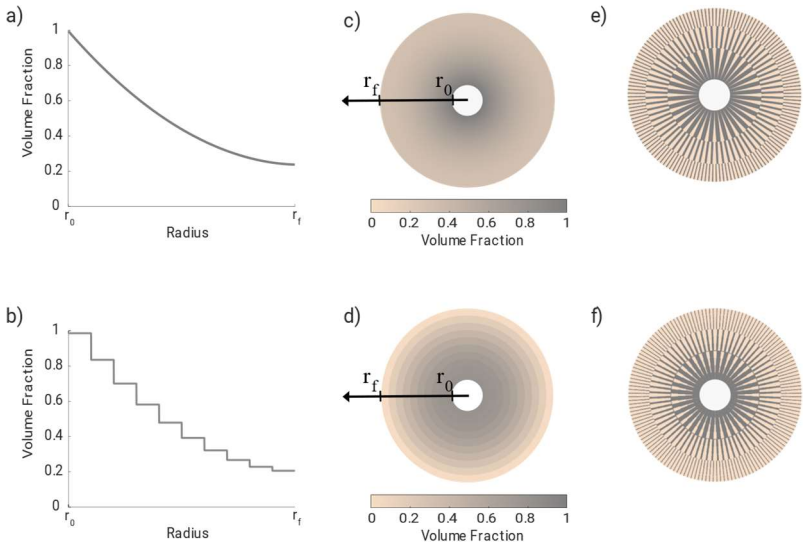

Figure 1.3 Volume fraction distribution in the form of a a) continuous second order polynomial and b) discrete volume fraction distribution. Representation of the volume fraction distribution as a c,d) effective medium system and e,f) a branching composite design.

In previous chapters, as in the majority of the current literature, thermal loads are assumed to be constant. Considering PCM applications necessitate transient applications due to the finite nature of the melting process, it is necessary to understand the thermal response of these materials to non-constant thermal loading. In Chapter 5 we execute an experimental study to characterize the response of PCM composites to harmonic thermal loading. The configurational basis of this experimental study is a PCM exposed to a periodic power input with a convective cooling boundary on the opposing side (Figure 1.4a). The physical manifestation of this configuration is accomplished with a heater, PCM and cold plate in series contained within an insulating container with the temperature measured at the boundaries using thermocouples (Figure 1.4b). Power input through the heating element is varied through the amplitude, offset and frequency, each with having a different effect on the resulting temperature rises. We observe there exists a regime within the thermal loading space which leads to temperature rises that are directly dampened from the effects of melting. This regime represents the key operational zone that should be targeted for in the application of these materials. Finally, we identify the shortcomings of this portion of the study, particularly, discrepancies with analytically predicted values and the origins of these discrepancies. Following from our experience from this experimental study we have modified the orientation and components of the experimental rig to move closer to an idealized system. The ongoing work on this front is described within Chapter 5.

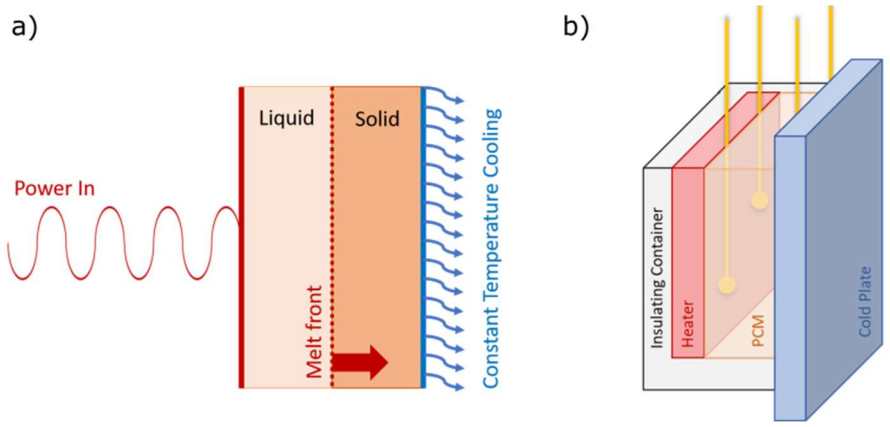

Figure 1.4 a) Schematic representation of the primary system under investigation consisting of a PCM slab with a periodic thermal load applied to one side and a convective cooling condition on the opposite side. b) Configuration of the experimental rig highlighting the heat source and cooling boundary as well as the location of thermocouples (yellow) in reference to the PCM under investigation.

1.4. References

[1] L. F. Cabeza, I. Martorell, L. Miró, A. I. Fernández, and C. Barreneche, "1 - Introduction to thermal energy storage (TES) systems," in *Advances in Thermal Energy Storage Systems*, L. F. Cabeza Ed.: Woodhead Publishing, 2015, pp. 1-28.

[2] G. Alva, Y. Lin, and G. Fang, "An overview of thermal energy storage systems," *Energy,* vol. 144, pp. 341-378, 2018.

[3] B. Zalba, J. M. Marín, L. F. Cabeza, and H. Mehling, "Review on thermal energy storage with phase change: materials, heat transfer analysis and applications," *Applied Thermal Engineering,* vol. 23, no. 3, pp. 251-283, 2003.

[4] L. Socaciu, "Thermal Energy Storage with Phase Change Material," *Leonardo Electronic Journal of Practices and Technologies,* vol. 11, pp. 75-98, 2012.

[5] H. Mehling and L. F. Cabeza, *Heat and cold storage with PCM*. Springer, 2008.

[6] R. Kandasamy, X.-Q. Wang, and A. S. Mujumdar, "Transient cooling of electronics using phase change material (PCM)-based heat sinks," *Applied Thermal Engineering,* vol. 28, no. 8, pp. 1047-1057, 2008.

[7] C. Barreneche, M. E. Navarro, A. I. Fernández, and L. F. Cabeza, "Improvement of the thermal inertia of building materials incorporating PCM. Evaluation in the macroscale," *Applied Energy,* vol. 109, pp. 428-432, 2013.

[8] F. L. Tan and C. P. Tso, "Cooling of mobile electronic devices using phase change materials," *Applied Thermal Engineering,* vol. 24, no. 2, pp. 159-169, 2004.

[9] D. Hale, M. Hoover, and M. ONeill, "Phase change materials handbook," 1971.

[10] P. Karimineghlani, E. Emmons, M. J. Green, P. Shamberger, and S. A. Sukhishvili, "A temperature-responsive poly (vinyl alcohol) gel for controlling fluidity of an inorganic phase change material," *Journal of Materials Chemistry A,* vol. 5, no. 24, pp. 12474-12482, 2017.

[11] A. Fallahi, G. Guldentops, M. Tao, S. Granados-Focil, and S. Van Dessel, "Review on solid-solid phase change materials for thermal energy storage: Molecular structure and thermal properties," *Applied Thermal Engineering,* vol. 127, pp. 1427-1441, 2017.

[12] J. Fukai, Y. Hamada, Y. Morozumi, and O. Miyatake, "Effect of carbon-fiber brushes on conductive heat transfer in phase change materials," *International Journal of Heat and Mass Transfer,* vol. 45, no. 24, pp. 4781-4792, 2002.

[13] J. Fukai, M. Kanou, Y. Kodama, and O. Miyatake, "Thermal conductivity enhancement of energy storage media using carbon fibers," *Energy Conversion and Management,* vol. 41, no. 14, pp. 1543-1556, 2000.

[14] A. Mills, M. Farid, J. Selman, and S. Al-Hallaj, "Thermal conductivity enhancement of phase change materials using a graphite matrix," *Applied Thermal Engineering,* vol. 26, no. 14-15, pp. 1652-1661, 2006.

[15] S. Pincemin, R. Olives, X. Py, and M. Christ, "Highly conductive composites made of phase change materials and graphite for thermal storage," *Solar Energy Materials and Solar Cells,* vol. 92, no. 6, pp. 603-613, 2008.

[16] P. P. Levin, A. Shitzer, and G. Hetsroni, "Numerical optimization of a PCM-based heat sink with internal fins," vol. 61, pp. 638-645, 2013.

[17] V. Shatikian, G. Ziskind, and R. Letan, "Numerical investigation of a PCM-based heat sink with internal fins," *International Journal of Heat and Mass Transfer,* vol. 48, no. 17, pp. 3689-3706, 2005.

[18] J. M. Khodadadi, L. W. Fan, and H. Babaei, "Thermal conductivity enhancement of nanostructure-based colloidal suspensions utilized as phase change materials for thermal energy storage: A review," *Renew Sust Energ Rev,* vol. 24, pp. 418-444, 2013.

[19] J. M. Khodadadi and S. F. Hosseinizadeh, "Nanoparticle-enhanced phase change materials (NEPCM) with great potential for improved thermal energy storage," *Int Commun Heat Mass,* vol. 34, no. 5, pp. 534-543, 2007.

[20] C. J. Ho and J. Y. Gao, "Preparation and thermophysical properties of nanoparticle-in-paraffin emulsion as phase change material," *Int Commun Heat Mass,* vol. 36, no. 5, pp. 467-470, 2009.

[21] M. A. Kibria, M. R. Anisur, M. H. Mahfuz, R. Saidur, and I. H. S. C. Metselaar, "A review on thermophysical properties of nanoparticle dispersed phase change materials," *Energ Convers Manage,* vol. 95, pp. 69-89, 2015.

[22] F. Yavari *et al.*, "Enhanced Thermal Conductivity in a Nanostructured Phase Change Composite due to Low Concentration Graphene Additives," *J Phys Chem C,* vol. 115, no. 17, pp. 8753-8758, 2011.

[23] L. Xia, P. Zhang, and R. Z. Wang, "Preparation and thermal characterization of expanded graphite/paraffin composite phase change material," *Carbon,* vol. 48, no. 9, pp. 2538-2548, 2010.

[24] Y.-J. Chen, D.-D. Nguyen, M.-Y. Shen, M.-C. Yip, and N.-H. Tai, "Thermal characterizations of the graphite nanosheets reinforced paraffin phase-change composites," *Composites Part A: Applied Science and Manufacturing,* vol. 44, pp. 40-46, 2013.

[25] X. Li *et al.*, "Advanced Nanocomposite Phase Change Material Based on Calcium Chloride Hexahydrate with Aluminum Oxide Nanoparticles for Thermal Energy Storage," *Energy & Fuels,* vol. 31, no. 6, pp. 6560-6567, 2017.

[26] N. S. Dhaidan, J. M. Khodadadi, T. A. Al-Hattab, and S. M. Al-Mashat, "Experimental and numerical study of constrained melting of n-octadecane with CuO nanoparticle dispersions in a horizontal cylindrical capsule subjected to a constant heat flux," *International Journal of Heat and Mass Transfer,* vol. 67, pp. 523-534, 2013.

[27] I. H. Kim, H. W. Sim, H. H. Hong, D. W. Kim, W. Lee, and D. K. Lee, "Effect of filler size on thermal properties of paraffin/silver nanoparticle composites," *Korean Journal of Chemical Engineering,* vol. 36, no. 6, pp. 1004-1012, 2019.

[28] Y. M. F. El Hasadi and J. M. Khodadadi, "Numerical Simulation of the Effect of the Size of Suspensions on the Solidification Process of Nanoparticle-Enhanced Phase Change Materials," *Journal of Heat Transfer,* vol. 135, no. 5, pp. 052901-052901-11, 2013.

[29] M. T. Barako, S. Lingamneni, J. S. Katz, T. Liu, K. E. Goodson, and J. J. J. o. A. P. Tice, "Optimizing the design of composite phase change materials for high thermal power density," vol. 124, no. 14, p. 145103, 2018.

[30] C. Y. Zhao, W. Lu, and Y. Tian, "Heat transfer enhancement for thermal energy storage using metal foams embedded within phase change materials (PCMs)," *Solar Energy,* vol. 84, no. 8, pp. 1402-1412, 2010.

[31] L. W. Fan and J. M. Khodadadi, "Thermal conductivity enhancement of phase change materials for thermal energy storage: A review," *Renew Sust Energ Rev,* vol. 15, no. 1, pp. 24-46, 2011.

[32] R. Kalbasi, M. Afrand, J. Alsarraf, and M. D. Tran, "Studies on optimum fins number in PCM-based heat sinks," *Energy,* vol. 171, pp. 1088-1099, 2019.

[33] P. P. Levin, A. Shitzer, and G. Hetsroni, "Numerical optimization of a PCM-based heat sink with internal fins," *International Journal of Heat and Mass Transfer,* vol. 61, pp. 638-645, 2013.

[34] S. F. Hosseinizadeh, F. L. Tan, and S. M. Moosania, "Experimental and numerical studies on performance of PCM-based heat sink with different configurations of internal fins," *Applied Thermal Engineering,* vol. 31, no. 17-18, pp. 3827-3838, 2011.

2. CONDUCTIVE HEAT TRANSFER IN LAMELLAR PHASE CHANGE MATERIAL COMPOSITES*

2.1. Nomenclature

Variables:

A	Area, (m^2)
$\hat{A}$	Effective cross-sectional area, (m^2)
C	Specific Heat for constant pressure, ($J \cdot g^{-1} \cdot K^{-1}$)
dt	Timestep length, (s)
Fo	Fourier number, (unitless)
k	Thermal conductivity, ($W \cdot m^{-1} \cdot K^{-1}$)
L	Latent heat of fusion, ($J \cdot g^{-1}$ or $J \cdot cm^{-3}$)
l	Length, (m)
q	Heat flow, (W)
Q''	Thermal energy capacity, ($J \cdot m^{-2}$)
q''	Heat flux, ($W \cdot m^{-2}$)
s	Location of the melt front (m)
St	Stefan number, (unitless)
t	Time, (s)
T	Temperature, (C)
V	Volume, (m^3)
x	Horizontal location, (m)
y	Vertical location, (m)
α	Thermal Diffusivity, ($m^2 \cdot s^{-1}$)
δ	Characteristic length, (m)
ϕ	Volume Fraction, (unitless)
λ	Solution to the transcendental Stefan problem, (unitless)
ρ	Density, ($g \cdot m^{-3}$)
τ	Characteristic time, (s)

Subscripts

b	Base
c	Cross-section of the fin
eff	Effective
cond	Highly thermally conductive material
i	Material and state index
j	Direction of thermal transport
l	Of the liquid
m	Melting
p	Pitch
PCM	Phase change material
q	x-index
r	y-index
s	Of the solid
tot	Total height of structure
v	Volumetric
w	Specific
0	At the y = 0 location (boundary condition)

Superscripts

⊥	Perpendicular to
||	Parallel to
p	time-index

2.2. Introduction

Phase change materials can play a useful role in pulsed or high-power thermal management systems due to their ability to buffer transient thermal loads. However, in many cases, practical engineering applications of phase change materials (PCMs) require a PCM component to be combined with a thermally conductive component (e.g., fibers [1, 2], flakes [3, 4], macroscopic fins [5, 6]), for the purpose of increasing heat transfer into the PCM volume. Analytical solutions of conductive heat transfer during melting or freezing are challenging due to the location of the solid/liquid interface representing a free boundary, which is not known a priori. [7-9] Exact solutions have only been established

for a few simple geometries and boundary conditions. [9-11] This challenge is exacerbated in the case of multi-component systems, since these systems introduce complex geometries and generally pose two- or three-dimensional (2D, 3D) problems. This barrier effectively limits the efficient design of thermal management systems containing PCM components. In the absence of exact analytical solutions, melting and solidification processes can be accurately described by higher order numerical approaches in two [6, 12-14] or three dimensions. [6, 15, 16] These approaches have been utilized extensively in the literature to investigate melting in a diverse range of geometries and boundary conditions, or by reduced order models [17, 18], which introduce tradeoffs between overall model fidelity and computational efficiency. The latter approach offers significant advantages for parametric design or optimization techniques due to the ability to rapidly investigate the response of a large number of potential material configurations to large number of external thermal loading conditions. However, the ability of reduced order models to adequately describe heat transfer during melting or solidification within complex multi-component structures over a valid range of conditions has not been adequately assessed, nor has the time and length scales over which they may be applied.

Previous investigations of melting and solidification of phase change material (PCM) systems containing additional elements have largely focused on either 1) micro- or nano-scale conductive particles introduced into and suspended within a PCM matrix, or 2) macroscopic thermally conductive foams or finned structures. On the micro- and nano- scale, a diverse range of nano-scale conductive additives and fillers have been investigated with the primary goal of increasing thermal conductivity, including metallic

nanoparticles,[19-22] carbon based additives,[1, 23-25] and oxide nanoparticles.[26, 27] In general, systems consisting of discrete micro- and nano-sized conductive particles are limited both by the small volume fraction of conductive material that is able to be accommodated without agglomerating or segregating, and by the non-negligible role of thermal interfacial resistances in these systems. [22, 28, 29]

Conversely, macro-scale multi-component systems (e.g., open foams and finned structures) can span a much wider range of volume fraction of constituent components than accessible in PCM materials containing conductive particles in suspension and are relatively easy to manufacture. 3D foams and finned structures have been assessed both numerically and experimentally to investigate the physical nature of the phase change process in these complicated structures,[30-32] and to identify some optimal configurations of the conductive components within the overall volume.[30, 33-35] As one salient example, lamellar structures consisting of alternating conductive and PCM phases have been investigated parametrically to assess how system parameters affect the magnitude or rate of heat absorbed from a heat source. Such investigations generally adopt a particular system configuration or geometry, which is modeled with varying degrees of fidelity, and perturb some aspect of the system (e.g., fin spacing, length and width, and boundary condition, thermal load type and magnitude), measuring the resulting internal temperature distributions and heat fluxes.[6, 36-38] While detailed simulation can reveal critical insights into the nature of the melting or solidification process, this approach is limited in its ability to predict a future response under different boundary conditions or for different internal structures.

Analytical expressions for heat flow and temperature distribution throughout a composite system undergoing a melting process have been proposed, but there is a lack of a cohesive investigation into the specific characteristic regimes and reduced order expressions corresponding to each behavioral regime.[39-41] In addition, there is a lack of concrete analytical expressions for how the time and length scales under investigation affect these characteristic behaviors. This knowledge would provide the opportunity to construct a multi-component PCM system with specific informed design parameters. By analogy, analytical descriptions of heat transfer from finned heatsinks and the optimal design of such heatsinks is a thermal management problem explored in great detail in the literature.[42, 43] The addition of PCMs adds a dynamic element that increases the complexity of the problem. However, similar analytical descriptions describing heat transfer in layered multicomponent systems containing PCMs as a function of their structure could reasonably be expected to introduce a new method of rapid intentional design of a component suited to a particular thermal management challenge.

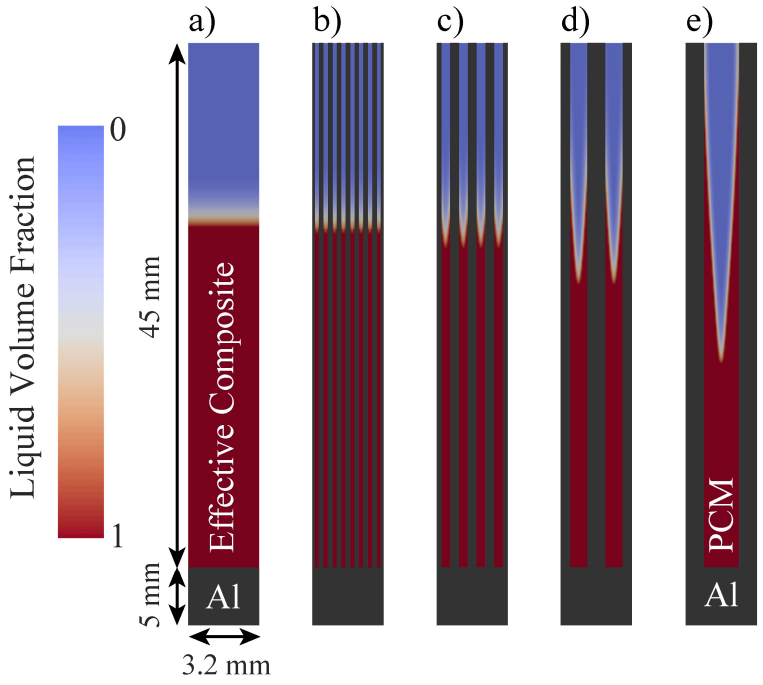

Figure 2.1 Figure illustrates the transition from a nearly flat melt profile and horizontal isothermal contours (for thin PCM layers; b, c) to melting along extended fin surfaces of PCM channel simultaneously (for thick PCM layers; d, e). Model was calculated by ANSYS for a volume 3.2 mm wide by 50 mm tall, with a 5 mm thick metal base; material properties used were those of Aluminum 6063, and LiNO3·3H2O as the PCM phase. Fins are equally spaced with a constant volume fraction of PCM for all volumes: b) 0.2 mm, c) 0.4mm, d) 0.8mm, e) 1.6 mm. For the volume illustrated in a), the layered structure is replaced with a composite material, with effective properties associated with 0.5 volume fraction of PCM and aluminum.

To achieve the underlying goal of developing a composite material which rapidly transports transient heat pulses away from a boundary, we are motivated to investigate lamellar two-component materials systems composed of a thermally conductive phase (generally a metal) which serves to conduct heat, and a PCM phase, which serves to store heat. As opposed to most previous efforts on melting of PCMs with macroscopic fins, we specifically focus on the limiting case where the thickness of each layer is small relative to the overall width of the layered material system (Figure 1.1). In such cases, the 1) geometries, 2) material properties, 3) relevant length scales and time scales involved, and 4) initial and boundary conditions of the system under consideration may result in temperature profiles which are well-described by a coherent quasi-one-dimensional (1D) solutions. This important transition in the shape of the melt front can be visualized by modeling melting in lamellar systems of decreasing layer thickness using the commercial finite element code ANSYS (Figure 2.1). Following previous observations that conductive heat transfer is less important at small layer thicknesses due to constrictions on fluid flow [6], we only simulate conductive heat transfer. At the limit where each layer becomes infinitesimally thin, we consider treating the system as a uniform composite material with effective homogenized properties attained from the volume fraction and distribution of different constituent phases (Figure 2.1,a); the details of this approach will be outlined later in this manuscript. Based on this observation, this study assesses the ability to efficiently and adequately describe heat transfer using two particular reduced order models. In the first case, we treat the complex material system as a single homogeneous material with some effective material properties calculated using the effective medium

approximation (EMA). In the latter case, we treat the system instead as an array of 1D fins, based on a modified version of the 1D fin equation.

Past attempts from literature at addressing melting in lamellar structure have varied widely in approach and especially scope. A significant portion of the literature has focused on describing heat transfer in PCM systems with mid to large associated Rayleigh numbers ($Ra>10^5$).[40, 44, 45] Previous studies of porous thermal energy storage systems have shown that convection heat transfer is insignificant even for $Ra \sim 10^5$ when the effective thermal conductivity of the medium is large.[46] The cases explored in this study exhibit similar Rayleigh numbers to previous studies, and preliminary estimations based on natural convection within a cavity result in natural convection heat fluxes 10-100x smaller than conduction heat flux associated with the moving liquid front.[47] It is worth noting that, for cases where the effective thermal conductivity is low (i.e. using ceramics or polymers as the conducting component), the natural convection would be comparable to conduction with phase change, and should be accounted for in those systems.

A composite material can be defined as having a set of effective, generally anisotropic, properties which can be used to model its macroscopic behavior, and which can be changed by changing the relative amount or distribution of the different constituent phases. Under the effective medium approximation (EMA), macroscopic properties of the material system are first attained through knowledge of volume fraction, size, shape, and distribution of different constituent phases which describe the microscale structure of the system.[48-50] Next, the volume can be assumed as a homogeneous composite material with effective properties. This method is a standard approach to describing elastic,[51, 52]

magnetic, [53-55] dielectric,[56, 57] electrical [55, 58, 59] and thermal transport [60, 61] properties of composite materials, and has successfully been employed to determine upper and lower bounds of these properties in either anisotropic (Voigt-Reuss or alternatively Maxwell-Eucken bounds) [62] or isotropic (Hashin-Strichman bounds) [53] cases respectively. The key challenge of this approximation is demonstrating that the EMA accurately captures transient phenomena across length-scales and time-scales of interest. This approach is generally accepted in the nano-composite field, but the accuracy of the EMA in describing the details of heat transport within the volume generally decreases with an increase in the ratio of the length scales of the features of interest to the length scales of the overall volume under consideration.[63-65] This works seeks to answer under what length and time scales we can use this approximation and how adequate is it in describing complex systems with melting and high conductivity components. We have previously demonstrated that this problem is tractable in lamellar systems if feature length scales are sufficiently small,[66] and that this approach accurately describes experimental measurements on such composite systems.[67]

Fin-based approximations describe the transfer of thermal energy rapidly through a conductive fin, then laterally into a surrounding volume, in this case a melting or freezing PCM. [68, 69] This approach builds on the substantial literature on fin geometries and fin-based heatsink structures,[6, 47, 68] but explicitly considers the role of the melting/freezing process in transferring heat from the fins into the surrounding PCM. Like the effective medium approximation, this approach effectively reduces a 2D or 3D problem into a 1D problem, allowing for less computationally expensive solutions.

However, this approximation involves simplifying assumptions, such as treating fins as non-interacting components, which is to say heat transfer is considered as flowing from the fin into surrounding PCM volumes separated by adiabatic barriers. Thus, it is reasonable to investigate conditions under which fin-based approximations hold and how these solutions might complement the regimes in which the EMA holds.

In this paper we develop approximate analytical solutions of conductive heat transfer in lamellar multi-component systems under EMA and fin-based approximations and test their accuracy against higher fidelity 2D numerical simulations. The overarching goal of the current work is to develop the two approximate solutions described above, and to evaluate their accuracy over varying parameters, under both constant temperature and constant heat flux boundary conditions. This work is unique in its approach to exploring simplified heat transfer in macroscopic systems containing a melting component. While the general approximate models discussed in this paper have been previously explored in different facets, their use as a descriptor of heat transfer in composites undergoing melting leaves much room for further development. In addition to an investigation into how well these equations apply to the systems in question, it must be questioned if there exist regimes of time and length scales where different models become more relevant.

In this work, we use numerical models to simulate heat transfer through a specific geometry of lamellar PCM/metal composite and use results to inform developed analytical expressions. The constituent components chosen in this study are aluminum and lithium nitrate trihydrate, a salt hydrate PCM, which are good candidates for heatsink design due to their favorable thermal properties. Four characteristic regimes in behavior of these

systems are observed, corresponding to 1) heat transfer through a metal interface layer, 2) transient evolution of melt profiles within the PCM lamellar layer, 3) quasi-steady melting within the PCM lamellar layer, and 4) sensible heating of an entirely molten PCM. We present sets of developed equations which predict the time scales at which transitions in behavior will occur under both constant temperature and constant heat flux boundary conditions. Comparing these approximate analytical solutions to a finite difference analysis (FDA) numerical model results in generally reasonable agreement, with the largest deviations derived from introducing approximate solutions to melting (i.e., the quasi-steady state approximation), where no exact analytical solution to the melting problem exists. The outcome of this study is a framework of approximate solutions that serve as design guidelines for developing multi-component PCM structures that address transient thermal management problems.

2.3. Theoretical Development

2.3.1. General Description of Phase Change Problem

The description of the melting or solidification of a material over time, *t*, under some specified geometry and boundary conditions is an example of a free boundary problem, where the location of the melt/solid interface, $s(t)$, is not known *a priori*. [7-9] Rather, $s(t)$ is a result of initial and boundary conditions imposed on the system. In this paper, we will describe the phase change problem in terms of melting of a solid. However, the complementary problem – solidification of a liquid – is readily attainable by appropriate modification of initial conditions, boundary conditions, and material properties within the phases.

In the case of a constant temperature boundary condition, $T(y = 0, t > 0) = T_0$, Neumann presented an exact solution to the 1D heat transfer problem in a Cartesian coordinate system. [10] The solution to the phase change problem is an expression describing the temperature profile within the system as a function of location and time, *T(y,t)*, as well as the location of the melt front as a function of time, *s(t)*. From this information, heat flux at any location at a certain time can be computed from Fourier's law.[11] This solution has since been presented in numerous reviews and texts. [8, 9, 11] For an initially solid substance starting at its melting temperature, T_{m}, the location of the melt front is given by:

$$s(t) = 2\lambda\sqrt{\alpha_l t}, \tag{2.1}$$

and the temperature profile in the liquid phase is given by:

$$\frac{T_l(y,t)-T_0}{T_m-T_0} = \frac{\mathrm{erf}(y/2\sqrt{\alpha_l t})}{\mathrm{erf}(\lambda)}. \tag{2.2}$$

In these expressions, α_l is the effective thermal diffusivity of the liquid, y is the vertical location, and λ is the solution to the transcendental equation

$$\lambda e^{\lambda^2}\mathrm{erf}(\lambda) = \frac{St_l}{\sqrt{\pi}}. \tag{2.3}$$

St_l is the Stefan number for the liquid which is defined as the ratio of sensible heat to latent heat

$$St_l = \frac{C(T_0-T_m)}{L_w}, \tag{2.4}$$

where *C* is the specific heat capacity and L_w is the specific latent heat. Combining Eq. 2.2 with Fourier's law, the heat flux, q'', at the boundary $(y = 0)$ held at a constant temperature is given by:

$$q''(0,t) = \frac{T_0 - T_m}{\sqrt{\pi}\sqrt{t}}\left(\frac{1}{\text{erf}\,(\lambda)} * \frac{k_l}{\sqrt{\alpha_l}}\right) \quad (2.5)$$

where k_l represents the thermal conductivity of the liquid phase.

2.3.2. Analytical Approaches to Heat Transfer in Lamellar Systems

We now introduce two approaches to model transient heat transfer in the combination PCM/metal system. The first approach, described in §2.2.2.1, homogenizes the properties of the lamellar layer and treats it as a single composite material with (anisotropic) effective properties. The second approach, described in §2.2.2.2, approaches the problem from the perspective of heat transfer through a high-conductivity fin into a surrounding medium, with the medium being a PCM. As opposed to traditional applications of fin equations, in this case, there is no mass transfer (i.e., fluid flow) past the fin.

2.3.2.1. Homogeneous Composite Approximation

Homogenization through an effective medium approximation (EMA) is considered to be valid when a material system behaves as a coherent system (i.e., when the length scales of the system are such that heat transfer can effectively be reduced to a 1D problem; (Figure 2.1). [48] In such a case, the effective properties of the homogenous composite depend on the properties of individual constituents, their proportions, and for transport properties, their shape and orientation. Intrinsic properties of the effective composite material (i.e., those that depend only on the volume fraction of constituents present; ρ, C, L_v, etc.) are described by a simple rule of mixtures

$$X_{\text{eff}} = \sum_i \phi_i X_i, \quad (2.6)$$

where ϕ_i denotes the volume fraction of constituent/phase, i, and X_i denotes the corresponding volumetric property. [70] In contrast, for the transport properties of a

material, geometry must be taken into account. [58-61] For these properties, the upper and lower bounds of the effective property is defined in directions parallel and perpendicular to conductive lamellae, respectively. [62]

$$k_{\text{eff}}^{||} = \phi_{\text{PCM}} k_{\text{PCM}} + \phi_{\text{cond}} k_{\text{cond}} \tag{2.7a}$$

$$(k_{\text{eff}}^{\perp})^{-1} = \phi_{\text{PCM}} (k_{\text{PCM}})^{-1} + \phi_{\text{cond}} (k_{\text{cond}})^{-1} \tag{2.7b}$$

For the purposes of this study, we will focus on the case where conductive lamellae are parallel to the direction of heat flow, $k_{\text{eff}}^{||}$. Thermal diffusivity is calculated using $k_{\text{eff}}^{||}$ and other properties calculated from Eq. 2.6. While this is the upper bound for thermal conductivity for 1D heat transfer in a Cartesian system, this will not necessarily hold for other geometries. [53]

Once effective material properties have been determined using Eq. 2.6 and Eq. 2.7, these effective properties can be used in analytical solutions of the general melting problem (§2.2.1), where the constituents are treated as a singular material undergoing melting. Alternatively, effective properties can be used to solve heat transfer numerically, with the advantage of reducing the order of a problem from a 2D or 3D problem to a 1D problem, with an associated reduction in computational cost. [9]

2.3.2.2. Fin Approximation

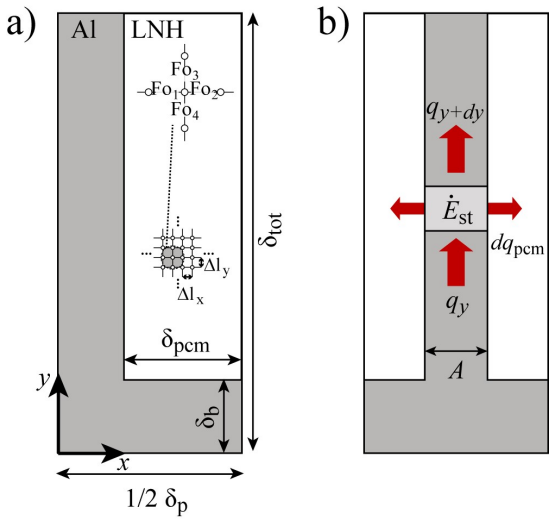

Figure 2.2 a) Geometry of FDA simulated composite showing the direction of Fourier numbers and node spacing. Structure is dictated by the pitch (δ_p), base height (δ_b), total height (δ_{tot}), and halfwidth of the PCM channel (δ_{PCM}). b) Geometry of fin model demonstrating a fin with cross sectional area (A) transferring heat into a finite thickness slab of PCM of width δ_{PCM}, with an adiabatic boundary. The applied boundary condition is applied to the bottom edge of the geometry and all other edges are adiabatic.

When the characteristic width-to-length ratio is sufficiently small in the system, heat flows first down the length of the metal fins, and then laterally into the PCM phase (particularly near the actively melting zone), as the low thermal conductivity of the PCM phase restricts heat flow vertically. [68] This particular behavior enables the use of a 1D fin approximation to describe heat flow within the lamellar system over time. We derive

the heat transfer equation for the fin using a differential volume energy balance, as shown schematically in Figure 2.2b. The overall energy balance in the fin is: [47, 71]

$$q_y - q_{y+dy} - dq_{\mathrm{PCM}} = \rho_{\mathrm{cond}} V C_{\mathrm{cond}} \frac{\partial T}{\partial t} \tag{2.8}$$

where q_y is the heat flow into the fin at location y, q_{y+dy} is the heat flow out of the fin at location $y + dy$, dq_{PCM} is the lateral heat flow out of the fin into the PCM material, and ρ_{cond}, V, and C_{cond} are the density, volume, and specific heat of the fin differential element, respectively.

The heat flow at location y is given by Fourier's law, accounting for a potentially non-uniform cross-sectional area of the fin,

$$q_y = -k_{\mathrm{cond}} A_c(y) \frac{\partial T}{\partial y}, \tag{2.9}$$

where k_{cond} is the thermal conductivity of the fin, and $A_c(y)$ is the cross-sectional area at location y. The heat flow at location $y + dy$ is given by the Taylor Series approximation of Eq. 2.9 at $y + dy$,

$$q_{y+dy} = q_y - \frac{\partial q_y}{\partial y} dy \tag{2.10}$$

and the heat flow laterally out of the fin is given by,

$$dq_{\mathrm{PCM}} = \frac{k_{\mathrm{PCM}}(T - T_m)}{\mathrm{erf}(\lambda)(\pi \alpha_{\mathrm{PCM}} t)^{1/2}} 2dy \tag{2.11}$$

which is the 1D solution for heat flux from the free boundary problem described above multiplied by the surface area of the differential fin volume that is exposed to the PCM phase. Combining Eq. 2.9 – 2.11 into Eq. 2.8 and simplifying yields the following differential equation:

$$\frac{\partial}{\partial y}\left(k_{\mathrm{cond}} A_c(y) \frac{\partial T}{\partial y}\right) - 2 \frac{k_{\mathrm{PCM}}(T - T_m)}{\mathrm{erf}(\lambda)(\pi \alpha_{\mathrm{PCM}} t)^{1/2}} = \rho_{\mathrm{cond}} A_c(y) C_{\mathrm{cond}} \frac{\partial T}{\partial t}, \tag{2.12}$$

that can be solved numerically over time (as detailed in §2.3.2).

While this approach does not lead to close-formed analytical solutions, it reduces the order of a problem from a 2D or 3D to a 1D heat transfer problem, leading to a notable reduction in computational cost.

2.4. Methods – Finite Difference

2.4.1. Fundamental Approximations

In order to create a reduced order model for describing conduction throughout the phase change process a number of simplifying assumptions are adopted in order to enhance the tractability of the numerical solution, but to retain the fundamental nature of the physical process being described:

(1) Material properties of both solid and liquid phases are independent of both temperature and time. This approximation may be made due to the fact that the change in properties are relative minor for the materials under investigation over the temperature range we test in this paper. [72, 73] As a direct example for LNH, the PCM under investigation in this work, a temperature shift from 35 º C to 45 º C leads to a 0.5% increase in thermal conductivity, no change in thermal diffusivity, and a 1% change in heat capacity. [72]

(2) The solid-liquid interface is a sharp well-defined boundary. While for some PCMs the melting process is smeared over a range of temperature values (e.g. paraffins), the PCMs under investigation in this work undergo a solid-liquid phase transition at a single well-defined temperature. However, even in the case that melting no longer occurs at a single temperature the underlying physics is minimally impacted.

(3) The density of the solid and liquid phases are equal (i.e., there is no fluid flow upon change of the location of the melt/solid interface). As with the previous two approximations, the density change, in reality, would be dependent on the particular PCM under investigation but is very minor in the context of this body of work (within 0.5 %). [72]

(4) Convection is negligible in the liquid phase. While convection plays an important role in some melting problems, it is strongly dependent on the problem geometry with respect to buoyancy forces, the duration of the melting period, the fluid viscosity, and the presence of geometric confinement. In this study, we focus on systems which are geometrically confined to small length scales, and which strongly limit the role of convection. [6, 39, 74] For these reasons, we consider the role of conduction and neglect convective heat transfer.

(5) To reduce the problem to its fundamental elements, we consider the case of the one-phase problem, where heat transfer only occurs in one phase (the liquid phase). That is, $T_{\mathrm{s}}(y > s(t), t > 0) = T_{\mathrm{m}}$. This simply dictates the initial condition of the system as having a uniform temperature profile that is set to the melting point of the PCM while being in the solid state.

(6) The role of contact resistance is neglected, as the relevant length scales investigated in this study greatly exceed the Kapitza length associated with interface thermal resistance. [75]

Below, we develop finite difference methods of decreased orders, 2D and 1D. This makes the problem of describing heat transfer in the complex systems more tractable and less

computationally expensive. These methods have been validated extensively through comparison to commercial high fidelity ANSYS packages and analytical expressions for single material conduction and has been supported by experimental results.

2.4.2. 2D Finite Difference Method

A finite difference analysis (FDA) was conducted to simulate conductive heat transfer through composite heatsink geometries. Creating a high-fidelity numerical model and comparing against approximate analytical solutions provides a test of solution accuracy over different time and length scales. [76] This numerical model is discussed in more detail in a previous work. [67] The FDA model simulates a given 2D area from the midpoint of the fin to the midpoint of the PCM channel (Figure 2.2a). By symmetry, this simulated area is representative of a fin structured heatsink with repeating reflected units of the modeled subsection. Each of the long sides and the top of the simulated area are treated as adiabatic boundaries while the bottom is the constant heat flux or temperature heat source. Again, we make the simplifying assumptions stated in §2.3.1.

The particular material system investigated in this study is aluminum 6063, selected as a light weight conductive alloy utilized in many heat exchangers, and lithium nitrate trihydrate ($LiNO_3 \cdot 3H_2O$) a salt hydrate phase selected for its high volumetric energy storage density, near room temperature melting point, and repeatable melting behavior (Table 2-1). The geometry of the system defined by the total height, δ_{tot}, base height, δ_{b}, fin pitch, δ_{p}, and volume fraction of metal in the fin, ϕ_{cond} (Figure 2.2a). Fin pitch, δ_{p} is defined as the width of a repeating unit of the lamellar heatsink and is twice the width of the simulated area. Through all simulations for direct comparison of aspect

ratios, δ_{tot} and δ_{b} were held constant and ϕ_{cond} is independent of location y. Nodes are created in an equally spaced array 500 × 50 nodes in the y direction) and x directions, respectively, and individually assigned a material and associated properties (Table 2-1). A thorough analysis of grid sizing was conducted to ensure model convergence and fidelity to both known analytical solutions, and to simulations the commercial FEA package, ANSYS.

Table 2-1 Material properties used in numerical simulations.

	Units		Aluminum 6063 [77]	$LiNO_3 \cdot 3H_2O$ [72]
k_s	W/mK		200	0.75
k_l	W/mK		-	0.58
L_v	MJ/m^3		-	408
L_w	J/g		-	287
α	mm^2/s		82.3	0.191
ρ	kg/cm^3		2.70	1.42
C	J/gK		0.9	2.76
Tm	K		-	303.25

An implicit method was selected to calculate the temperature throughout the composite heatsink in numerical simulations. For each timestep, *dt*, the temperature of any node must satisfy:

$$(Fo_1 + Fo_2 + Fo_3 + Fo_4 + 1)T_{q,r}^{p+1} - Fo_1 T_{q,r-1}^{p+1} - Fo_2 T_{q,r+1}^{p+1} - Fo_3 T_{q-1,r}^{p+1} - Fo_4 T_{q+1,r}^{p+1} = T_{q,r}^{p} \quad (2.13)$$

where Fo_j denotes the Fourier number calculated as:

$$Fo_j = \frac{\Delta t(k_{q,r} + k_{q',r'})}{2\rho_{q,r} C_{q,r} \Delta l^2} \quad (2.14)$$

and the subscripts of T, q and r, refer to the location of each node in the simulated geometry and q' and r' refer to the neighboring node in the direction j. Additionally, the distance across the node is represented by Δl in the direction j. The temperature change of each node and the fraction of the node that melts during a timestep is calculated using the total energy stored within a node. In the case of a constant temperature boundary condition, the temperature of the non-adiabatic wall is held at a fixed value, and heat flux is calculated numerically. In the case of a constant heat flux boundary condition the non-adiabatic wall satisfies:

$$(Fo_1 + Fo_2 + 2Fo_3 + 1)T_{q,r}^{p+1} - Fo_1 T_{q,r-1}^{p+1} - Fo_2 T_{q,r+1}^{p+1} - 2Fo_3 T_{q-1,r}^{p+1} = T_{q,r}^{p} + \frac{2q_0'' \Delta t}{\rho_{q,r} C_{q,r} \Delta y} \qquad (2.15)$$

The initial state of the system is entirely in the solid state, and total enthalpy of each node is tracked to calculate the melt fraction of a node for a particular time. After each time step, excess temperature above the melting temperature for a node which has not completely melted is used to calculate a new melt fraction, and the temperature of the node is adjusted accordingly. This approach has the effect of limiting melting to occur at a single discrete temperature, which is an accurate description of melting of at an invariant point (e.g., of the salt hydrate phase considered in this study). This method also requires using a sufficiently small time step to avoid numerical artifacts associated with melting more than a single node in each time step, a condition which was rigorously evaluated during validation of the numerical code.

Time steps were chosen to increase exponentially from dt = 5.5 ms (at t = 0 s) to dt = 4 s (at t = 5,000 s) to balance model fidelity and simulation run times. A series of linear varying timestep simulations were completed to test the effect of fine time

increments on model convergence. Timesteps for the final model were chosen to be smaller than fine convergent linear models for short timescales, in early melting stages, and increase past the linear timestep size thereafter (at ~10 s).

2.4.3. 1D Finite Difference Approximation

The 1D finite difference approximation treats heat transfer from each conductive layer as a single fin, and follows similarly to the full 2D model, with the addition of a heat flux term that accounts for heat flow into the PCM layer, which is dependent on both location and time, as given below.

$$Fo_j\left[\hat{A}_{q+1}T_{q+1}^{p+1} + \hat{A}_{q-1}T_{q-1}^{p+1} - 2A_qT_q^{p+1}\right] - \frac{2k_{\mathrm{PCM}}\left(T_q^{p+1}-T_q\right)}{erf(\lambda_q)\left(\pi\alpha_{\mathrm{PCM}}\tau_q^{p+1}\right)^{1/2}}\frac{\Delta t}{\rho_{cond}C_{cond}} = A_q\left(T_q^{p+1} - T_q^{p}\right) \quad (2.16)$$

This has a similar effect as the approach of considering homogeneous composite properties in that it reduces the order of a 2D composite structure to essentially a 1D heat transport problem. In this case, differences in cross-sectional areas of the fin between nodes must be taken into account, where summing the thermal resistances between each node produces an effective cross-sectional area.

$$\hat{A}_{q\prime} = \frac{2}{\frac{1}{A_{q\prime}}+\frac{1}{A_q}} \quad (2.17)$$

The approximate solution to the transcendental variable from the Stefan problem described above is used here, valid for $St << 1$,

$$\lambda_q = \sqrt{\frac{St_q}{2}} \quad (2.18)$$

where St must be calculated for each element at each timestep, given below.

$$St_{\mathrm{q}} = \frac{C_{\mathrm{PCM}}\left(T_q^{p}-T_m\right)}{L_{\mathrm{w}}} \quad (2.19)$$

Because the time and location of the melt front are not independent parameters in this problem, we can calculate an effective "melt front propagation time" based on the current location of the melt front, as given below.

$$\tau_q^p = \frac{2x_q^{p^2}}{\alpha_{\mathrm{PCM}} St} \tag{2.20}$$

This time is then incremented by the timestep chosen for the solver,

$$\tau_q^{p+1} = \tau_q^p + \Delta t \tag{2.21}$$

The solution to the temperature profile at the next time is determined using standard linear algebra solvers, and a new melt front location is determined at each node for the next time step,

$$s_q^{p+1} = \sqrt{\frac{\alpha_{\mathrm{PCM}} St(\tau_{\mathrm{q+1}})}{2}} \tag{2.22}$$

until the melt front has exceeded the distance from the fin surface to the half-width of the PCM layer thickness. Once this condition has been satisfied for a given node, the term accounting for melt-front propagation in Eq. 2.16 becomes zero, and the problem reduces to 1D conduction through a metal slab. It is important to point out that this solution assumes quasi-steady state melt-front propagation, which is valid only for small temperature rises. [78] Additionally, this model does not account for the sensible heat in the PCM domain in the time before melting is completed. Hence, this model is inaccurate for extremely high values of temperature rise or surface heat flux, as discussed in more detail in later sections.

2.5. Results and Discussion

2.5.1. Characteristic Times, Constant Temperature

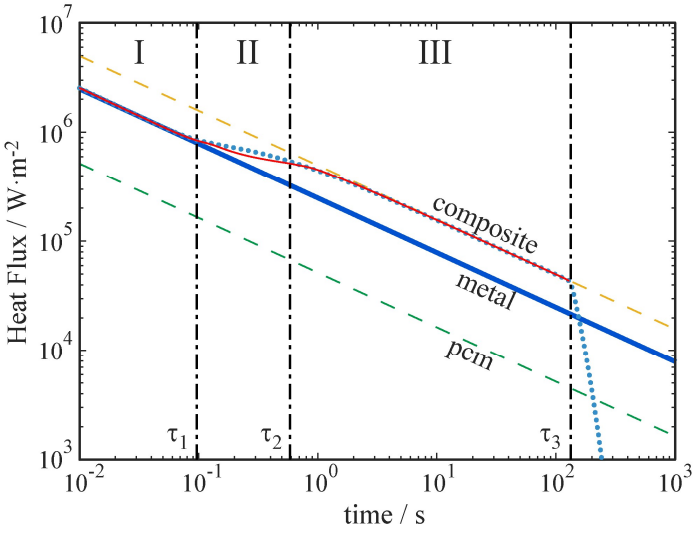

Figure 2.3 2D FDA simulation results for time-dependent heat flux across the base into a lamellar composite with equal volume fraction ($\phi = 0.5$) for a fine pitch ($\delta_p = 0.4$ mm) with a metal base of δ_b = 5 mm thick, and with constant temperature boundary condition ($T_0 - T_m$ = 20 ºC) (red line). Straight lines represent the exact analytical solution for heat flux into a volume composed entirely of PCM (dotted green), a homogeneous composite ($\phi = 0.5$; dotted yellow) or semi-infinite slab of metal (solid blue). Dotted blue line represents the 1D FDA simulation, which includes a base of metal overlaid by a homogeneous composite. Three characteristic regimes separated by critical times τ_1, τ_2, and τ_3 (calculated with Eq. 2.25, 2.27 and 2.32), represent: I) heat diffusion through the metal base, II) development of melt profile within PCM channels, and III) propagation of melt front through the lamellar composite.

Heat transfer through lamellar systems is governed by different behavior across different time regimes, based on the geometry of the system. In the case of a multi-component PCM lamellar systems with a finite thickness base, we have identified three general regimes for a constant temperature boundary condition and two regimes for a constant heat flux boundary condition. For a constant temperature boundary condition, we observe regimes of: 1) conduction through a finite thickness (single constituent) base, 2) transitional period and formation of the solid-liquid interface within PCM channels, and 3) quasi-steady melting of the PCM lamellae (Figure 2.3). This is most clearly observed at small temperature differences but at larger temperature differences as well. In this section, we derive critical time constants to demarcate the boundaries between these three regimes. The objective for this section is to establish the critical time constants which demarcate the boundaries between these three regimes, as a function of geometry (ϕ_{PCM}, pitch, height), material properties, and boundary conditions.

2.5.1.1. Heating of Solid Base, $0 < t < \tau_{1,T_0}$

At the initiation of heating for the constant temperature boundary condition, incident heat at the base propagates through the base metal slab, and heat transfer in the overall system is governed by 1D conduction based on the thermal properties of the base material. For short time periods, we treat this as a semi-infinite medium:

$$q''_{1,T_0} = \frac{k_{\mathrm{cond}}(T_0 - T_{\mathrm{m}})}{\sqrt{\pi \alpha_{\mathrm{cond}} t}} \tag{2.23}$$

After some characteristic time, τ_{1,T_0}, heat reaches the lamellar PCM/metal layer and during an initial transitional period, goes towards melting PCM at the base of the PCM channels.

During this period, the heat flow is given by Fourier's law through the base between the applied base temperature and the melting temperature of the PCM:

$$q''_{2,T_0} = \frac{k_{\text{cond}}(T_0 - T_{\text{m}})}{\delta_{\text{b}}} \tag{2.24}$$

where δ_{b} is the thickness of the base material (Figure 2.2). Equating Eq. 2.23 and 2.24 and solving for time gives the characteristic time for transition from base heating to heating the lamellar layer:

$$\tau_{1,T_0} = \frac{\delta_{\text{b}}^2}{\pi \alpha_{\text{cond}}} \tag{2.25}$$

which is independent of the geometry of the overlying lamellar layer.

The general conclusion from this analysis is that the metal base serves as a thermal bottleneck, throttling heat transfer to the simple conduction through a single phase until a characteristic time, τ_{1,T_0}, as defined by Eq. 2.25.

2.5.1.2. Onset of Melting of PCM, $\tau_{1,T_0} < t < \tau_{2,T_0}$

Following the initial temperature rise in the base, heat begins to flow into PCM channels, and forms a melt front within the channel. The period $\tau_{1,T_0} < t < \tau_{2,T_0}$ is characterized by a transition from semi-infinite heat flow through the base to semi-infinite heat flow through the homogeneous composite. We will first delineate τ_{2,T_0} under a limiting approximation of narrow fins (i.e., small δ_{p}, where δ_{p} represents the pitch of the lamellar system). After this, we expressly discuss the role of δ_{p} in τ_{2,T_0}

For small δ_{p}, the melt front is roughly flat, and so it fully develops very near the base. For constant temperature boundary conditions, τ_{2,T_0} is given by a heat balance when Eq. 2.24 is equal to the heat flow through the effective homogeneous composite.

$$q''_{3,T_0} = \frac{k_{\text{eff}}(T_0 - T_{\text{m}})}{\text{erf}\,(\lambda)\sqrt{\pi\alpha_{\text{eff}}t}} \tag{2.26}$$

Equating q''_{2,T_0} (Eq. 2.24) with q''_{3,T_0} (Eq. 2.26) results in a transition time

$$\tau_{2,T_0} = \frac{\delta_{\text{b}}^2}{\pi\alpha_{\text{eff}}}\left(\frac{k_{\text{eff}}}{k_{\text{cond}}\text{erf}\,(\lambda)}\right)^2 \tag{2.27}$$

While the heat balance approach is accurate for systems of sufficiently small pitches (as will be presented in subsequent sections) a second model is necessary for wider pitches to take into account the effect of increasing width on the critical time. As illustrated in Figure 2.3, composite behavior in fin structured heatsinks occurs after the melt profile has been fully established and continues until the melt front begins to experience edge effects. In order to consider the influence of the critical composite time τ_{2,T_0}, we calculate the time it takes to establish the melt profile as the time necessary to melt the PCM channel from the outer edge to the centerline of the channel. From the constant temperature boundary condition, the exact solution for the location of the melt front is given by Eq. 2.1. This may be rearranged and, replacing $s(t)$ with δ_{PCM} results in:

$$\tau_{2,T_0} = \frac{1}{\alpha_{\text{PCM}}}\left(\frac{\delta_{\text{PCM}}}{2\lambda_{\text{PCM}}}\right)^2 \tag{2.28}$$

This approach neglects τ_{1,T_0}, and thus provides a lower bound estimate of τ_{2,T_0}. Comparing the critical time to develop a melt profile in Eq. 2.28 with the critical time required to reach quasi-steady flow in the homogeneous medium in Eq. 2.27 and solving for δ provides a critical channel width that denotes the feature size required to achieve homogeneous composite behavior, which has typical values on the order of ~100 μm for metal/PCM lamellar systems

$$\tau_{2,T_0} = \begin{cases} \frac{\delta_b^2}{\pi\alpha_{eff}}\left(\frac{k_{eff}}{k_{cond}\mathrm{erf}\,(\lambda)}\right)^2 & \delta_{PCM} < 2\lambda_{pcm}\sqrt{\frac{\delta_b^2\alpha_{PCM}}{\pi\alpha_{eff}}\left(\frac{k_{eff}}{k_{cond}\mathrm{erf}\,(\lambda)}\right)^2} \\ \frac{1}{\alpha_{PCM}}\left(\frac{\delta_{PCM}}{2\lambda_{PCM}}\right)^2 & \delta_{PCM} > 2\lambda_{PCM}\sqrt{\frac{\delta_b^2\alpha_{PCM}}{\pi\alpha_{eff}}\left(\frac{k_{eff}}{k_{cond}\mathrm{erf}\,(\lambda)}\right)^2} \end{cases} \quad (2.29)$$

2.5.1.3. Steady Melting of PCM, $\tau_{2,T_0} < t < \tau_{3,T_0}$

For constant temperature boundary conditions, the total thermal energy that the system can absorb is the total sensible and latent heat associated with a uniform temperature rise of the whole system

$$Q'' = (\delta_{tot} - \delta_b)\left[\rho_{eff}C_{eff}(T_0 - T_m) + L_{v,eff}\right] \quad (2.30)$$

where δ_{tot} is the total height of the thermal energy storage (TES) system. This total energy storage per area must be equal to the integral of the heat flux over time, which can be integrated using the characteristic times and heat fluxes described above

$$Q'' = \int_0^{\tau_{1,T_0}} q_1''\,dt + \int_{\tau_{1,T_0}}^{\tau_{2,T_0}} q_2''\,dt + \int_{\tau_{2,T_0}}^{\tau_{3,T_0}} q_3''\,dt \quad (2.31)$$

Assuming that the first two regimes store very little heat relative to the third regime, the total time to exhaust the latent heat capacity of the PCM system reduces to:

$$\tau_{3,T_0} = \left[\frac{L_{v,eff}(\delta_{tot}-\delta_b)\mathrm{erf}\,(\lambda)\sqrt{\pi\alpha_{eff}}}{2k_{eff}(T_0-T_m)} + \frac{\delta_b}{\mathrm{erf}\,(\lambda)\sqrt{\pi\alpha_{eff}}}\left(\frac{k_{eff}}{k_{cond}}\right)\right]^2 \quad (2.32)$$

2.5.1.4. Summary of Critical Times

The heat flux over time for the constant temperature boundary conditions can be summarized as follows (assuming small feature sizes, as discussed in section 2.4.1.2).

$$q_s''(t) = \begin{cases} \frac{k_{cond}(T_0-T_m)}{\sqrt{\pi\alpha_{cond}t}}, & 0 < t < \tau_{1,T_0} = \frac{\delta_b^2}{\pi\alpha_{cond}} \\ \frac{k_{cond}(T_0-T_m)}{\delta_b}, & \tau_{1,T_0} < t < \tau_{2,T_0} = \frac{\delta_b^2}{\pi\alpha_{eff}}\left(\frac{k_{eff}}{k_{cond}}\right)^2 \\ \frac{k_{eff}(T_0-T_m)}{\mathrm{erf}\,(\lambda)\sqrt{\pi\alpha_{eff}t}}, & \tau_{2,T_0} < t < \tau_{3,T_0} = \left[\frac{L_{v,eff}(\delta_{tot}-\delta_b)\mathrm{erf}\,(\lambda)\sqrt{\pi\alpha_{eff}}}{2k_{eff}(T_0-T_m)} + \frac{\delta_b}{\mathrm{erf}\,(\lambda)\sqrt{\pi\alpha_{eff}}}\left(\frac{k_{eff}}{k_{cond}}\right)\right]^2 \end{cases} \quad (2.33)$$

It should be noted that the magnitude of boundary conditions increases, the critical times reported will still hold within a reasonable amount of error but deviate more as the role of sensible heat becomes more increasingly significant compared to the role of latent heat.

2.5.2. Characteristic Times, Constant Heat Flux

For constant heat flux boundary condition, we do not observe an equivalent regime II for the range of heat fluxes investigated in this study. As the magnitude of the heat flux across the boundary is increased, the role of sensible heat becomes increasingly large compared to the role of the latent heat. This effectively leaves two regimes of 1) conduction through the finite thickness (single constituent) base and 2) melting of the lamellar layer. An equivalent approach can be taken to the critical times of constant heat flux as was applied for constant temperature for equivalent behaviors.

2.5.2.1. Heating of Solid Base, $0 < t < \tau_{1,q_0''}$

As in the constant temperature boundary condition case, the first regime is characterized by the time it takes for conduction through the base material. In the case of a constant heat flux boundary condition, the relationship between surface temperature of the base and surface heat flux is given by

$$T_{0,q_0''} = \frac{2q_0''}{k_{cond}}\sqrt{\frac{\alpha_{cond}t}{\pi}} + T_m \tag{2.34}$$

which can be used to solve for the time at which PCM melting initiates by inserting Eq. 2.24 for the heat flux and solving for time.

$$\tau_{1,q_0''} = \frac{\pi}{\alpha_{cond}}\left(\frac{\delta_b}{2}\right)^2 \tag{2.35}$$

As with the constant temperature boundary condition, this time acts as a bottleneck for heat transfer through the system.

2.5.2.2. Melting of Lamellar Layer, $\tau_{1,q_0''} < t < \tau_{2,q_0''}$

For constant heat flux boundary conditions, the total time to change the phase of the composite is simply given from an energy balance over the whole volume:

$$\tau_{2,q_0''} = \frac{L_{\mathrm{v,eff}}(\delta_{\mathrm{tot}} - \delta_{\mathrm{b}})}{q_0''} \tag{2.36}$$

This leaves us with a simple expression to describe the total time it takes to melt all the PCM within the system.

2.5.2.3. Summary of Critical Times

While in the constant temperature boundary condition we track heat flux at the surface, for the constant heat flux boundary condition we track temperature. The surface temperature over time for the constant heat flux boundary condition is summarized below.

$$T_0(t) - T_m = \begin{cases} \frac{2q_0''}{k_{cond}}\sqrt{\frac{\alpha_{cond} t}{\pi}}\,, & 0 < t < \tau_{1,q_0''} = \frac{\pi}{\alpha_{cond}}\left(\frac{\delta_b}{2}\right)^2 \\ \frac{{q_0''}^2}{k_{eff} L_{v,eff}}\left(t - \tau_{1,q_0''}\right) + \frac{q_0''\delta_b}{k_{cond}}\,, & \tau_{1,q_0''} < t < \tau_{2,q_0''} = \frac{L_{v,eff}(\delta_{tot} - \delta_b)}{q_0''} \end{cases} \tag{2.37}$$

While a third regime between these two in which the melt front was establishing was theorized and demonstrated to emerge for sufficiently small heat flux values, for practical applications, this summary is sufficient.

2.5.3. Internal Heat Fluxes During Melting

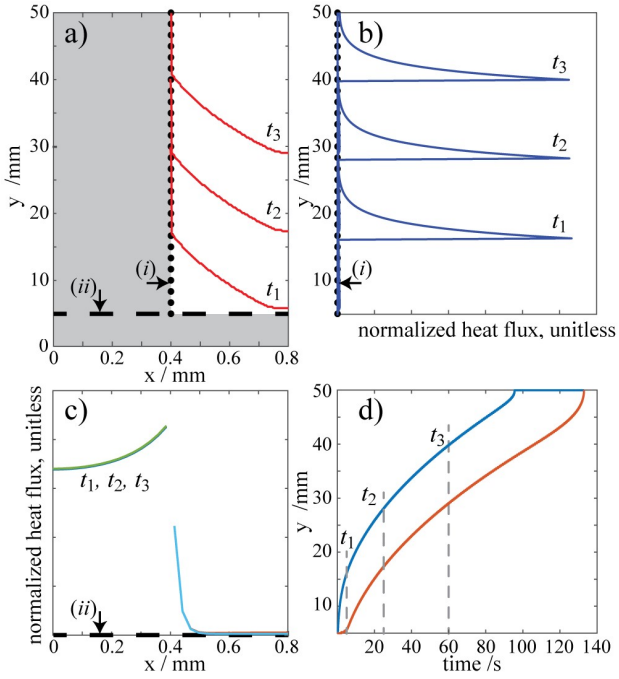

Figure 2.4 A lamellar composite with equal volume fraction PCM and metal ($\phi = 0.5$; $\delta_p = 1.6$ mm; $\delta_b = 5$ mm), and with constant temperature boundary condition ($T_0 - T_m = 20$ ºC). a) Melt front (red line) at three points in time (t_1, t_2, t_3). b) Normalized horizontal heat flux across vertical fin surface (i) designated by dotted line at three points in time. c) Normalized vertical heat flux across horizontal plane (ii) designated by dashed line, which are nearly indistinguishable for times t_1, t_2, t_3. Heat flux is normalized by the maximum heat flux for that time, to illustrate the relative distribution of heat flux across a particular plane. d) Height of melt front along the vertical fin surface (blue), and at the mid-point of the PCM channel (red) as a function of time, illustrating the nearly constant height of the melt front meniscus.

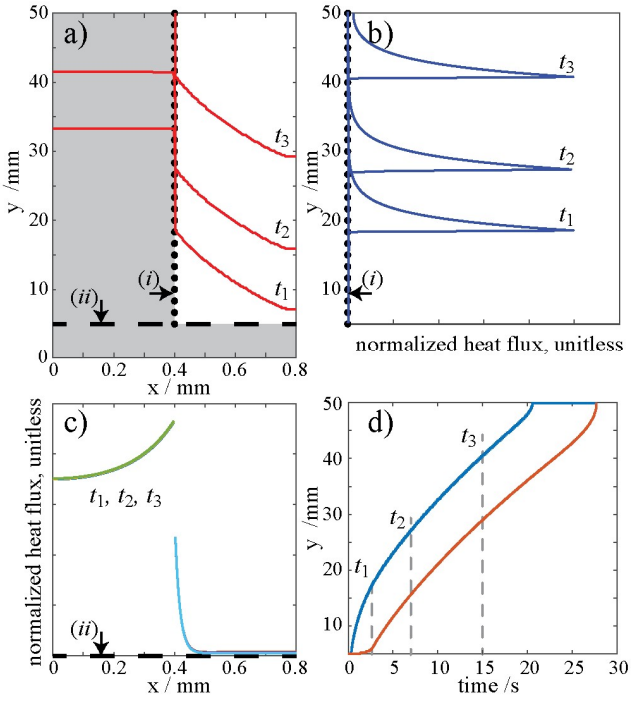

Figure 2.5 Lamellar composite with equal volume fraction PCM and metal ($\phi = 0.5$; $\delta_p = 1.6$ mm; $\delta_b = 5$ mm), and with constant heat flux boundary condition ($q_0'' = 100\ \mathrm{W \cdot cm^{-2}}$). a) Melt front (red line) at three points in time (t_1, t_2, t_3). b) Normalized horizontal heat flux across vertical fin surface (i), and c) vertical heat flux across horizontal plane (ii), using normalization procedure described for Figure 2.4, and which are nearly indistinguishable for times t_1, t_2, t_3. d) Height of melt front along the vertical fin surface (blue), and at the mid-point of the PCM channel (red) as a function of time, illustrating the nearly constant height of the melt front meniscus.

During melting of lamellar multi-component systems containing a PCM, a melt front meniscus is established within each PCM channel (at time τ_{2,T_0}), which propagates upward with an approximately conserved shape until finite edge effects are encountered (Figure 2.4a, Figure 2.5a). Plotting the height (distance in *y*) of the melt front adjacent to the fin with the height of the melt front at the midpoint of the PCM channel demonstrates that there exists a short transitional period during which the melt profile develops its characteristic profile ($\tau_{1,T_0} < t < \tau_{2,T_0}$), followed by a progressive translation of the melt front upwards ($\tau_{2,T_0} < t < \tau_{3,T_0}$), during which time, the gap between edge meniscus height remains nearly constant (Figure 2.4d, Figure 2.5d). In order to analyze trends in internal heat flow within the system, we monitor the relative magnitude and position of heat flux passing through two internal surfaces of the composite: *i)* the vertical surface between a conductive layer and a PCM layer (Figure 2.4b, Figure 2.5b), and *ii*) the horizontal surface at the top of the metal base (Figure 2.4c, Figure 2.5c). As the heat flux throughout the composite decreases with time (as the melt front moves away from the heat source), it is useful to normalize by the maximum heat flux at each given time, in order to focus on the relative distribution of heat flux within the system over time. Tracking the normalized heat flux from the base into the lamellar layer illustrates that after the melt front within the PCM has fully developed, the vast majority of the heat travels into the fin (Figure 2.4c, Figure 2.5c), flows vertically along the *y* direction, and flows laterally into the PCM channels near the melt zone. Lateral heat flux is maximized at the height of the melt front adjacent to the fin (Figure 2.4b, Figure 2.5b). Furthermore, the general shape of the normalized heat flux profile remains constant while traveling upward until the finite

boundary of the system is reached. Equivalent behavior was observed for the constant heat flux and constant temperature boundary condition cases.

Taken together, these observations support the underlying premise of both 1) the fin model, as well as 2) the homogeneous composite model. First, these results confirm the assumption that the fins act as conductive channels to transport heat away from the interface to the height at which melting occurs, at which point heat is transferred laterally into the PCM. Second, as long as the pitch of the lamellar system is relatively small, the tendency for the internal fin temperature to rise beyond the melting temperature is limited by rapid lateral heat transfer into PCM (which is subject to incipient melting along the fin). At the small length scale limit, this leads to quasi-1D heat transfer vertically through the system.

2.5.4. Constant Temperature Boundary Condition

2.5.4.1. Variable Pitch

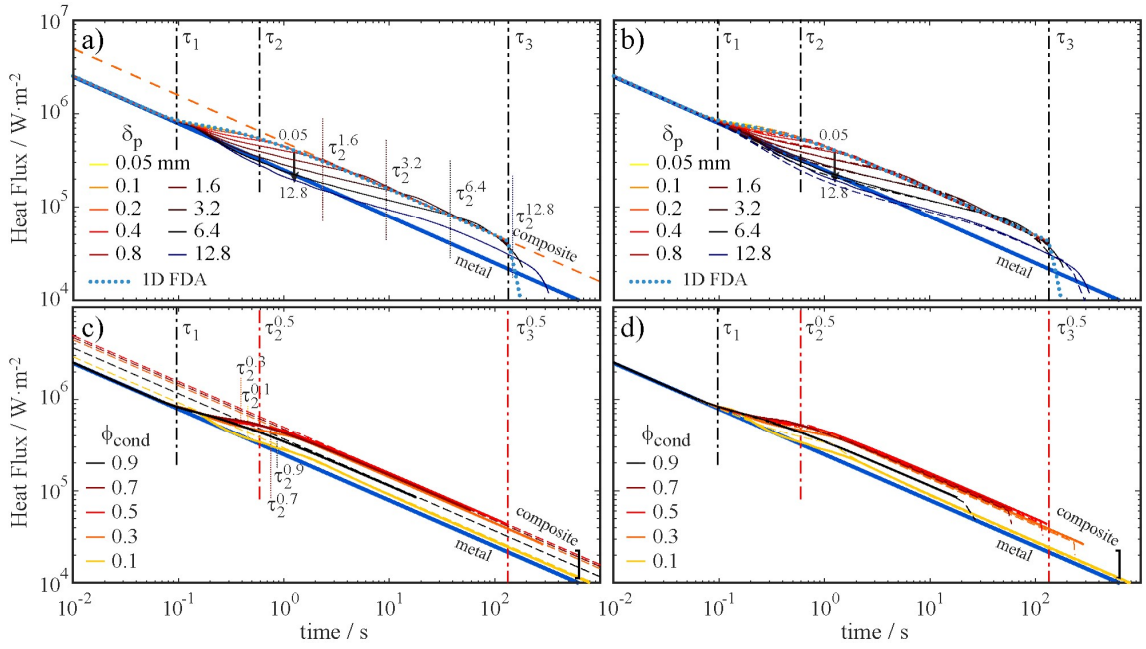

Figure 2.6. Time-dependent heat flux into lamellar composites with a constant temperature boundary condition ($T_0 - T_m$ = 20 ºC). a), b) Varying pitch at a constant volume fraction PCM and metal ($\phi = 0.5$; δ_b = 5 mm) with τ_1, τ_2, and τ_3 calculated with Eq. 2.25, 2.30 and 2.32, respectively. Solid lines represent 2D FDA results, while dashed lines represent a) exact analytical solutions using the homogeneous composite approximation, and b) 1D fin approximation. Dotted line represents a 1D FDA result, with the lamellar bulk treated with effective composite properties. c), d) Volume fraction dependence at a constant pitch ($\delta_p = 0.4$ mm) with τ_1, τ_2, and τ_3 calculated with Eq. 2.25, 2.29 and 2.32, respectively. Solid lines represent 2D FDA results, while dashed lines represent c) exact analytical solutions using the homogeneous composite approximation, and d) 1D fin approximation. Thick blue lines represent the analytical solution to heat diffusion into a semi-infinite metal slab.

Varying the pitch separating PCM lamella in the mixed material layer alters the time necessary to reach composite behavior (τ_{2,T_0}), and the heat flux across the boundary during this transitional period ($\tau_{1,T_0} < t < \tau_{2,T_0}$). To understand the dependence of conductive heat transfer on the spacing of the fins, a series of analytical and numerical tests were run, following the approaches and models described in previous sections. Keeping a constant interface temperature ($T_0 = T_m + 20$ °C), and a constant volume fraction ($\phi_{cond} = 0.5$), a series of 9 FDA simulations were run with pitches ranging from 0.05 mm to 12.8 mm, each run doubling the pitch of the previous run (Figure 2.6c,d). Larger pitches take longer times to establish a constant melt profile leading to a composite behavior occurring at later times. As calculated previously, for small pitches (<0.5 mm) using the heat balance method (Eq. 2.27) leads to good agreement with τ_{2,T_0}. However, for larger pitches, the time for the melt front to travel the half-width of the PCM channel (Eq. 2.28) better describes when the system begins to act as a composite.

1D FDA of the homogenous composite model (using effective properties) converges to the 2D FDA results at small pitches ($\delta_p < \sim 0.5$ mm depending on the dictated volume fraction; Figure 2.6c), supporting the general use of the composite approach when δ_{PCM} is below a critical value (Eq. 2.29). Furthermore, analytical expressions describing heat transfer through homogeneous composites adequately describe heat flux during the period of quasi-steady melting ($\tau_{2,T_0} < t < \tau_{3,T_0}$). Because the homogeneous composite model does not recognize any horizontal length scales, this model does not capture pitch dependency on heat transfer. However, outside of the transitional period ($\tau_{1,T_0} < t < \tau_{2,T_0}$), heat transfer is adequately described.

In contrast, the fin model captures some aspects of heat transfer during the transitional period (Figure 2.6d), although it systematically underestimates heat transfer immediately after τ_1, in part because it neglects any heat transfer from the base vertically into PCM channels. When vertical node spacing in the FDA is greatly shortened the numerical artifact of the first nodes melting is lessened and the results are closer to the fin model but never converge. We demonstrate the applicability of critical times for ΔT = 20 °C (Figure 2.6) and for a lower thermal driving force ΔT = 1 °C and show over this temperature range the expressions of these critical times still hold.

2.5.4.2. Variable Volume Fraction

Increasing the volume fraction of metal has the effect of decreasing the time required to reach composite behavior (τ_{2,T_0}), while simultaneously altering the limiting heat flux once composite behavior is achieved ($\tau_{2,T_0} < t < \tau_{3,T_0}$). Keeping a constant interface temperature ($T_0 = T_m + 20$ °C), and a constant pitch ($\delta_p = 0.4$ mm), a series of 9 FDA simulations were run with volume fractions ranging from 0.1 to 0.9 (Figure 2.6a,b). Results from the FDA can be compared against the analytical solutions for the homogeneous material for each volume fraction (Figure 2.6a) and against the results from the fin approximation (Figure 2.6b). In the beginning stages of heat absorption into the PCM, a higher volume fraction of PCM will result in higher heat fluxes, but once melting begins the opposite will be true. Composite behavior (τ_{2,T_0}) is achieved more rapidly in cases of larger ϕ_{cond} because for a fixed δ_p, the PCM channel width, $2\delta_{\mathrm{PCM}}$, decreases, causing the evolution of the melt front to proceed rapidly. Furthermore, the changing effective properties of the material the characteristic composite behavior ($\tau_{2,T_0} < t <$

τ_{3,T_0}) is dependent on volume fraction, with the highest heat transfer occurring at $\phi_{\text{cond}} \approx$ 0.5. Finally, expressions presented for critical times agree fairly well with transitions in behavior. Again, simulations run at a lower thermal driving force $\Delta T = 1\ ^{\circ}C$, illustrate that critical times still hold fairly well over this range of constant temperature boundary conditions.

2.5.5. Constant Heat Flux Boundary Condition

2.5.5.1. Variable Pitch

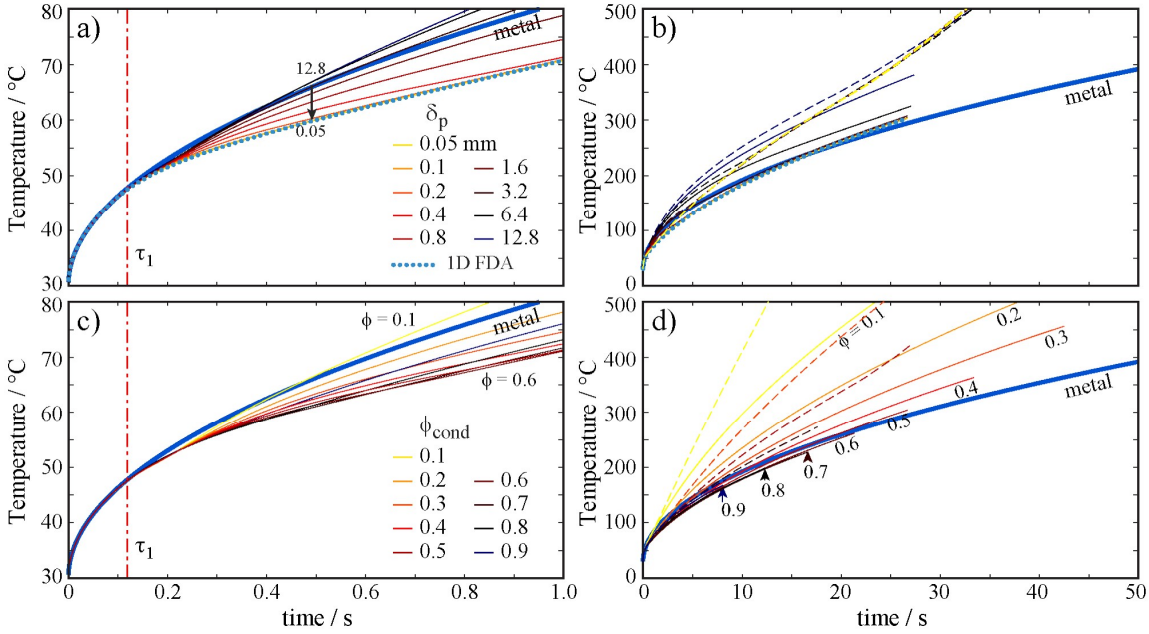

Figure 2.7 Time-dependent heat flux into lamellar composites with a constant heat flux boundary condition ($q_0'' = 100\,\mathrm{W \cdot cm^{-2}}$). a), b) Varying pitch at a constant volume fraction PCM and metal ($\phi = 0.5$; δ_b = 5 mm) with τ_1 calculated with Eq. 2.35. Solid lines represent 2D FDA results. Dotted line represents a 1D FDA result, while the thick blue line represents the analytical solution to heat diffusion into a semi-infinite metal slab. In b) dashed lines represent 1D fin approximation. c), d) Volume fraction dependence at a constant pitch ($\delta_p = 0.4$ mm) with τ_1 calculated with Eq. 2.35. Solid lines represent 2D FDA results, while the thick blue line represents the analytical solution to heat diffusion into a semi-infinite metal slab.

Under constant heat flux boundary conditions, varying lamella pitch introduces a longer transitional period of time before a system achieves quasi-steady melting (Figure 2.7c,d). For all constant heat flux simulations in this study, the input was chosen to be 100 $W \cdot cm^{-2}$. The first regime is characterized by an interfacial temperature rise during conduction through a metal base (Figure 2.7c, Eq. 2.34), followed by an approximately linear increase in surface temperature during melting of the composite (Figure 2.7d, Eq. 2.37). Varying the pitch increases the interfacial temperature during the transitional period relative to that of the small-pitch limit (Figure 2.7c,d). In these cases, the large pitch effectively limits heat absorption by melting PCM in the channel, resulting in an increase of interfacial temperature.

1D FDA of the homogenous composite model (using effective properties) converges nearly exactly to the 2D FDA results at small pitches ($\delta_p < \sim 0.1$ mm; Figure 2.7c), supporting the general use of the composite approach when δ_{PCM} is below a critical value. Furthermore, analytical expressions describing heat transfer through homogeneous composites adequately describe heat flux during the period of quasi-steady melting ($\tau_{1,q_0''} < t < \tau_{2,q_0''}$) for low heat fluxes, where the quasi-steady state approximation holds. It should be pointed out that for 100 $W \cdot cm^{-2}$, the quasi-steady state approximation is not entirely adequate, resulting in a progressive deviation from a linear interfacial temperature rise with time due to the role of sensible heating in the system (Figure 2.7d). Because the homogeneous composite model does not recognize any horizontal length scales, this model does not capture pitch dependency on heat transfer. In contrast, the fin model captures some aspects of heat transfer during the transitional period. We demonstrate the

applicability of critical times for q" = 100 W·cm^{-2} (Figure 2.7) and for a lower thermal driving force q" = 10 W·cm^{-2}, and show over this temperature range the expressions of these critical times still hold.

2.5.5.2. Variable Volume Fraction

For a constant heat flux boundary condition, increasing the volume fraction of metal minimizes the slope of the temperature change over small timescales. As in the previous case, the heat flux was set as 100 W·cm^{-2}, and the pitch was held constant at 0.4 mm. For each volume fraction, the PCM begins melting at the end of the plateau and is then limited by the lack of possible conduction causing sensible heat to increase. For cases in which there is a higher percentage of PCM, this increase is progressively more rapid. This leads to a pivotal point where, before this time, higher PCM volumes exhibit lower temperatures and after this time higher metallic volumes exhibit lower temperatures. Over longer timescales, as in the constant temperature case, the highly metallic elements will increase in temperature due to the lack of capacitive ability and $\phi_{\text{cond}} \approx 0.5$ will yield the lowest temperatures. Again, simulations run at a lower thermal driving force q" = 10 W·cm^{-2} illustrate that critical times still hold fairly well over this range of constant temperature boundary conditions.

2.6. Conclusions

Lamellar systems containing a melting component combined with conductive elements present a unique challenge in developing expressions for conductive heat transfer, resulting in few analytical solutions for such systems. Due to the challenging nature of free boundary problems and the introduction of non-trivial geometries, exact

solutions describing these systems are unlikely but approximate solutions offer great promise. In this body of work, we explored two approximate analytical solutions treating a lamellar PCM system as a 1) homogeneous composite medium with effective properties and 2) a singular fin in an infinite PCM surrounding. Analyzing these models led to the identification and mathematical expression of distinct characteristic thermal regimes and critical times. Comparing results of approximate models with varying parameters and boundary conditions against 2D FDA numerical calculations validates the use of approximate models for the end-member case where the thickness of PCM layers is small. These lengthscales and timescales are demonstrated to be intimately coupled. For example, for the material system and geometry considered herein, the homogeneous composite approximation holds fairly well for time scales greater than ~1 s when the thickness of the PCM layer is less than ~1 mm, but only for longer times (greater than ~100 s) when the thickness of the PCM layer increases to ~10 mm (Figure 2.6). In contrast, the 1D fin approximation described herein provides a more accurate description of heat transfer at shorter time periods when the melt front meniscus is being established, but at a cost of overestimating temperature rise at a heated surface for high heat fluxes due to the approximation of a small Stefan number (Eq. 2.18). Expressions developed were tested across low and relatively high boundary conditions and were shown to still be valid.

Importantly, within the bounds considered within this study, both the reduced order approaches and the higher fidelity 2D FDA simulations indicate a number of specific outcomes which are counterintuitive to traditional finned heatsink design. For example, for any particular volume fraction of metal and PCM, heat flux across a base held at a

constant temperature boundary condition is maximized by reducing the pitch of lamellar spacing (i.e., the thickness of the PCM layer). Similarly, for a constant heat flux boundary condition, the temperature rise at the base is minimized by reducing the pitch of lamellar spacing. In both cases, the limit to increasing heat flux or decreasing temperature rise is achieved when the critical length scale of the composite material is small enough that it can be treated using homogenized effective properties. This observation holds over a wide range of boundary conditions, volume fractions of metal / PCM, and material properties even outside of the data presented in this study. For these cases, isothermal temperature contours are essentially flat, and the temperature of the conductive layers extends above and below the melting temperature of the PCM; that is, the concept of fin efficiency is no longer a predictor of optimal design for lamellar composite structures in the limit where PCM layer thickness is small. However, multiple previous numerical investigations have illustrated that in these cases, the increase in conductive heat transfer rates more than offset the decreased role of convective heat transfer in these systems.[6, 14, 37, 38] Thus, we anticipate that considering lamellar structures as composite materials will facilitate rational design of systems particularly in the case where high rates of heat transfer play important roles. Using the prescribed analytical solutions as a framework, for a known application, allows for deliberate design in the creation of systems which 1) can be treated as composites for particular time scale problems, and 2) which can offer favorable tradeoffs in energy and cooling power densities.

2.7. References

[1] J. Fukai, Y. Hamada, Y. Morozumi, and O. Miyatake, "Effect of carbon-fiber brushes on conductive heat transfer in phase change materials," *International Journal of Heat and Mass Transfer,* vol. 45, no. 24, pp. 4781-4792, 2002.

[2] J. Fukai, M. Kanou, Y. Kodama, and O. Miyatake, "Thermal conductivity enhancement of energy storage media using carbon fibers," *Energy Conversion and Management,* vol. 41, no. 14, pp. 1543-1556, 2000.

[3] A. Mills, M. Farid, J. Selman, and S. Al-Hallaj, "Thermal conductivity enhancement of phase change materials using a graphite matrix," *Applied Thermal Engineering,* vol. 26, no. 14-15, pp. 1652-1661, 2006.

[4] S. Pincemin, R. Olives, X. Py, and M. Christ, "Highly conductive composites made of phase change materials and graphite for thermal storage," *Solar Energy Materials and Solar Cells,* vol. 92, no. 6, pp. 603-613, 2008.

[5] P. P. Levin, A. Shitzer, and G. Hetsroni, "Numerical optimization of a PCM-based heat sink with internal fins," vol. 61, pp. 638-645, 2013.

[6] V. Shatikian, G. Ziskind, and R. Letan, "Numerical investigation of a PCM-based heat sink with internal fins," *International Journal of Heat and Mass Transfer,* vol. 48, no. 17, pp. 3689-3706, 2005.

[7] J. Stefan, "Über die Theorie der Eisbildung, insbesondere über die Eisbildung im Polarmeere," *Annalen der Physik,* vol. 278, no. 2, pp. 269-286, 1891.

[8] J. M. Hill, *One-dimensional Stefan problems: an introduction* (Pitman monographs and surveys in pure and applied mathematics). Harlow, Essex, England : New York: Longman Scientific & Technical ; Wiley, 1987.

[9] V. Alexiades and A. D. Solomon, *Mathematical modeling of melting and freezing processes*. Washington : Hemisphere Pub. Corp., 1993.

[10] H. Weber and B. Riemann, *Die partiellen Differential-Gleichungen der mathematischen Physik nach Riemann's Vorlesungen bearb*. F. Vieweg & sohn, 1919.

[11] H. S. Carslaw and J. C. Jaeger, *Conduction of heat in solids*, 2nd ed. ed. Oxford : Clarendon Press, 1959.

[12] R. Velraj, R. V. Seeniraj, B. Hafner, C. Faber, and K. Schwarzer, "Experimental analysis and numerical modelling of inward solidification on a finned vertical tube for a latent heat storage unit," *Solar Energy,* vol. 60, no. 5, pp. 281-290, 1997.

[13] O. Mesalhy, K. Lafdi, A. Elgafy, and K. Bowman, "Numerical study for enhancing the thermal conductivity of phase change material (PCM) storage using high thermal conductivity porous matrix," *Energy Conversion and Management,* vol. 46, no. 6, pp. 847-867, 2005.

[14] M. Gharebaghi and I. Sezai, "Numerical investigation of a phase change material (PCM) module with internal fins," in *ASME/JSME 2007 Thermal Engineering Heat Transfer Summer Conference collocated with the ASME 2007 InterPACK Conference*, 2007: American Society of Mechanical Engineers, pp. 115-120.

[15] S. K. Roy and B. L. Avanic, "Turbulent heat transfer with phase change material suspensions," *International Journal of Heat and Mass Transfer,* vol. 44, no. 12, pp. 2277-2285, 2001.

[16] R. Sabbah, M. M. Farid, and S. Al-Hallaj, "Micro-channel heat sink with slurry of water with micro-encapsulated phase change material: 3D-numerical study," *Applied Thermal Engineering,* vol. 29, no. 2, pp. 445-454, 2009.

[17] K. A. R. Ismail and R. Stuginsky Jr, "A parametric study on possible fixed bed models for pcm and sensible heat storage," *Applied Thermal Engineering,* vol. 19, no. 7, pp. 757-788, 1999.

[18] K. A. R. Ismail and J. R. Henríquez, "Numerical and experimental study of spherical capsules packed bed latent heat storage system," *Applied Thermal Engineering,* vol. 22, no. 15, pp. 1705-1716, 2002.

[19] J. M. Khodadadi, L. W. Fan, and H. Babaei, "Thermal conductivity enhancement of nanostructure-based colloidal suspensions utilized as phase change materials for thermal energy storage: A review," *Renew Sust Energ Rev,* vol. 24, pp. 418-444, 2013.

[20] J. M. Khodadadi and S. F. Hosseinizadeh, "Nanoparticle-enhanced phase change materials (NEPCM) with great potential for improved thermal energy storage," *Int Commun Heat Mass,* vol. 34, no. 5, pp. 534-543, 2007.

[21] C. J. Ho and J. Y. Gao, "Preparation and thermophysical properties of nanoparticle-in-paraffin emulsion as phase change material," *Int Commun Heat Mass,* vol. 36, no. 5, pp. 467-470, 2009.

[22] M. A. Kibria, M. R. Anisur, M. H. Mahfuz, R. Saidur, and I. H. S. C. Metselaar, "A review on thermophysical properties of nanoparticle dispersed phase change materials," *Energ Convers Manage,* vol. 95, pp. 69-89, 2015.

[23] F. Yavari *et al.*, "Enhanced Thermal Conductivity in a Nanostructured Phase Change Composite due to Low Concentration Graphene Additives," *J Phys Chem C,* vol. 115, no. 17, pp. 8753-8758, 2011.

[24] L. Xia, P. Zhang, and R. Z. Wang, "Preparation and thermal characterization of expanded graphite/paraffin composite phase change material," *Carbon,* vol. 48, no. 9, pp. 2538-2548, 2010.

[25] Y.-J. Chen, D.-D. Nguyen, M.-Y. Shen, M.-C. Yip, and N.-H. Tai, "Thermal characterizations of the graphite nanosheets reinforced paraffin phase-change composites," *Composites Part A: Applied Science and Manufacturing,* vol. 44, pp. 40-46, 2013.

[26] X. Li *et al.*, "Advanced Nanocomposite Phase Change Material Based on Calcium Chloride Hexahydrate with Aluminum Oxide Nanoparticles for Thermal Energy Storage," *Energy & Fuels,* vol. 31, no. 6, pp. 6560-6567, 2017.

[27] N. S. Dhaidan, J. M. Khodadadi, T. A. Al-Hattab, and S. M. Al-Mashat, "Experimental and numerical study of constrained melting of n-octadecane with CuO nanoparticle dispersions in a horizontal cylindrical capsule subjected to a constant heat flux," *International Journal of Heat and Mass Transfer,* vol. 67, pp. 523-534, 2013.

[28] I. H. Kim, H. W. Sim, H. H. Hong, D. W. Kim, W. Lee, and D. K. Lee, "Effect of filler size on thermal properties of paraffin/silver nanoparticle composites," *Korean Journal of Chemical Engineering,* vol. 36, no. 6, pp. 1004-1012, 2019.

[29] Y. M. F. El Hasadi and J. M. Khodadadi, "Numerical Simulation of the Effect of the Size of Suspensions on the Solidification Process of Nanoparticle-Enhanced Phase Change Materials," *Journal of Heat Transfer,* vol. 135, no. 5, pp. 052901-052901-11, 2013.

[30] M. T. Barako, S. Lingamneni, J. S. Katz, T. Liu, K. E. Goodson, and J. J. J. o. A. P. Tice, "Optimizing the design of composite phase change materials for high thermal power density," vol. 124, no. 14, p. 145103, 2018.

[31] C. Y. Zhao, W. Lu, and Y. Tian, "Heat transfer enhancement for thermal energy storage using metal foams embedded within phase change materials (PCMs)," *Solar Energy,* vol. 84, no. 8, pp. 1402-1412, 2010.

[32] L. W. Fan and J. M. Khodadadi, "Thermal conductivity enhancement of phase change materials for thermal energy storage: A review," *Renew Sust Energ Rev,* vol. 15, no. 1, pp. 24-46, 2011.

[33] R. Kalbasi, M. Afrand, J. Alsarraf, and M. D. Tran, "Studies on optimum fins number in PCM-based heat sinks," *Energy,* vol. 171, pp. 1088-1099, 2019.

[34] P. P. Levin, A. Shitzer, and G. Hetsroni, "Numerical optimization of a PCM-based heat sink with internal fins," *International Journal of Heat and Mass Transfer,* vol. 61, pp. 638-645, 2013.

[35] S. F. Hosseinizadeh, F. L. Tan, and S. M. Moosania, "Experimental and numerical studies on performance of PCM-based heat sink with different configurations of internal fins," *Applied Thermal Engineering,* vol. 31, no. 17-18, pp. 3827-3838, 2011.

[36] X. Q. Wang, C. Yap, and A. S. Mujumdar, "A parametric study of phase change material (PCM)-based heat sinks," *International Journal of Thermal Sciences,* vol. 47, no. 8, pp. 1055-1068, 2008.

[37] C. X. Guo and W. J. Zhang, "Numerical simulation and parametric study on new type of high temperature latent heat thermal energy storage system," *Energy Conversion and Management,* vol. 49, no. 5, pp. 919-927, 2008.

[38] M. Gharebaghi and I. Sezai, "Enhancement of Heat Transfer in Latent Heat Storage Modules with Internal Fins," *Numerical Heat Transfer, Part A: Applications,* vol. 53, no. 7, pp. 749-765, 2007.

[39] P. Lamberg and K. Sirén, "Analytical model for melting in a semi-infinite PCM storage with an internal fin," *Heat and Mass Transfer,* journal article vol. 39, no. 2, pp. 167-176, 2003.

[40] M. Vynnycky and S. Kimura, "An analytical and numerical study of coupled transient natural convection and solidification in a rectangular enclosure," *International Journal of Heat and Mass Transfer,* vol. 50, no. 25-26, pp. 5204-5214, 2007.

[41] Y. Dutil, D. R. Rousse, N. Ben Salah, S. Lassue, and L. Zalewski, "A review on phase-change materials: Mathematical modeling and simulations," *Renew Sust Energ Rev,* vol. 15, no. 1, pp. 112-130, 2011.

[42] Y. Peles, A. Kosar, C. Mishra, C. J. Kuo, and B. Schneider, "Forced convective heat transfer across a pin fin micro heat sink," *International Journal of Heat and Mass Transfer,* vol. 48, no. 17, pp. 3615-3627, 2005.

[43] A. D. Kraus, J. Welty, and A. Aziz, "Extended surface heat transfer," 2000.

[44] Z. Yang and S. V. Garimella, "Melting of Phase Change Materials With Volume Change in Metal Foams," *Journal of Heat Transfer,* vol. 132, no. 6, 2010.

[45] Z. Zhang and A. Bejan, "Solidification in the presence of high Rayleigh number convection in an enclosure cooled from the side," *International Journal of Heat and Mass Transfer,* vol. 33, no. 4, pp. 661-671, 1990.

[46] C. Beckermann and R. Viskanta, "Natural convection solid/liquid phase change in porous media," *International journal of heat and mass transfer,* vol. 31, no. 1, pp. 35-46, 1988.

[47] F. P. Incropera and D. P. DeWitt, *Fundamentals of heat and mass transfer*, 5th ed. New York: J. Wiley (in English), 2002.

[48] T. C. Choy, *Effective Medium Theory: Principles and Applications*. Oxford University Press, 2016.

[49] D. E. Aspnes, "Local-Field Effects and Effective-Medium Theory - a Microscopic Perspective," *Am J Phys,* Article vol. 50, no. 8, pp. 704-709, 1982.

[50] G. W. Milton, *The theory of composites. Graeme W. Milton* (Cambridge monographs on applied and computational mathematics:). Cambridge ; New York : Cambridge University Press, 2002.

[51] B. E. Hornby, L. M. Schwartz, and J. A. Hudson, "Anisotropic effective-medium modeling of the elastic properties of shales," vol. 59, no. 10, pp. 1570-1583, 1994.

[52] E. J. Garboczi and J. G. Berryman, "Elastic moduli of a material containing composite inclusions: effective medium theory and finite element computations," *Mech Mater,* vol. 33, no. 8, pp. 455-470, 2001.

[53] Z. Hashin and S. A. Shtrikman, "A Variational Approach to the Theory of Effective Magnetic Permeability of Multiphase Materials," *Journal of Applied Physics,* vol. 33, pp. 3125-3131, 1962.

[54] L. Z. Wu, J. Ding, H. B. Jiang, L. F. Chen, and C. K. Ong, "Particle size influence to the microwave properties of iron based magnetic particulate composites," *Journal of Magnetism and Magnetic Materials,* vol. 285, no. 1, pp. 233-239, 2005.

[55] J. C. Maxwell, *A treatise on electricity and magnetism*. Oxford: Clarendon Press, 1873.

[56] B. Sareni, L. Krähenbühl, A. Beroual, and C. Brosseau, "Effective dielectric constant of random composite materials," *Journal of Applied Physics,* vol. 81, no. 5, pp. 2375-2383, 1997.

[57] Y. Rao, J. Qu, C. P. Wong, and T. Marinis, "A Precise Numerical Prediction of Effective Dielectric Constant for Polymer-Ceramic Composite Based on Effective-Medium Theory," Periodical no. 4, p. 680, 2000.

[58] R. Landauer, "Electrical conductivity in inhomogeneous media," *AIP Conference Proceedings,* vol. 40, no. 1, pp. 2-45, 1978.

[59] D. Stroud, "Generalized effective-medium approach to the conductivity of an inhomogeneous material," *Physical Review B,* vol. 12, no. 8, pp. 3368-3373, 1975.

[60] C.-W. Nan, R. Birringer, D. R. Clarke, and H. Gleiter, "Effective thermal conductivity of particulate composites with interfacial thermal resistance," *Journal of Applied Physics,* Article vol. 81, no. 10, p. 6692, 1997.

[61] B. Ghanbarian and H. Daigle, "Thermal conductivity in porous media: Percolation-based effective-medium approximation," *Water Resources Research,* vol. 52, no. 1, pp. 295-314, 2015.

[62] W. Voigt, "Ueber die beziehung zwischen den beiden elasticitatsconstanten isotroper korper," *Annalen der Physik und Chemie,* vol. 38, pp. 573-587, 1889.

[63] M. I. Mishchenko, Z. M. Dlugach, and N. Zakharova, "Direct demonstration of the concept of unrestricted effective-medium approximation," vol. 39, no. 13, pp. 3935-3938, 2014.

[64] C. Liu, R. L. Panetta, and P. Yang, "Inhomogeneity structure and the applicability of effective medium approximations in calculating light scattering by inhomogeneous particles," vol. 146, pp. 331-348, 2014.

[65] M. Kahnert, "Modelling radiometric properties of inhomogeneous mineral dust particles: Applicability and limitations of effective medium theories," *J Quant Spectrosc Ra,* vol. 152, pp. 16-27, 2015.

[66] P. J. Shamberger and T. S. Fisher, "Cooling power and characteristic times of composite heatsinks and insulants," *International Journal of Heat and Mass Transfer,* vol. 117, pp. 1205-1215, 2018.

[67] M. E. Deckard, J. Felts, and P. J. Shamberger, "Cooling Power and Thermal Buffering in Composite Heatsinks," in *2018 17th IEEE Intersociety Conference*

on Thermal and Thermomechanical Phenomena in Electronic Systems (ITherm), 29 May-1 June 2018 2018, pp. 109-116, doi: 10.1109/ITHERM.2018.8419501.

[68] Y. A. Çengel, *Heat transfer : a practical approach*, 2nd ed. New York: McGraw-Hill (in English), 2004.

[69] F. P. Incropera, *Fundamentals of Heat and Mass Transfer*. John Wiley \& Sons, 2006.

[70] D. R. Askeland and P. P. Phulé, *The science and engineering of materials*. Springer, 2003.

[71] Y. A. Çengel and A. J. Ghajar, *Heat and mass transfer : fundamentals & applications*, 5th ed. New York, NY : McGraw Hill Education, 2015.

[72] P. J. Shamberger and T. Reid, "Thermophysical Properties of Lithium Nitrate Trihydrate from (253 to 353) K," *Journal of Chemical & Engineering Data,* vol. 57, no. 5, pp. 1404-1411, 2012.

[73] W. R. Humphries and E. I. Griggs, *A design handbook for phase change thermal control and energy storage devices*. NASA Huntsville, AL, 1977.

[74] S. S. Sundarram and W. Li, "The effect of pore size and porosity on thermal management performance of phase change material infiltrated microcellular metal foams," *Applied Thermal Engineering,* vol. 64, no. 1, pp. 147-154, 2014.

[75] W. A. Goddard, D. Brenner, S. E. Lyshevski, and G. J. Iafrate, *Handbook of Nanoscience, Engineering, and Technology*. CRC Press, 2012.

[76] H. Henry and A. A. Stavros, "Mathematical modelling of solidification and melting: a review," *Modelling and Simulation in Materials Science and Engineering,* vol. 4, no. 4, 1996.

[77] A. H. Committee, "Metals Handbook: Vol. 2, Properties and selection–nonferrous alloys and pure metals," *American Society for Metals, Metals Park, OH,* 1978.

[78] L. M. Jiji and S. Gaye, "Analysis of solidification and melting of PCM with energy generation," *Applied Thermal Engineering,* vol. 26, no. 5, pp. 568-575, 2006.

3. OBJECTIVE ORIENTED PHASE CHANGE MATERIAL COMPOSITE HEAT SINK DESIGN*

3.1. Nomenclature

Variables:

C_{p}	Specific heat at constant pressure, $(J\ kg^{-1}\ K^{-1})$
f	Melt fraction
k	Thermal conductivity, $(W\ m^{-1}\ K^{-1})$
L_{v}	Volumetric latent heat of fusion, $(J\ kg^{-1})$
q''	Heat flux, $(W\ m^{-2})$
r	Radius, (m)
Ra	Rayleigh number, (unitless)
St	Stefan number, (unitless)
t	Time, (s)
T	Temperature, (C)
y	Vertical location, (m)
δ	melt front location, (m)
ρ	Density, $(\mathrm{k}g\ m^{-3})$
ϕ	Volume fraction, (unitless)

	Intrinsic material property

Subscripts:

0	At heated boundary, y=0 or $r=r_0$
cart	Based in Cartesian coordinates
cyl	Based in Cylindrical coordinates
eff	Effective
f	Farthest edge of system
i	Constituent index
l	Of the liquid
m	Melting
metal	Metal
OPT	Optimal
PCM	Phase change material
thresh	Threshold

3.2. Introduction

Thermal energy storage (TES) systems containing phase change materials (PCMs) have been established as highly efficient components for transient cooling [1, 2] but are hindered by a lack of cohesive geometry and composition design guidelines, resulting in underperforming PCM structures developed through arbitrary or empirical methods. While the basic principles of heat transfer during melting and solidification processes are well-understood [3-5], the translation of the fundamental physics into rational module

design principles for this type of nonlinear thermal device are not well-defined. This is contrasted with other common thermal management components such as heat sinks [6, 7], heat pipes [8-10], heat exchangers [6, 11] which have had extensive development of definite design principles. TES systems can be primarily defined by their (1) power density, which describes the rate of heat transfer through the material, and their (2) energy density, which quantifies the amount of the thermal energy that can be absorbed [12-15]. Phase change materials (PCMs) are notable for their high energy density, which can be utilized through the phase transition, but are often lacking in power density [12, 16]. As a result, it is often desirable to combine high thermal conductivity materials with PCMs to form high performance composites, within which the composition or structure may be tuned to modify resultant system properties [13, 15]. Currently, it is not understood how composition and architecture can be used to select for a chosen response profile or thermal buffering capacity under realistic application constraints.

Thermal buffering capacity is a term which can be used as a description of the performance of a TES cooling device, which describes a TES system's ability to dampen transient thermal loads and can be considered in terms of heat absorption rate or temperature, depending on the boundary condition applied. The characteristic response of a standard PCM system is demonstrated schematically in Figure 1a under an applied heat flux thermal load, and in Figure 3.1b for an applied constant temperature thermal load. For constant boundary conditions with an applied constant temperature thermal load, the heat flux into the material system is an appropriate performance metric for thermal

buffering capacity, whereas for an applied heat flux thermal load the temperature of the heated boundary is the appropriate choice.

Composite materials can be defined as systems containing two or more components, where the properties of those materials can be combined to calculate a set of effective properties which accurately model the composite's macroscopic behavior. PCM composite systems take many geometries which most often fall into the categories of: composite dispersions [17-20], macro-/micro- porous media (eg. lattices or foams) [13, 21-25] , and finned heat sinks [26-28]. Additionally, composites systems can also be formed using combinations of characteristic elements from these categories such as the fins and foams [29-31] or fins and dispersions [32-34]. Each category metal/PCM assemblies can be described as an ideal composite in the limit of small constituent spacing, where the length scales of heat transfer between the conductive material and the PCM become sufficiently small such that the temperature profile is effectively even and moves as a uniform front [35-38]. One advantage of treating the system as a homogeneous material is the resulting simplification of the melting problem from a 3D, or 2D, configuration (Figure 3.1c,f) to a 1D configuration (Figure 3.1d,g). This saves significant computational expense in numerical simulations, allowing for rapid testing of varying configurations and presents the opportunity for simplified analytical solutions to non-trivial configurations and scenarios, as detailed in the following sections. This approximation will break down in the presence of high convective driving forces, associated with large Rayleigh ($Ra > 10^6$, for systems with high effective thermal conductivity) [39, 40], and in cases of wide constituent spacing [35, 37]. However, with

this limitation being known, constituent spacing can be selected such that the requirement of small spacing is met and when this is true, even with relatively high driving forces, the role of convection has been shown to play a very small role in comparison to conductive forces [27, 41].

When designing PCM composite systems, the proportion and configuration of components within these structures directly dictates the direction and magnitude of heat transfer within the system [13, 14]. The most common thermal management components are rectangular slabs, corresponding to planar heat sources, or cylindrical annuluses, corresponding to line or circular pipe heat sources, both of which are investigated in this work. These systems are commonly filled with rectangular or radial fins (Figure 3.1c,f), respectively, because they are easily manufactured and can access a large range of volume fractions, which are inaccessible by nanocomposites [20, 42] or more complex structures [13, 43]. These structures also represent the upper limit of anisotropic heat transfer parallel to the direction of heat flow [44].

The bulk of previous work on PCM composite design has focused on experimental or numerical empirical testing of similar geometries and selecting the highest performing system within a sample set of thermal configurations [28, 41, 45-47]. Differing thermal configurations can be defined as permutations of materials, boundary conditions, time scales, coordinate bases, critical performances metrics, thermal loading, and length scales, where each configuration will correspond to a specific optimal design. These empirical studies only provide limited insight into the characteristics of specific high-performance systems by optimizing a particular subset of thermal configurations, but their results do

not provide widely applicable design guidelines for the broader design space. Moreover, the data provided in these studies is sparse in comparison to the overall degrees of freedom in the design space. Therefore, these studies are unlikely to identify underlying correlations and design rules.

Analytical optimization efforts often focus on identifying useful figures of merit which identify the point of component mixing where the thermally capacitive and conductive elements best balance each other to maximize the rate of heat absorption from the heated boundary under simple thermal loads [13, 48, 49]. These approaches are useful as a starting place for PCM based designs, but these solutions assume a quasi-infinite volume, therefore not accounting for geometric constraints or efficient utilization of allotted space. This assumption is sufficient for lower power applications, and very large available volumes, but for most real-world design applications, it becomes necessary to account for finite available volumes. The otherwise lack of sensitivity toward finite volumes in the literature is partially addressed in work by Lu through the development of a methodology to select for allowable heat pulses for a given PCM body with specified geometry and an upper threshold temperature limit [50]. While this methodology is useful for determining operating parameters, it is not trivial to translate to system design and is limited to the selection of constant heat flux pulses in Cartesian coordinates and only explores one optimization goal.

For finite volumes, the time corresponding to the completion of melting marks the point where subsequent times experience a rapid decrease in performance for both thermal load types and corresponds to the limit of the PCM's thermal buffering capacity (Figure

3.1a,b) [35]. Previous work by Bransier found that this point of melting completion could be used as a design tool for dimension selection [51]. The author showed that the width of a PCM slab, perpendicular to a planar thermal load, should be chosen such that the time at which optimization is occurring should correspond to the complete melting of the system. This emphasizes the impact the constraint of a finite volume places on the design problem, which is very common in application.

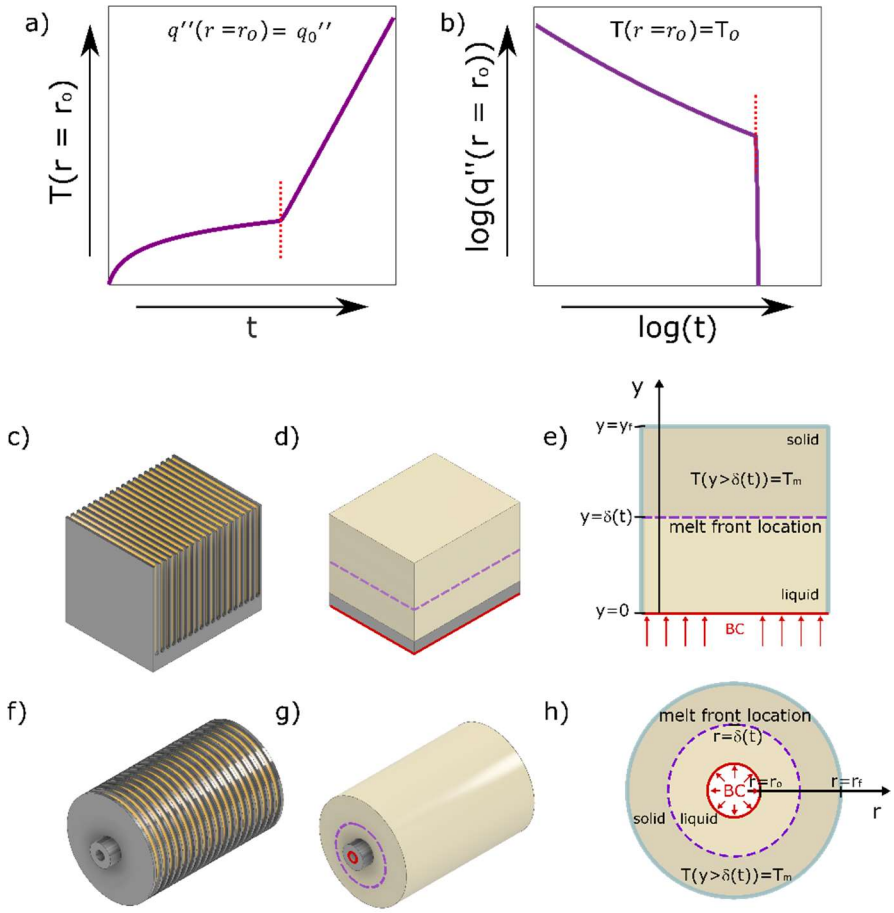

Figure 3.1. Characteristic responses of PCM volumes to an applied a) heat flux (q'') or b) temperature (T) boundary condition with the melting completion time indicated with a red dashed line. Schematic of c,f) finned composite system, approximated as a d,g)homogeneous composite and, e,h) fundamental configuration of the thermal problem with a c,d,e) Cartesian and f,g,h) cylindrical coordinate basis. Solid red lines indicate the boundary where the thermal load is applied, and the dashed purple lines indicate the uniformly distributed melt front location.

In this work we seek to develop a methodology that will allow the tailoring of a specific thermal response through composition selection of the thermally conductive and capacitive elements in a dynamic PCM thermal system. Furthermore, we seek to address the role of a volume constraint on the resulting optimization, as this is a facet of the design problem that is not often addressed by current literature but is critical for most applications. To this end, we establish a comprehensive analytical framework describing this optimal composition for highest thermal buffering capacity with the objective to either 1) maximize the thermal buffering of the heated boundary at a given time, or 2) maximize the time the desired buffering effect occurs. To ensure the widespread applicability of this work, the breadth of our frameworks includes constant temperature and constant heat flux boundary conditions, where we consequently analyze thermal buffering in terms of the complementary boundary variable not being fixed. We also complete our analysis for both Cartesian and cylindrical based systems, allowing this work may be applied to a large variety of applications. For each combination of coordinate systems, performance metrics, and boundary conditions, an optimal volume fraction is analytically identified and compared against analogous numerical and experimental results, both from the existing body of literature and original results. The analytical solutions contained herein are meant to provide a practical guideline for the design of PCM composite systems for thermal management when the application is known. This provides an unprecedented degree of design insight currently lacking in the current literature, especially considering the breadth of thermal configurations and design objectives contained in this work.

3.3. Methods

3.3.1. Problem Statement

In the pursuit of optimal composite design, we consider the composite to act as a singular effective medium through the homogeneous composite approximation (§ 3.3.1.2) and utilize the quasi-steady state (QSS) approximation (§ 3.3.1.3) to describe internal heat transfer and melt dynamics.

The system of study is initially defined at the melting point, entirely in the solid state. The appropriate heating boundary condition of either a constant temperature or heat flux is applied to a single boundary and all other boundaries are adiabatic (Figure 3.1e,h). It is assumed in our analytical and numerical approaches that the solid and liquid phases are distinct and their respective material properties are not dependent on temperature. Furthermore, convective heat and mass transfer are considered negligible in our model, confining heat transfer to conductive pathways, which is practical for the small length scales we are considering. At such length scales, where the composite approximation is most valid, the associated Rayleigh numbers become relatively small, indicating negligible levels of convective heat transfer, as previously discussed [39]. In this limit, the interaction between fluid viscosity and geometric confinement balances the buoyant forces and convective heat transfer is dwarfed by conductive heat transfer [27, 40, 41]. Furthermore, this is also the limit in which the time for heat penetration from the conductive fin into the PCM becomes increasingly small and the thermal front converges to a uniform distribution, consistent with a singular effective medium [35, 36]. As volume fraction limits to 0, where there is no metal in the system, a manufacturability limit will

be reached, and our assumptions will break down. However, if a design problem yields a solution with the sole goal of increasing thermal capacitance, the singularly PCM system is expected to still be the highest performing solution.

The material composites developed and analyzed herein are composed of octadecane and aluminum alloy, AlSi12 (Table 3-1). Octadecane was chosen for its near room temperature melting point, high latent heat, and ease of incorporation. In our analytical and numerical models, the melting temperature is approximated as a single well-defined temperature which is an assumption that varies in accuracy depending on the PCM in question. Octadecane is known to melt over a range of temperatures which can vary depending on the sample purity. For the material used in this study, the full width at half maximum range of the melting peak was measured with DSC to be 3.3 °C for a moderate heating rate of 10 °C/min, which is relatively small when compared to the total heating range under investigation here. This demonstrates that while approximating the melting temperature as discrete adds a level of approximation to our experimental comparisons, it is still a reasonable approximation to make and we have observed that using a low value within the melting range has shown strong comparisons to experimental results. AlSi12 was chosen for our related additive manufacturing capabilities and for its high thermal conductivity. To manufacture optimally performing systems, the aluminum alloy structures are designed through the analytical optimization system described herein, these structures are then manufactured by powder bed laser fusion and infiltrated with octadecane, as further discussed in section ∮ 3.2.3.

Table 3-1 Material properties used in original numerical simulations and analytical modelling.

	Units	AlSi12 alloy	Octadecane
k_l	$W\ m^{-1}\ K^{-1}$	-	0.15
k_s	$W\ m^{-1}\ K^{-1}$	80	0.36
L_v	J m^{-3}	-	1.74 x10^8
ρ	$kg\ m^{-3}$	2700	712
C_p	$J\ kg^{-1}\ K^{-1}$	900	2200
T_m	C	-	28

3.3.2. Finite Difference Analysis

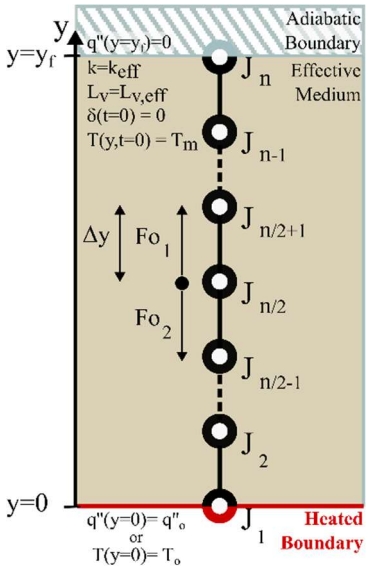

Figure 3.2. Schematic visualization of the computational space under consideration demonstrating the setup of the system and the means for using Fourier numbers (Fo) to simulate heat transfer between evenly spaced (Δy) nodes (J_1 – J_n) from the heated boundary (J_1) to the adiabatic boundary (J_n).

In this work, numerical investigations are utilized to characterize heat transfer and, specifically, the time-dependent temperature rise, and quantity of heat absorbed by a composite PCM volume under externally applied boundary conditions. We use 1D finite difference analysis (FDA) models simulating conductive heat transfer through Cartesian and cylindrical PCM composite geometries, which have been established and tested in previous work (Figure 2.2) [35, 36, 52]. The fundamental assumptions of the FDA models

include 1) the material properties of the solid and liquid phases are not dependent on temperature, 2) melting occurs at a singular temperature, 3) the interface between phases is well-defined, 3) the densities of the solid and liquid phases are equal leading to no mass transfer upon phase change and 4) no convection occurs in the liquid phase. These assumptions also carry through to the analytical models contained in this work.

Within the FDA, nodes are linearly spaced between boundaries and node characteristics are given by the system geometry and effective properties (Figure **3.2**). For all simulations executed in this work, the initial state of the bulk is completely in the solid state and held at the melting temperature. A singular boundary node is set to apply a thermal load of either an applied constant heat flux or temperature and the opposing boundary node is adiabatic. For every timestep, the heat transfer between nodes is calculated using an implicit backward Euler method, from which the temperature and melt fraction of each node is determined. To this end, for a Cartesian coordinate basis the heat equation is given by:

$$\frac{1}{\partial y}\left(k\frac{\partial T}{\partial y}\right)=\rho C_p\frac{\partial T}{\partial t}+L_v\frac{\partial f}{\partial t}, \tag{3.1}$$

where y, ρ, C_p, T, t, k and L_v represent distance, density, specific heat capacity, temperature, time, thermal conductivity, and volumetric latent heat, respectively [6]. The melt fraction of a given node volume is represented by f, where the possible values are; 0 which represents not at all melted, 1 which represents completely melted and intermediate values represent partial melting. Within equation 3.1 the left-hand side of the equation represents the rate of heat transfer through the given volume and the right-hand side of the equation represents the heat absorbed by the volume through sensible

(term 1) and latent (term 2) heating. The same concepts of energy conservation can also be applied to a cylindrical coordinate basis, yielding the heat equation:

$$\frac{1}{r}\frac{1}{\partial r}(kr\frac{\partial T}{\partial r})=\rho C_p\frac{\partial T}{\partial t}+L_v\frac{\partial f}{\partial t}, \tag{3.2}$$

where the r is radial distance [6]. Within the FDA, once the melting temperature of a given node is reached, the node will absorb thermal energy into the latent heat until the volume is completely melted before beginning to sensibly heat leading to a singular well-defined front.

Fidelity of FDA model is directly dependent on timestep length and node spacing. Timesteps are chosen to be most fine at earliest times (10^{-7} s) increasing by 10^{-7} s each step. A total of 2,000 nodes are distributed between the two boundaries of the simulated volume. This combination of values yields the highest relationship between fidelity and computational expense. Timesteps and number of nodes were chosen such that full convergence was observed between tests of increasingly smaller timesteps and larger number of nodes. Accuracy of the resulting finite difference model was tested against ANSYS simulations, analytical models, and experimental data [35, 52]. Simulated heat transfer continues until an end condition is met, determined by the thermal conditions and objective function being designed for, as a given time or performance threshold.

3.3.3. Experimental Verification

To supplement thorough numerical testing, a set of experimental tests are done to further validate the proposed analytical framework. Cylindrical metal finned structures are fabricated from Aluminum alloy, AlSi12 (3D Systems, PS2585-18), using laser powder

bed fusion (ProX 200), which is selected for its ability to generate high resolution features (beam spot diameter: 80 μm) with low porosity (< 1 vol.%). This process is completed using the ProX 200 machine which claims a surface roughness up to an average of 5 μm. The metal structures are longitudinally uniform with radially branching fins designed to maintain a target uniform volume fraction throughout the cylindrical volume, while maintaining a maximum spacing of 1 mm in order to satisfy the composite effective properties assumption [35, 53]. These cylindrical structures are designed with consistent parameters: 38.1 mm axial length, 3.6 mm inner radius, 1.5 mm metal base width and outer radius of 19.1 mm, with a maximum uncertainty of ± 0.2% on all fabrication dimensions. Metal structures are filled with molten PCM and refrigerated to solidify.

Insulating layers of silicone foam are used to enclose the experimental test rig and prevent environmental heat transfer. Cylindrical composites are initial initially held isothermally at 22 °C where all the PCM is in the solid state. A cartridge heater is used to apply a constant heat flux thermal load of 7.3 ± 0.3 W·cm^{-2} to the inner radius of the cylindrical composite (CIR-10151/120V, Omega), where the uncertainty represents the combined uncertainty of the cartridge heater surface area and the measured heater power. Thermistors, with a variability of ± 1 ℃, are attached to inner wall of the composite and are used to record temperature while the system undergoes heating (MP3022, TE Tech) [53].

3.4. Theoretical Development

3.4.1. Analytical Foundation

3.4.1.1. Limiting Regimes

Within this work, for every configuration of interest we define an individual solution for the *rate limited* and *volume limited* regimes. These solutions are presented as optimal volume fractions, ϕ, which refer specifically to the volume fraction of metal within the system. In the *rate limited* regime, the performance of the system is limited by the rate at which heat can be absorbed into the system. The *rate limited* regime case is effectively equivalent to an infinite medium because the melt front has no interaction with the edges of the system. Consequently, in this case it may be recommended that the system size be decreased to cut down on the total mass and volume of the thermal management system and cut down on unused volumes. Figure 3.3(c,d) demonstrates that the *rate limited* optimum is the absolute optimal performance the system may have to a thermal load.

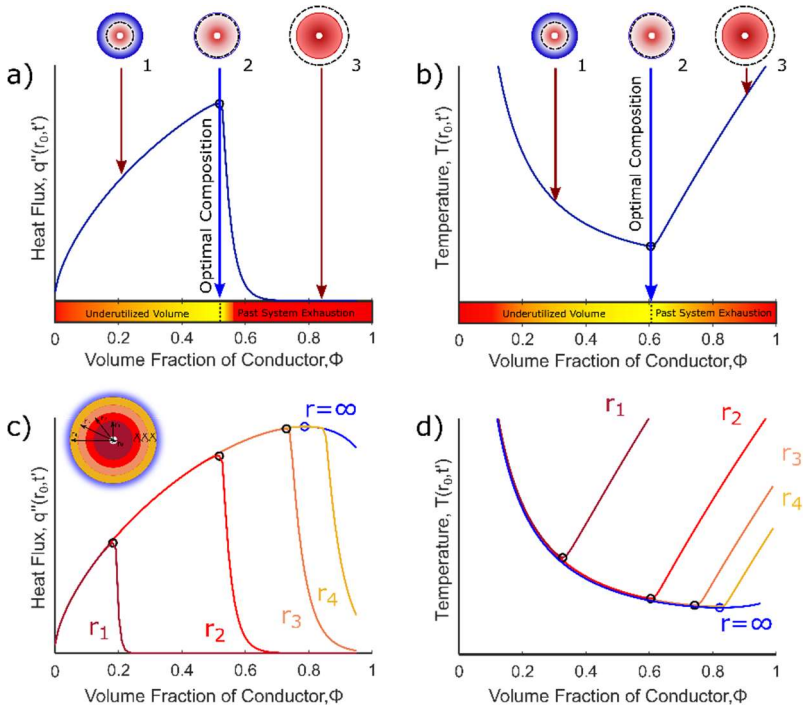

Figure 3.3. Compositional dependence of a) final heat flux, when a constant temperature boundary condition is applied ($T(r = r_0) = T_0$), and b)final temperature, when a constant heat flux boundary condition is applied ($q''(r = r_0) = q''_0$), at time, t', with respect to the volume fraction of metal ϕ. d) For a series of varying radii, the compositional dependence of performance at a given time is explored for e) constant temperature and f) constant heat flux boundary conditions. In the volume limited regime (r_1, r_2, r_3), the optimal composition is affected by the finite boundary and in the rate limited regime (r_4), the optimal composition coincides with an infinite system.

When a volume constraint is taken into account, the composition predicted by using a *rate limited* calculation may no longer be optimal (Figure 3.3c,d), leading to the definition of a second regime designated as the *volume limited* regime. Since the *rate limited* optimum does correspond to the highest possible performance given no volume constraints, it follows that a system designer may wish to relax volume constraints to achieve the highest performance optimum if possible. However, in many cases volume constraints may be inflexible and using the *rate limited* optimum would lead to extremely poor performance, which emphasizes the importance of utilizing the *volume limited* regime when necessary. In this case the performance is now limited by the total thermal capacity of the system and the optimum is determined by the composition leading to full utilization of the volume (Figure 3.3a,b). The primary objective of the *volume limited* regime is to add additional capacitance preventing the onset of detrimental effects of melting completion. This leads to a decrease in volume fraction with increasing times of interest or thermal loading magnitude.

The optimal composition is dependent on problem specific factors such as, material properties, geometric constraints, performance metric and thermal loading. Once the thermal and geometric parameters of the optimization problem are defined, the *rate limited* optimum, and the *volume limited* optimum should both be calculated and the lesser of the two values should be selected as the true optimum (Figure 3.3c,d).

3.4.1.2. Homogeneous Composite Approximation

The homogenous composite approximation treats a multicomponent material system as a single medium, where the effective properties are calculated from: the constituent material properties, the relative volume fraction of constituent components, and their distributions. Previous literature has shown that in the effective medium limit, where decreased the constituent components are well-mixed and separated by small length scales, thermal transport in PCM systems can be calculated using the homogeneous composite approximation [35-37, 54]. As previously discussed, for such composites, this limit corresponds to behavior where the time for heat penetration from the conductive fin into the PCM becomes increasingly small and convective heat transfer is dwarfed by conductive heat transfer [35, 40]. The homogeneous composite approximation represents the upper limit of heat transfer for these systems and defines the objective of optimizing component spacing within a composite, i.e. optimal component spacing corresponds to the limit where performance converges with the homogeneous composite model [13, 35, 36]. The validity of this approximation has been demonstrated in both Cartesian and cylindrical coordinate systems [35, 37], and the critical point of spacing for use of this approximation is analytically described for Cartesian systems [35].

For intrinsic properties, the resulting effective properties are determined solely through constituent volume/proportions, whereas extrinsic transport properties, such as thermal conductivity, also consider the specific internal geometries. For intrinsic properties, the effective property, X_{eff}, can be calculated as:

$$X_{\text{eff}} = \sum_i \phi_i X_i, \tag{3.3}$$

where each constituent volumetric material property, X_i, is scaled by the constituent volume fraction, ϕ_i [55]. For the case of heat transport parallel to the heat source the effective thermal conductivity, k_{eff}, follows the upper bound associated with conductive elements arranged in parallel along the direction of heat transfer and can also be calculated as:

$$k_{\text{eff}} = \sum_i \phi_i k_i, \tag{3.4}$$

where the thermal conductivity of each constituent is denoted by k_i [44, 55]. While this configuration corresponds to anisotropic heat transfer perpendicular to the heat source, other methods of calculating transport properties can be applied to other configurations. For example, microencapsulated PCM structures [56] would represent systems with highly isotropic heat transfer from which transport properties could be determined using the calculation described by Hashin and Shtrikman [57] and alternatively referred to as the Maxwell–Eucken bounds. Additionally, specific heat transfer models have been developed for alternating layers [55, 58], and lattice structures [59, 60], among others.

3.4.1.3. Quasi-Steady State (QSS) approximation

In addition to the homogeneous composite approximation, the melting problem in composite systems can further be simplified using the quasi-steady state (QSS) approximation. This approximation assumes the conduction time through the liquid is short relative to the melt time. These assumed conditions lead to constant temperature gradients within the liquid phase ($\frac{\partial^2 T_l}{\partial y^2} = 0, \frac{\partial^2 T_l}{\partial r^2} = 0$), making the analytical melting problem more tractable [61-63]. This assumption is considered valid for very low Stefan numbers (St << 1), which implies the role of sensible heat is very small compared to the

role of latent heat at the melt front interface [63-66]. Therefore, this approximation is most suitably applied for materials with very high latent heat values under low to moderate magnitude thermal loads, which is highly applicable for a large portion of PCM applications.

3.4.2. Approximate Equations

In subsequent sections we establish the fundamental heat transfer equations which are used to develop an analytical optimization framework. More complete derivations described in the following sections are discussed in works by Hill [61] and Alexiades [62] among others.

3.4.2.1. Cartesian Melting Descriptions – Applied Heat Flux BC

We first consider the 1D cartesian melting problem with an applied constant heat flux boundary condition. We set the boundary at location, $\mathrm{y} = 0$, which corresponds to the planar interface between the heat source and the PCM composite layer. Heat flows in the positive y direction away from this source. Using the QSS approximation, the increase in temperature at the heated boundary, $\Delta T_0 = T(\mathrm{y} = 0) - T_{\mathrm{m}}$, is:

$$\Delta T_0(\mathrm{t}) = \frac{q_0'' \delta(t)}{k_{\mathrm{eff}}}, \quad y = 0, \tag{3.5}$$

where q_0'' corresponds to the applied thermal heat flux at the boundary, k_{eff} corresponds to the effective thermal conductivity and $\delta(t)$ represents the location of the melt front as a function of time, which is given by:

$$\delta(t) = \frac{q_0'' t}{L_{\mathrm{v,eff}}}, \tag{3.6}$$

where $L_{\mathrm{v,eff}}$ represents the effective volumetric latent heat of the composite. Combining equations 3.5 and 3.6 yields the equation for the temperature rise at the heated boundary over the initial temperature of the material, ΔT_0, as a function of time:

$$\Delta T_0(\mathrm{t}) = \frac{{q_0''}^2 t}{k_{\mathrm{eff}} L_{\mathrm{v,eff}}}, \;\; y = 0. \tag{3.7}$$

3.4.2.2. Cartesian Melting Descriptions – Applied Constant Temperature BC

For the complementary problem of an applied constant temperature boundary condition, at $y = 0$ the heat flux into the system through the heated boundary interface (q_0'') is given as:

$$q_0''(t) = k_1 \frac{\Delta T_0}{\delta(t)}, \tag{3.8}$$

where ΔT_0 is the difference between the applied temperature of the heated boundary and the initial temperature set to T_{m} ($\Delta T_0 = T(y = 0) - T_{\mathrm{m}}$). Additionally, the location of the melt front, $\delta(t)$, can be expressed as:

$$\delta(t) = \sqrt{\frac{2k_{\mathrm{eff}}\Delta T_0 t}{L_{\mathrm{v}}}}. \tag{3.9}$$

Substituting equation 3.9 into equation 3.8 allows for the expression of heat flux into the system in terms of boundary condition and material properties as a function of time:

$$q_0''(t) = \sqrt{\frac{L_{\mathrm{v,eff}} k_{\mathrm{eff}} \Delta T_0}{2t}}, \;\; y = 0. \tag{3.10}$$

3.4.2.3. Cylindrical Melting Descriptions – Applied Heat Flux BC

We assume approximately the same configuration to establish analogous equations for cylindrical systems with the boundary at location r_0, which corresponds to the cylindrical interface between the heat source and the PCM composite heat sink. The heat

flows through the composite in the r direction away from this source until reaching the outer boundary at r_{f}. For the boundary condition of an applied heat flux, the QSS solution the temperature rise at the inner radius boundary ($\Delta T_0 = T(r = r_0) - T_{\mathrm{m}}$) can then be described as:

$$\Delta T_0(\mathrm{t}) = -\frac{q_0'' r_0}{k_{\mathrm{eff}}}\left\{\ln\left(\frac{r_0}{\delta(t)}\right)\right\},\ r = r_0, \tag{3.11}$$

where the melt front location $\delta(t)$ in the radial direction is given by:

$$\delta(t) = \sqrt{\frac{2q_0'' r_0 t}{L_{\mathrm{v,eff}}} + {r_0}^2}. \tag{3.12}$$

Combining equations (3.11) and (3.12) yields the equation for temperature rise at the inner radius boundary as a function of time:

$$\Delta T_0(\mathrm{t}) = \frac{q_0'' r_0}{k_{\mathrm{eff}}}\left\{\ln\left(\sqrt{\frac{2q_0'' t}{r_0 L_{\mathrm{v,eff}}} + 1}\right)\right\},\ r = r_0. \tag{3.13}$$

3.4.2.4. Cylindrical Melting Descriptions – Applied Constant Temperature BC

Lastly the necessary equation for Cylindrical based melting systems with an applied constant temperature boundary condition at the inner radius completes our analytical basis. The key equation for heat flux into the system through the inner radius heated boundary is expressed as:

$$q_0''(t) = -k_{\mathrm{eff}}\frac{\Delta T_0}{r_0 \ln(r_0/\delta(t))},\ r = r_0. \tag{3.14}$$

Furthermore, the location of the melt front travelling radially through the system is given as:

$$\delta(t)\big(1 + \ln(r_0/\delta(t))\big) = r_0 - \frac{k_{\mathrm{eff}}\Delta T_0 t}{r_0 L_{\mathrm{v,eff}}}. \tag{3.15}$$

Due to the nature of the of the above location it is not possible to analytically isolate $\delta(t)$ but numerical methods can be used to further advance design capabilities.

3.4.3. Deriving Optimums

To create expressions for an optimal volume fraction of components, it is first necessary to define the objective that we are designing for. For an applied heat flux boundary condition, we will be considering the design objectives of: minimizing T_0 at a given optimization time, t', (∮ 3.3.3.1) and maximizing the duration the heated boundary can stay below a given allowable temperature threshold, T_{thres} (∮ 3.3.3.2). For an applied constant temperature boundary condition, we will be considering the design objectives of: maximizing q''_0 at a given optimization time, t', (∮ 3.3.3.3) and maximizing the duration the system can stay above a minimum allowable heat flux, q''_{thres} , i.e., dissipating at least a given level of power (∮ 3.3.3.4). The collection of all these objectives and geometries allows for this work to be broadly applied to many common applications.

In the following sections we derive analytical expressions for optimal volume fraction. An expression is derived for every combination of coordinate basis (Cartesian/cylindrical), boundary condition (applied $\Delta T_0 / q''_o$), and design objective. Furthermore, independent expressions are developed for the *rate limited* and *volume limite*d regimes. In the *rate limited* regime, the volume fraction is selected based on the rate the material can absorb heat. In the *volume limited* regime, the volume fraction is selected based on the thermal capacitance limits. From the resulting volume fraction

values for each regime, the lower volume fraction of the two will be the optimal design choice, as discussed in ∮ 3.3.1.1.

For the design objective of optimizing a specific performance metric at a given time (∮3. 3.3.1, ∮ 3.3.3.3), in the *rate limited* regime the performance metric, determined by the given boundary condition, is maximized analytically with respect to volume fraction to identify the optimum. The optimum in the *volume limited* regime is identified such that PCM melting completes at the time under investigation to select for a more thermally capacitive competition, delaying the drop in performance associated with melting completion.

For the design objective of maximizing the time for achieving a given minimum level performance (∮ 3.3.3.2, ∮ 3.3.3.4), in the *rate limited* regime the allowable time is maximized analytically with respect to volume fraction to identify the optimum. The *volume limited* optimal volume fraction is obtained by an analytical balancing of rate of thermal absorption and thermal capacitance. This is achieved by selecting a volume fraction such that the time to complete PCM melting corresponds with the time the threshold of performance is met.

3.4.3.1. Boundary Condition: Applied Heat Flux

$$\boldsymbol{q''(y = 0|\, r = r_o) = q''_o}$$

Objective Function: Minimize the Temperature at a Given Time

$$\textbf{min } \big(\boldsymbol{T(y = 0|\, r = r_o, t)}\big) \textbf{ for } \boldsymbol{t = t'}$$

Consider first the case of a constant defined heat flux, $q''(y = 0|\, r = r_o) = q''_o$, that will operate for a specific amount of time, with the goal of minimizing the temperature

of the heated surface at a particular optimization time, $\min\left(T(y=0|\, r=r_o,t)\right)$ for $t=t'$.

To optimize the system when in the *rate limited* regime for Cartesian based systems equation 3.7 is rewritten as a function of volume fraction:

$$\Delta T_0 = \frac{{q_0''}^2 t}{(k_{\mathrm{metal}}(\phi)+k_{\mathrm{PCM}}(1-\phi))L_{\mathrm{v,PCM}}(1-\phi)}, \tag{3.16}$$

where the minimum temperature rise corresponds to:

$$\phi_{\mathrm{OPT,cart}} = \frac{(\mathrm{k_{metal}}-2\mathrm{k_{PCM}})}{2(\,\mathrm{k_{metal}}-\mathrm{k_{PCM}})}. \tag{3.17}$$

Under the rate limited regime for this configuration, the optimal volume fraction is exclusively a function of the thermal conductivity of the constituent materials.

When pursuing the objective of minimizing the temperature at a given time for cylindrical based systems, the temperature rise at the inner radius, equation 3.13, can be minimized similarly.

$$(k_{\mathrm{metal}}(\phi)+k_{\mathrm{PCM}}(1-\phi))\, q_0'' r_0 t' - L_{\mathrm{v,PCM}}(1-\phi)^2\left(\frac{2q_0'' r_0 t'}{L_{\mathrm{v,PCM}}(1-\phi)} + {r_0}^2\right)(\mathrm{k_{metal}}-\mathrm{k_{PCM}})\ln\left(\sqrt{\frac{2q_0'' t'}{L_{\mathrm{v,PCM}} r_0(1-\phi)}+1}\right)=0 \tag{3.18}$$

This equation can then be solved numerically to determine the volume fraction that will minimize the temperature of a given system with no edge effects at a given time. Unlike the Cartesian case, optimal volume fraction for cylindrical systems in the *rate limited* regime is dependent on time and geometry.

For a Cartesian system in the *volume limited* regime, the optimal volume fraction can be solved using equation 3.6 and setting the melt front location to the edge of the system ($\delta(t)=y_f$). Substituting in the effective property calculation for latent heat, and solving for volume fraction yields:

$$\phi_{\mathrm{OPT,cart}} = 1 - \frac{q_0'' t'}{y_{\mathrm{f}} L_{\mathrm{v,PCM}}} \quad . \tag{3.19}$$

In this case the optimal volume fraction is determined by the height of the system, the latent heat, the heat flux load and the time at which the system is being optimized.

The same approach may be taken for *volume limited* cylindrical systems, using equation 3.12 and setting the melt front location equal to the outer radius ($\delta(t) = r_f$). Substituting in the effective property calculation for latent heat, and solving for volume fraction yields:

$$\phi_{\mathrm{OPT,cyl}} = 1 - \frac{2 q_0'' r_0 t'}{L_{\mathrm{v,PCM}} ({r_{\mathrm{f}}}^2 - {r_0}^2)}. \tag{3.20}$$

This expression follows the same form as the cartesian result (eq 3.19) while accounting for radially varying thermal mass.

3.4.3.2. Boundary Condition: Applied Heat Flux

$$\boldsymbol{q''(y = 0 | \, r = r_o) = q_o''}$$

Objective Function: Maximize the Time to Stay Below a Given Threshold Temperature

$$\textbf{max (t) for } \boldsymbol{T(y = 0 | \, r = r_o) < T_{\mathrm{thresh}}}$$

For the next objective we can consider a power source that can be run up until a defined upper temperature limit is reached, T_{thresh}. It is crucial in this scenario to have a design method to prevent the overheating and damage to the power source component or surrounding system. This upper limit can also be defined as a temperature threshold:

$$\Delta T_{\mathrm{thresh}} = T_{\mathrm{thresh}} - T_{m,} \tag{3.21}$$

which cannot be exceeded.

For this objective, when the system is *rate limited*, the solution can be obtained simply through isolating the time component. Rearranging equation 3.7 for time and substituting in effective property calculations yields:

$$t = \frac{(k_{\text{metal}}(\phi)+k_{\text{PCM}}(1-\phi))L_{\text{v,PCM}}(1-\phi)\Delta T_0}{q_0''^2} \tag{3.22}$$

Maximizing this equation when $\Delta T_0 = \Delta T_{thres}$, yields the same volume fraction as the previous Cartesian *rate limited* response described by equation 3.17. This is expected because the optimal volume fraction in the Cartesian coordinate system does not vary with time or melt front location.

The cylindrical *rate limited* case will differ between design objectives due to the time and geometric dependance of the melt front circumference and associated volume. For this regime, equation 3.13 can be taken and rearranged for time. Substituting the effective material properties for the latent heat and thermal conductivity, we attain the expression for heat a specific time as a function of volume fraction:

$$t = \frac{r_0 L_{\text{v,PCM}}(1-\phi)(\text{e}^{2\Delta T_0\left(k_{\text{PCM}}(1-\phi)+k_{\text{metal}}(\phi)\right)/q_0'' r_0} - 1)}{2q_0''}. \tag{3.23}$$

Maximizing equation 3.23 then yields the following optimal composition:

$$\phi_{\text{OPT,cyl}} = \frac{2\Delta T_{thres}\ (k_{metal}-k_{PCM})-q_0'' r_0}{2\Delta T_{thres}\ (k_{metal}-k_{PCM})}. \tag{3.24}$$

For Cartesian based systems, the limiting factor of thermal capacitance can be described using the time to complete melting, equation 3.6, with an effective latent heat calculation to get:

$$t = \frac{\text{L}_{\text{v,PCM}}(1-\phi)(y_{\text{f}})}{q_0''}. \tag{3.25}$$

This can then be substituted into equation 3.16, setting $\Delta T_0 = \Delta T_{\text{thresh}}$, and simplified to get the optimal volume fraction of the *volume limited* regime as:

$$\phi_{\text{OPT,cart}} = \frac{y_f q_0'' - \text{k}_{\text{PCM}}(\Delta T_{\text{thresh}})}{\Delta T_{\text{thresh}}(\text{k}_{\text{metal}} - \text{k}_{\text{PCM}})}. \tag{3.26}$$

The same approach from the Cartesian development can then be applied to Cylindrical based systems for the *volume limited* regime. Taking the equation for melt front location (eq. 3.12) and rearranging to get the time to complete melting yields:

$$t = \frac{(r_{\text{f}}^2 - r_0^2) L_{\text{v,PCM}}(1-\phi)}{2 r_0 q_0''}. \tag{3.27}$$

Substituting the time of melting completion from equation 3.27 into equation 3.13, setting $\Delta T_0 = \Delta T_{\text{thresh}}$, and solving for volume fraction then results in the equation:

$$\phi_{\text{OPT,cyl}} = \frac{q_0'' r_0 \, ln\left(r_0/r_{\text{f}}\right) + \Delta T_{\text{thresh}} k_{PCM}}{\Delta T_{\text{thresh}}(k_{PCM} - k_{\text{metal}})}. \tag{3.28}$$

3.4.3.3. Boundary Condition: Applied Constant Temperature

$$\mathbf{T}(\boldsymbol{y = 0 \,|\, r = r_o}) = \boldsymbol{T_o}$$

Objective Function: Maximize the Heat Flux at a Given Time

$$\textbf{max } \left(\boldsymbol{q''(y = 0 \,|\, r = r_o, t)}\right) \textbf{ for } \boldsymbol{t = t'}$$

In addition to considering system with an applied heat flux, it is also useful to develop optimization of systems with an applied constant temperature boundary condition. An applied constant temperature boundary is most closely analogous to the cooling of a heat pipe with a roughly isothermal liquid circulating through the system. If it is known that there will be a thermal load for a given amount of time, it may be desirable to maximize the heat absorption up to a given time based on the thermal loads of the system.

Within this configuration, first we develop an optimization for Cartesian geometries in the *rate limited* regime. Using an effective properties substitution in equation 3.10 the heat flux into a Cartesian system is given by:

$$q_0'' = \sqrt{\frac{(\mathrm{k_{metal}}(\phi) + \mathrm{k_{PCM}}(1-\phi))(\mathrm{L_{v,PCM}}(1-\phi))\Delta T_0}{2t}}. \tag{3.29}$$

The maximization of this equation then yields the optimum described by equation 3.17, and is consistent across all *rate limited* solutions in Cartesian based systems.

The cylindrical system under an applied constant temperature boundary condition presents a much more challenging problem due to the transcendental nature of the solution for the melt front location. To optimize for this case a numerical method is used to test across all volume fractions for the composition that will yield the largest flux at the time of optimization using equations 3.14 and 3.15.

In the applied constant temperature boundary condition case, the *volume limited* optimal volume fraction is calculated using the equation for melt front location (eq. 3.9) and substituting in the effective latent heat and thermal conductivity:

$$y_\mathrm{f} = \sqrt{\frac{2(\mathrm{k_{metal}}(\phi) + \mathrm{k_{PCM}}(1-\phi))\Delta T_0 t}{\mathrm{L_{v,PCM}}(1-\phi)}}. \tag{3.30}$$

This equation can then be solved to identify the optimal volume fraction as:

$$\phi_{\mathrm{OPT,cart}} = \frac{\mathrm{L_{v,PCM}} y_\mathrm{f}^2 - 2\,\mathrm{k_{PCM}} t' \Delta T_0}{\mathrm{L_{v,PCM}} y_\mathrm{f}^2 + 2\,t' \Delta T_0 (\mathrm{k_{metal}} - \mathrm{k_{PCM}})}. \tag{3.31}$$

Applying the same approach to the cylindrical case, equation 3.15 for the location of the melt front can be used with effective material properties substituted as follows:

$$\delta(t)\big(1 + \ln(r_0/\delta(t))\big) = r_0 - \frac{(\mathrm{k_{metal}}(\phi) + \mathrm{k_{PCM}}(1-\phi))\Delta T_0 t}{r_0\,\mathrm{L_{v,PCM}}(1-\phi)}. \tag{3.32}$$

This expression can then be solved, replacing $\delta(t)$ with the outer radius of the system r_{f} and solving for the volume fraction as:

$$\phi_{\mathrm{OPT,cyl}} = \frac{r_{\mathrm{f}}\, r_0\, \mathrm{L_{v,PCM}}(1+\ln(r_0/r_{\mathrm{f}})) - \mathrm{L_{v,PCM}} r_0{}^2 + \mathrm{k_{PCM}} t' \Delta T_0}{r_{\mathrm{f}}\, r_0\, \mathrm{L_{v,PCM}}(1+\ln(r_0/r_{\mathrm{f}})) - \mathrm{L_{v,PCM}} r_0{}^2 + t' \Delta T_0 (\mathrm{k_{PCM}} - \mathrm{k_{metal}})}. \tag{3.33}$$

3.4.3.4. Boundary Condition: Applied Constant Temperature

$$\mathbf{T}(\boldsymbol{y = 0 \mid r = r_o}) = \boldsymbol{T_o}$$

Objective Function: Maximize the Time to Stay Above a Threshold Heat Flux

$$\textbf{max (t) for } \boldsymbol{q''(y = 0 \mid r = r_o) < q''_{thresh}}$$

The last objective we consider is to maximize the time (t) to stay above a threshold heat flux, q''_{thresh}, when an applied constant temperature boundary condition is applied. This can also be explained as ensuring the absorption of at least a certain level of heat for the longest amount of time. If an application seeks to operate components for as long as possible and the cooling components remain relatively isothermal the development below will be the most useful.

For the Cartesian case this can be calculated using equation 3.10 and rearranging to get:

$$t = \frac{(\mathrm{k_{metal}}(\phi) + \mathrm{k_{PCM}}(1-\phi))(\mathrm{L_{v,PCM}}(1-\phi))\Delta T_0}{2\, q_0''^2} \tag{3.34}$$

Maximizing this equation with respect to volume fraction, when $q_0'' = q''_{\mathrm{thresh}}$, yields equation 3.17 consistent once again across all *rate limited* Cartesian optimizations.

As previously discussed, analytical solutions for cylindrical systems under constant temperature loads are not apparent. Therefore, for the objective of maximizing the time of obtaining at least a given level of heat flux in the *rate limited* regime, we take

a numerical approach. Testing across a sample space of volume fractions with corresponding effective properties, equation 3.14 can be used to determine the melt front location where the system would reach the heat flux threshold. This radius can then be substituted into equation 3.15 to calculate the corresponding time where the heated boundary would intersect with the chosen heat flux. From this the maximum time value can be taken and the corresponding volume fraction identified.

For the Cartesian case in the *volume limited* regime for the objective of staying above a minimum threshold heat flux into the system for the longest time, equation 3.9 can be used, rearranging for time:

$$t = \frac{{y_f}^2 \, \mathrm{L_{v,PCM}}(1-\phi)}{2(\,\mathrm{k_{metal}}(\phi) + \mathrm{k_{PCM}}(1-\phi))\Delta T_0} \tag{3.35}$$

Equation 3.10 can also be rearranged for time as follows:

$$t = \frac{(\,\mathrm{k_{metal}}(\phi) + \mathrm{k_{PCM}}(1-\phi))(\mathrm{L_{v,PCM}}(1-\phi))\Delta T_0}{{q_0''}^2} \tag{3.36}$$

Equation 3.35 and 3.36 can then be set equal and simplified to get the optimal volume fraction of:

$$\phi_{\mathrm{OPT,cart}} = \frac{q''_{\mathrm{thresh}} y_{\mathrm{f}} - \mathrm{k_{PCM}}\Delta T_0}{\Delta T_0(\mathrm{k_{metal}} - \mathrm{k_{PCM}})} \tag{3.37}$$

which is a direct translation of equation 3.26, yielding the same form while utilizing different variables as boundary conditions.

To identify the equivalent result for the cylindrical system equation 3.14 can be used, substituting the thermal conductivity for an expression of effective properties:

$$q_0'' = -(\,\mathrm{k_{metal}}(\phi) + \mathrm{k_{PCM}}(1-\phi))\frac{\Delta T_0}{r_0 \ln(r_0/\delta(t))} \tag{3.38}$$

The q_0'' value can then be assigned the minimum heat flux value given, q_{thres}'' , and the melt front location can be assigned to the outer radius ($\delta(t) = r_{\mathrm{f}}$). The volume fraction can then be solved for as:

$$\phi_{\mathrm{OPT,cyl}} = \frac{q''_{\mathrm{thresh}} r_0 \ln(r_0/r_{\mathrm{f}}) + \Delta T_0 \mathrm{k_{PCM}}}{\Delta T_0 (\mathrm{k_{PCM}} - \mathrm{k_{metal}})} \tag{3.39}$$

3.4.4. Analytical Summary

Table 3-2 summarizes the analytical framework derived in section 3.3.3, providing a guideline for optimal volume fraction selection across the different design objectives, limiting regimes, boundary conditions and coordinate systems.

Table 3-2 Compilation of equations describing optimal volume fraction with various thermal configurations and objectives for PCM composites.

Cartesian

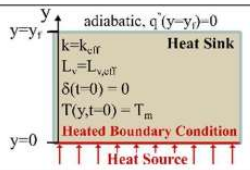

Heated Boundary Condition: Applied Heat Flux, $q''(y=0)=q_o''$
Objective Functions:
Minimize the temperature at a given time
Maximize the time to stay below a given threshold temperature

Objective Function	Rate Limited	Volume Limited
min $(T(y=0,t))$ for $t=t'$	$\phi_{cart}=\frac{(k_{metal}-2k_{PCM})}{2(k_{metal}-k_{PCM})}$ equation 3.17, § 3.3.3.1	$\phi_{cart}=1-\frac{q_0''t'}{y_f L_{v,PCM}}$ equation 3.19, § 3.3.3.1
max (t) for $T(y=0)<T_{thresh}$	$\phi_{cart}=\frac{(k_{metal}-2k_{PCM})}{2(k_{metal}-k_{PCM})}$ equation 3.17, § 3.3.3.2	$\phi_{cart}=\frac{y_f q_0'' - \Delta T_{thresh} k_{PCM}}{\Delta T_{thresh}(k_{metal}-k_{PCM})}$ equation 3.26, § 3.3.3.2

Heated Boundary Condition: Applied Temperature, $T(y=0)=T_o$
Objective Functions:
Maximize the heat flux at a given time
Maximize the time to stay above a threshold heat flux

Objective Function	Rate Limited	Volume Limited
max $(q''(y=0,t))$ for $t=t'$	$\phi_{cart}=\frac{(k_{metal}-2k_{PCM})}{2(k_{metal}-k_{PCM})}$ equation 3.17, § 3.3.3.3	$\phi_{cart}=\frac{L_{v,PCM}y_f^2 - 2k_{PCM}t'\Delta T_0}{L_{v,PCM}y_f^2 + 2t'\Delta T_0(k_{metal}-k_{PCM})}$ equation 3.31, § 3.3.3.3
max (t) for $q''(y=0)<q''_{thresh}$	$\phi_{cart}=\frac{(k_{metal}-2k_{PCM})}{2(k_{metal}-k_{PCM})}$ equation 3.17, § 3.3.3.4	$\phi_{cart}=\frac{q''_{thresh}y_f - k_{PCM}\Delta T_0}{\Delta T_0(k_{metal}-k_{PCM})}$ equation 3.37, § 3.3.3.4

Cylindrical

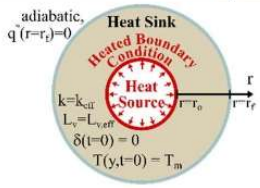

Heated Boundary Condition: Applied Heat Flux, $q''(r=r_o)=q_o''$
Objective Functions:
Minimize the temperature at a given time
Maximize the time to stay below a given threshold temperature

Objective Function	Rate Limited	Volume Limited
min $(T(r=r_o,t))$ for $t=t'$	Solve Equation 3.18 numerically equation 3.18, § 3.3.3.1	$\phi_{cyl}=1-\frac{2q_0''r_0t'}{L_v(r_f^2-r_0^2)}$ equation 3.20, § 3.3.3.1
max (t) for $T(r=r_o)<T_{thresh}$	$\phi_{cyl}=\frac{2\Delta T_{thresh}(k_{metal}-k_{PCM})-q_0''r_0}{2\Delta T_{thresh}(k_{metal}-k_{PCM})}$ equation 3.24, § 3.3.3.2	$\phi_{cyl}=\frac{q_0''r_0\ln(r_0/r_f)+\Delta T_{thresh}k_{PCM}}{\Delta T_{thresh}(k_{PCM}-k_{metal})}$ equation 3.28, § 3.3.3.2

Heated Boundary Condition: Applied Temperature, $T(r=r_o)=T_o$
Objective Functions:
Maximize the heat flux at a given time
Maximize the time to stay above a threshold heat flux

Objective Function	Rate Limited	Volume Limited
max $(q''(r=r_o,t))$ for $t=t'$	Maximize equation 3.14 for q'' using equation 3.15 to calculate $\delta(t')$ equations 3.14/3.15, § 3.3.3.3	$\phi_{cyl}=\frac{r_f r_0 L_{v,PCM}(1+\ln(r_0/r_f)) - L_{v,PCM}r_0^2 + k_{PCM}t'\Delta T_0}{r_f r_0 L_{v,PCM}(1+\ln(r_0/r_f)) - L_{v,PCM}r_0^2 + t'\Delta T_0(k_{PCM}-k_{metal})}$ equation 3.33, § 3.3.3.3
max (t) for $q''(r=r_o)<q''_{thresh}$	Maximize equation 3.15 for t using equation 3.14 to calculate $\delta(t)$ when $q''(r=r_o)=q''_{thresh}$ equations 3.14/3.15, § 3.3.3.4	$\phi_{cyl}=\frac{q''_{thresh}r_0\ln(r_0/r_f)+\Delta T_0 k_{PCM}}{\Delta T_0(k_{PCM}-k_{metal})}$ equation 3.39, § 3.3.3.4

3.5. Results and Discussion

Throughout the following sections we assess the functionality and applicability of the above developed analytical models through comparison to numerical and experimental results from original work and examples from the existing literature. Temperature and heat flux values are chosen to generally reflect the thermal loads of low to moderate power thermal management systems.

3.5.1. Original Experimental Results

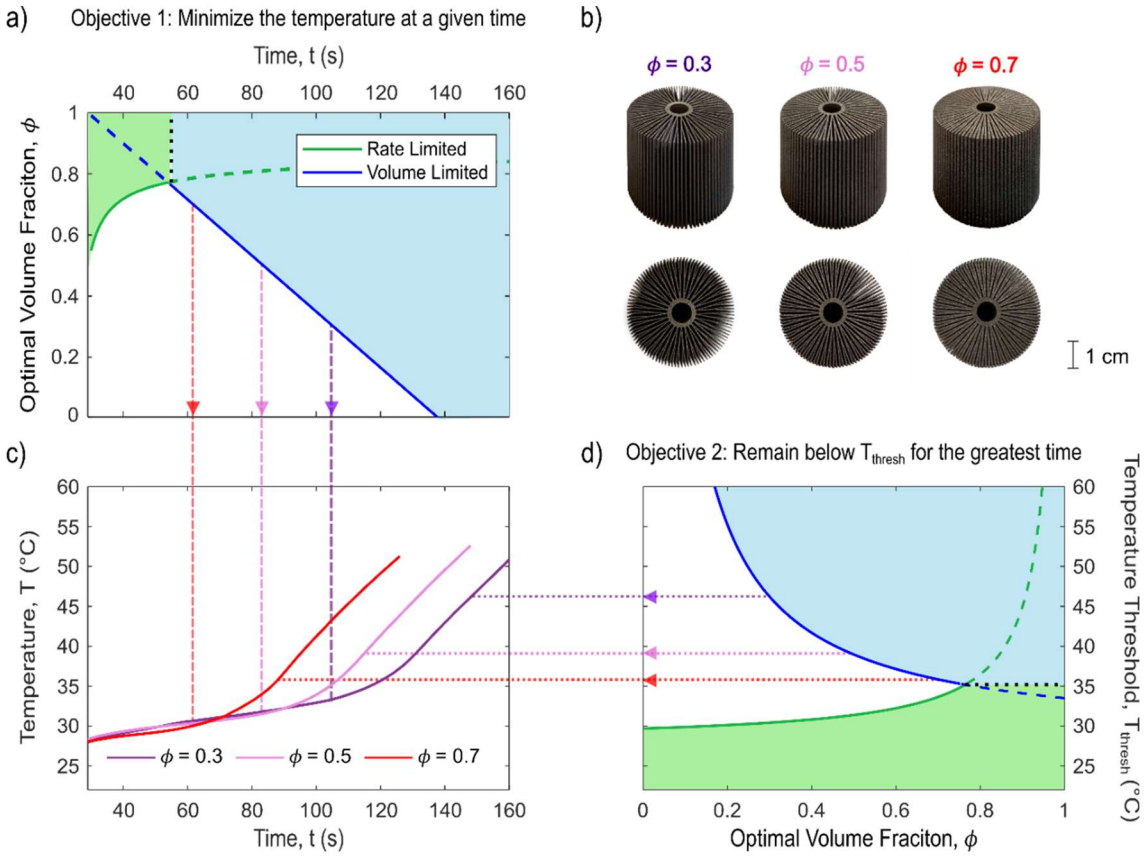

Figure 3.4. Analytical results a) for the goal of minimizing the temperature at a given time the optimal volume fraction can be described over time. b) Photographs of the 3D printed physical aluminum systems for each of the volume fractions used in experimental results (0.3, 0.5, 0.7). Analytical results can be compared against c) experimental results for a Cylindrical finned heat sink under a heat flux load of 7.3 Wcm^{-2}, $q''(r = r_o) =$ 7.3 Wcm^{-2}, with volume fractions 0.3, 0.5, and 0.7. Analytical results d) for the goal of maximizing the time to stay below a given temperature the optimal volume fraction can be described for varying temperature increases. Dashed arrows indicate the relationship between the analytical results and behavior of the 3 tested structures.

To create a practical comparison for the analytical model developed herein we experimentally compare systems with different volume fractions and observe how the optimal system changes over time. Using 3D printed aluminum three systems were printed with metal volume fractions of 0.3, 0.5, and 0.7 (Figure 3.4b). Temperature is measured at the base of the structures. While higher volume fractions can achieve lower temperatures at shorter times, their lower composition of PCM causes them to melt faster, leaving the lower volume fractions to become the highest performing systems at longer times (Figure 3.4c). This is consistent with the models and analysis contained in previous sections.

The analytical framework developed above is applied to an experimental dataset to assess the practical applicability of the models. In Figure 3.4 we demonstrate the changes in predicted optimal volume fraction using the objective of minimizing temperature at a given time (Figure 3.4a) or maximizing the time below a given temperature (Figure 3.4d) for a set internal boundary condition of 7.3 $W cm^{-2}$. These can be directly compared to the experimental data showing the temperature of the different volume fraction systems over time (Figure 3.4c). In all cases, the analytical model was able to predict the highest performing system out of the three tested.

For the optimization metric of minimizing the temperature at a given time, we select times of 76.4 s, 54.6 s, and 32.7 s after the onset of melting, which correspond with the volume fractions of 0.3, 0.5, and 0.7 (Figure 3.4a). Because it is not possible to initialize the experiment isothermally exactly at the melting temperature, equation 3.20 is compensated with time (t) renormalized by the melting time ($t - t_m$) (Figure 3.4a). This

adds a new level of approximation to our analysis because the system does not isothermally heat from its starting temperature of 22 ℃ but is shown to minimally affect the accuracy of our models for this case. For each optimization time we accurately select the optimal performing composite composition out of the sample set which corresponds closely to the onset of edge effects, as expected, and predicted times corresponding with the completion of melting are correct to within approximately 10%.

For the optimization metric of maximizing the time below a given temperature, we select temperature thresholds of 46.3 ℃, 39.0 ℃, and 35.9 ℃, which correspond with the volume fractions of 0.3, 0.5, and 0.7 (Figure 3.4d). These optimums are predicted by equation 3.28 and reveal that the experimentally measured temperature values seen here are lower than analytically predicted values, which is also confirmed by equivalent numerical testing using our finite element model. This discrepancy is primarily attributed to 1) temperature heterogeneities near the free surface where the temperature is measured due to heat loss to the surrounding environment, 2) the contribution of the thermal mass of the cartridge heater itself, as well as interfacial resistances between the heater and the base of the composite PCM, 3) shortcomings of the QSS-based solutions, which neglect the role of sensible heat, and 4) potentially minor convective effects which increase at lower volume fractions, longer times and higher temperatures. Regardless, the predicted optimums still provide approximate guide for the true optimums here and the validity of optimization through this performance metric is further explored numerically and through experimental work in the existing literature in the sections below.

3.5.2. Numerical Comparison

In addition to experimental results, the analytical trends described in this work can be validated through direct comparison to numerical simulations. Numerical methods are useful in their ability to control every aspect of the system, as well as gather large quantities of data when compared with experimental methods. We use a previously established 1D finite difference model to test systems which employs the same homogenous composite approximation as our numerical development above [35, 36, 52].

3.5.2.1. Applied Heat Flux

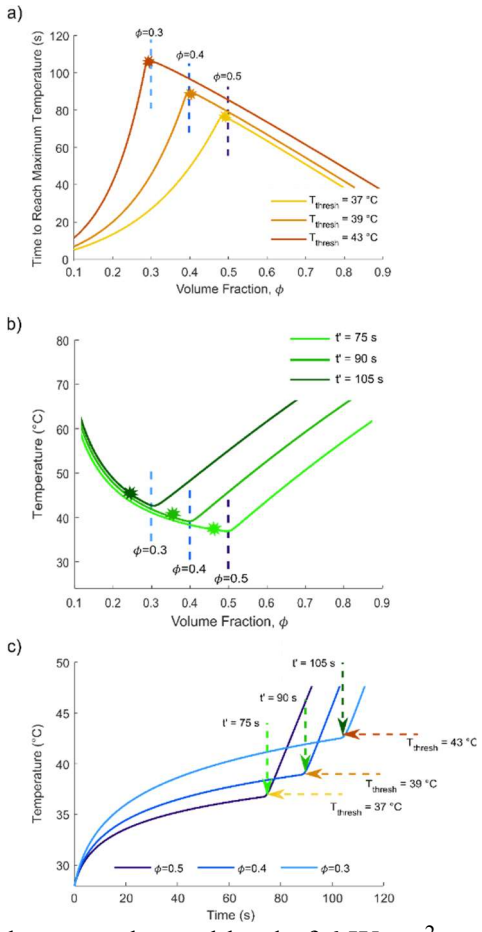

Figure 3.5 For a cylindrical system thermal load of 6 Wcm^{-2} we present numerical results detailing the relationship between material compositions to a) the time at which PCM composites will reach the threshold temperature and b) the final boundary temperature at a given time. a,b) Volume fractions 0.3, 0.4, and 0.5 are denoted and asterisks indicate the optimal volume fractions predicted by analytical models above for each given end condition. c) Full simulation numerical results for a system under a thermal load of $q''(r = r_o) = 6$ Wcm^{-2}, with 75 s, 90 s, 105 s denoting the times at which we are optimizing to minimize temperature and 37 °C, 39 °C and 43 °C denoting defined threshold temperatures which we wish to stay below for the longest amount of time.

Figure 3.5 compares numerical and analytical optimization approaches for the given problem of optimizing a cylindrical system under a constant heat flux boundary condition. In our numerical methodology, the system is defined with a given composition and thermal load and continuously simulated until a given end condition is reached, defined as either reaching a given threshold temperature (Figure 3.5a) or reaching a given time (Figure 3.5b), depending on the design objective. The simulation basis is iterated to test a wide range of volume fractions in a short amount of time, for a cylindrical system thermal load of 6 Wcm^{-2}. There exists a clear pivot point in the volume fraction space which corresponds to the maximum value of the selected performance metric (Figure 3.5a,b). Through a comparison to full simulation runs (Figure 3.5c) it is evident that these optimums correspond to the point at which the PCM melting completes.

The predictions of the analytical model can be directly compared to the results given by the numerical model (Figure 3.5a,b). For the cases shown here the analytical solution predicts results in the *volume limited* regime which is expected since the full simulation results show the optimum is related to the completion of melting. Asterisks are used in Figure 3.5a-b to denote predicted analytical optimums calculated by equation 3.28 (Figure 3.5a) and equation 3.20 (Figure 3.5b). We observe that for either design objective the model is in strong alignment with the exhaustive results, demonstrating the accuracy of the model while highlighting the benefit of significantly reduced computational expense. It was also discovered that the models predicting optimal volume fraction for the goal of keeping the boundary temperature below a given threshold were more accurate than models created for the goal of minimizing temperature at a given time. This effect

originates from the difference in time between the melt front reaching the outer boundary of the systems and completely melting the system, causing the true optimum to occur at the latter instance.

3.5.2.2. Applied Constant Temperature

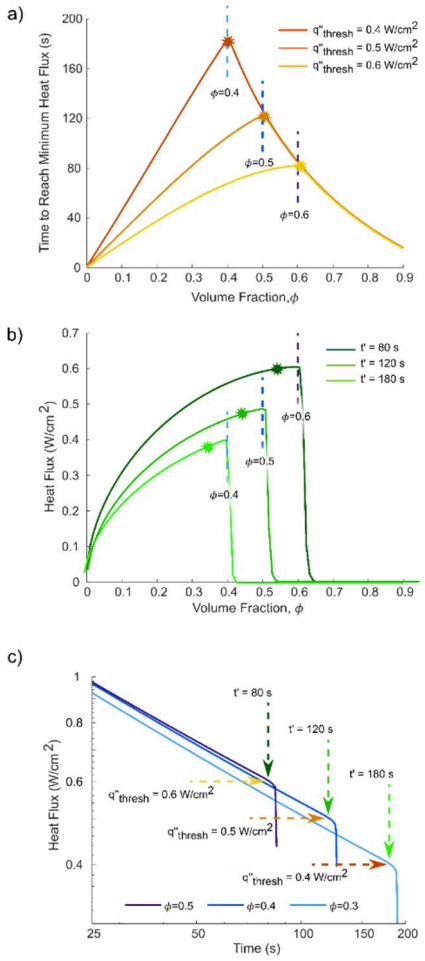

Figure 3.6. For a cylindrical system thermal load of $29\ ^{\circ}C$ we present numerical results detailing the relationship between material compositions to a) the time at which composites will reach the set threshold heat flux and b) the final boundary heat flux at a given time. a,b) Volume fractions 0.4, 0.5, and 0.6 are denoted and asterisks indicate the optimal volume fractions predicted by analytical models above for each given end condition. c) Full simulation numerical results for a system under a thermal load of $T(r = r_o) = 29\ ^{\circ}C$, with 80 s, 120 s, 180 s denoting the times at which we are optimizing to maximize heat flux and $0.4\ \mathrm{Wcm^{-2}}$, $0.5\ \mathrm{Wcm^{-2}}$ and $0.6\ \mathrm{Wcm^{-2}}$ denoting defined threshold heat fluxes which we wish to stay above for the longest amount of time.

Figure 3.7 compares numerical and analytical optimization methodologies for the analogous problem of optimizing a cylindrical system under a constant temperature thermal load. For this boundary condition, the numerical simulation is run until the end condition of either falling below a threshold level of heat removal performance (Figure 3.6a) or reaching a given time (Figure 3.6b), depending on the design objective. For a cylindrical system thermal load of 29 °C , it can again be observed that there exists a clear pivot point in the volume fraction space which corresponds to the optimum of the performance being selected for (Figure 3.6a,b). In the same fashion as the constant power boundary condition a comparison to full simulation runs (Figure 3.6c) shows that these optimums correspond to the point at which the PCM melting completes, indicating that the application parameters fall within the *volume limited* regime. Asterisks are used in Figure 5a-b to denote predicted analytical optimums calculated by equation 3.39 (Figure 3.6a) and equation 3.33 (Figure 3.6b), where we observe strong agreement between predicted and numerically determined optimums.

Comparison between analytical and numerical results contained in Figure 3.6 represents a very low magnitude boundary condition (29 °C) compared to the melting temperature (28 °C). This decision was made to demonstrate a more accurate portion of the parameter space. As was the case for the constant heat flux boundary condition, higher magnitude boundary conditions and longer times will decrease the accuracy of the model. Similarly, to the constant power case, the goal of maximizing the heat absorbed at a given

time does not perfectly predict the numerical optimum (Figure 3.6b). In contrast, the goal of maximizing the time the system is achieving at least a given minimum threshold heat flux leads to higher accuracy predictions, which is attributed to the time needed to melt the entirety of the outer radius simulated node.

3.5.2.3. Applicability Range

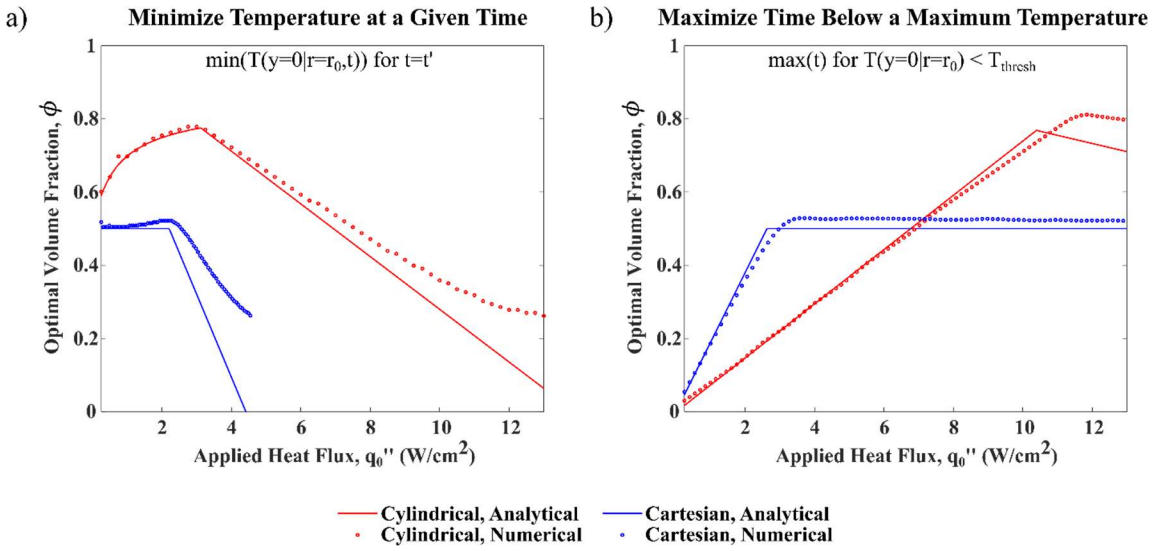

Figure 3.7 Optimal volume fraction given by numerical results (dotted points) and analytical predictions (solid lines) in cylindrical (red) and Cartesian (blue) based systems a) for the objective of minimizing temperature at 60 s ($t' = 60\ s$) after thermal load onset and b) maximizing the time below a maximum threshold temperature of 38 ℃ ($T_{thres} = 38$ ℃) for a system under varying thermal loads in.

As discussed in previous sections the accuracy of the models developed in this paper is highly dependent on the desired parameters of the application and originates largely a result of selecting the QSS solution for melting as an analytical basis. Therefore, it is necessary to explore the limits of the applicability of these models to understand how they may be applied to real systems. When comparing numerically observed and analytically predicted results we calculate high R^2 values indicating high predictive

performance. Dividing our analysis between regimes using analytical predictions leads to coefficients of determination with consistent values of $R^2 \approx 1$ within the *rate limited* regime and an average of $R^2 \approx 0.93$ within the *volume limited* regime.

For the objective of minimizing temperature at a given time, the *rate limited* regime yields very high-fidelity predictions while the *volume limited* regime is the least accurate of the prediction regions studied here. Calculations of coefficients of determination show that the cylindrical results within this regime are the least accurate with $R^2 \approx 0.76$, compared to the Cartesian results with $R^2 \approx 0.97$, although the narrower range of inquiry within the Cartesian testing can contribute to this observation. Within the *volume limited* regime, our predictions align very strongly with numerical predictions at lower magnitudes of thermal loading but deviate with increased boundary condition magnitude (Figure 3.7a). This is to be expected as the QSS solution is most valid when the role of sensible heat is small compared to the role of latent heat and will become less valid at longer times and higher thermal load. The deviation effects of the boundary magnitude are shown for a singular optimization time and will deviate more at longer times and have higher agreement at shorter times. It can be inferred from these results that, at high heat fluxes, if the model predicts a very low volume fraction in the *volume limited* regime, an offset towards higher volume fractions should be considered.

For the objective of maximizing the time below a given temperature, the accuracy of the model is shown to be much less dependent on operating parameters (Figure 3.7b). In the *volume limited* regime both coordinate basis system classifications show extremely high agreement. In the *rate limited* regime, for both the Cartesian and cylindrical based

systems, the analytical models slightly underpredicts the numerically predicted optimum but this is held relatively constant with varying optimization parameters. For this objective, coefficients of determination are found to have consistent values of $R^2 \approx 1$.

3.5.3. Application to Previously Reported Experiments

3.5.3.1. Critical Evaluation of Numerical Simulations

In addition to testing our analytical optimization against the original experimental and numerical data presented above, we are also able to draw on the existing literature to verify that our predictions are widely applicable. A 2015 study by Pakrouh et al. represents a quintessential study within the current PCM composite design space wherein different design configurations are used to empirically assess trends in performance [41]. This study employed a 3D computational fluid dynamics (CFD) model to simulate heat transfer through PCM based pin fin composite heatsinks under a thermal load of 1.02 W/cm^2, where the distribution of fins is uniform and rectilinear.

One of the most significant advantages to comparing our optimization methodology to existing datasets is to further justify the assumptions and approximations used throughout the development of this work. The CFD employed in the Pakrouh study diverges in the fundamental assumptions from the analytical and numerical models in this work in several ways, such as, 1) We approximate a macroscopic finned system as a 1D uniform composite which contrasts with the full 3D simulations executed in the Pakrouh study, 2) which also includes a metal base that we exclude. 3) The 3D simulation is initialized at a uniform temperature of 27 °C, while our models assume a uniform temperature distribution at the melting temperature starting from the solid state, which is

compensated by the time to start melting in our following analysis. 4) Furthermore, in our work we assume a finite, well-defined, melting temperature while the PCM used in the Pakrouh study melts over a 5 °C range, from which we select the lowest value for our direct comparisons. 5) Finally, the CFD directly investigates the role of convection which is not included in our models. Consistent with previous literature and our claims, smaller spacing of fins led to minimal levels of convection even in the late stages of melting. Considering the sum of all these differences, our ability to predict optimal performances within the context of this work can greatly increase the confidence in our optimization methodology.

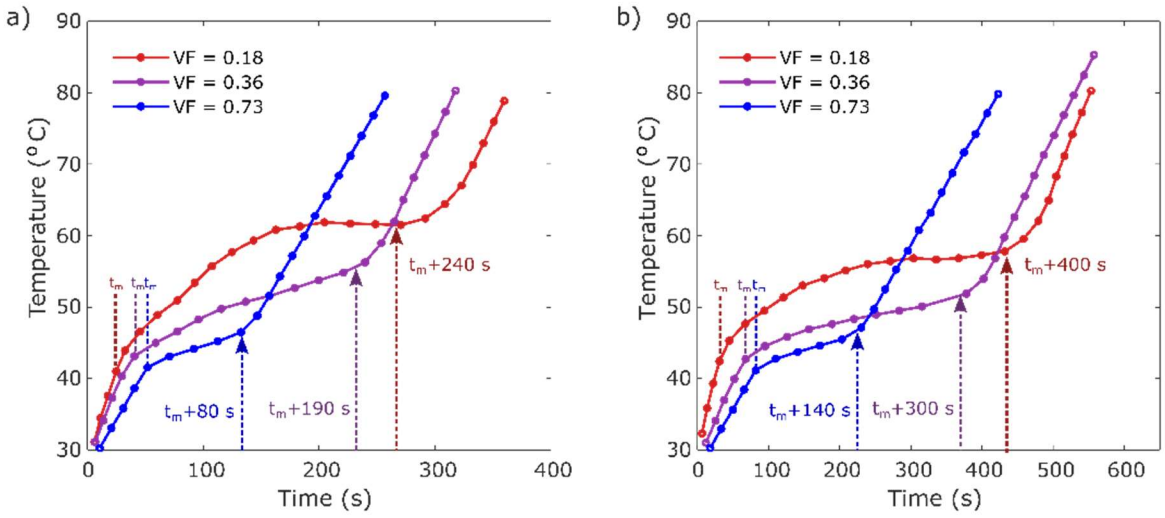

Figure 3.8. Base temperature evolution with time for metal volume fractions of 0.18, 0.36 and 0.73 with a fin height of (a) 15 mm and (b) 25 mm. Dashed lines labeled with tm indicate the datapoint corresponding to the start of melting when the lowest temperature of the melting range is reached, and dashed arrows indicate optimization times that correspond to the given compositions (within 3 %) when pre-selecting a volume limited solution. Modified from Pakrouh et al, 2015 **(**https://creativecommons.org/licenses/by/3.0/**)** [35].

For this paper we test the performance metric of optimizing performance, corresponding to minimizing temperature, at a given time. For the given materials, aluminum, and the commercial paraffin RT44 HC (T_m=41-45 °C), the rate limited optimum would be ϕ=0.5 (equation 3.17), which is not sampled at within the dataset.

Consequently, we can analyze the lower volume fractions as optimal systems for different times and, while the highest of these volume fractions (ϕ=0.73) will never be optimal, applying the solution for the volume limited regime still allows us to assess the applicability of the equations and assumptions we are working with. For the shorter fin height, 15 mm, we propose the optimization times of 80s, 190s, and 240s after the beginning of melting, which corresponds to the optimal volume fractions of 0.73, 0.35 and 0.18 (equation 3.19, Figure 3.8a). For the 23 mm extended fin systems, we propose the optimization times of 140s, 300s, and 400s after the beginning of melting which correspond to optimal metal volume fractions of 0.71, 0.38 and 0.18 (equation 3.19, Figure 8b). For each of the optimization times selected, it is evident that the selected volume fraction yields the lowest temperature out of the three related volume fraction systems (Figure 3.8). Furthermore, we confirm the optimality of the pivot point corresponding to the completion of melting as well as our ability to predict when it will occur. Our prediction is especially strong at the high volume fractions, which is explainable by the relationship between the increasing distance between fins, ranging from 1 mm to 8 mm, and the role of convection. Even at the lowest volume fractions where convection is certainly playing a role, we are still able to accurately select an optimal volume fraction and predict the approximate time of melting completion.

3.5.3.2. Critical Evaluation of Experimental Observations

Another selection from the existing literature that can be used to directly asses the applicability of our optimization methodology is work by Tamraparni et al. from 2021 which sought optimal designs of lamellar PCM composites primarily using numerical and

experimental methods [36]. The experimental aspects of this work serve as a useful validation of the real-world validation of the methodology we have developed. This work is especially useful because it represents one of the more complete experimental datasets within the literature and a thorough examination of different volume fraction systems under various heat flux conditions can be found in the supplemental information of this work (

Figure **3.9**).

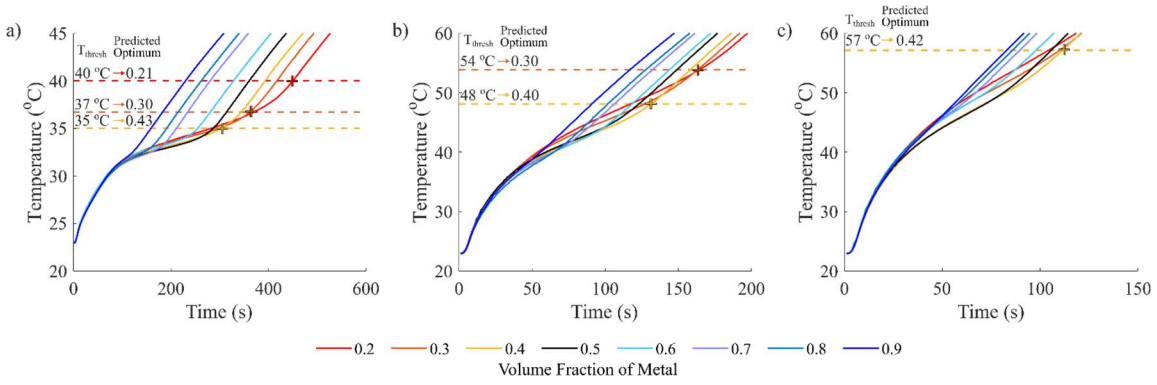

Figure 3.9. Temperature vs time plots systems for Cartesian based octadecane and aluminum alloy composites with varying volume fraction of metal for heat flux boundary conditions of (a) 1.45 W cm^{-2}, (b) 4.8 W cm^{-2} and (c) 7.25 W cm^{-2}. Dashed horizontal lines indicate a temperature threshold and are labeled with the volume fraction predicted to satisfy the optimization of maximizing the time to stay below the threshold. Modified with permission from Tamraparni et al, 2021 [36].

Using equation 3.17, a rate limited optimal volume fraction can be calculated as 0.5, which can clearly be observed as the highest performing composition across thermal loads and performance metrics throughout the study. Therefore, any volume fractions higher than this value can be rejected as possible optimums, which is confirmed within a reasonable level of randomness. For further analysis we consider the performance metric of maximizing the time the heated boundary can stay below a given maximum value in the volume limited regime. For the lowest power dataset, 1.45 W cm^{-2}, we propose temperature thresholds of 35 °C, 37 °C, and 40 °C which correspond to a predicted optimal composition of 0.43, 0.3 and 0.21 volume fraction of metal respectively (equation 3.26,

Figure **3.9**a). As the heat flux is increased, the lowest volume fractions fall out of our analysis frame. Therefore, we propose two temperature thresholds for the 4.8 W cm^{-2} dataset of 48 °C, and 54 °C which correspond to a predicted optimal composition of 0.4 and 0.3 volume fraction of metal respectively (equation 3.26,

Figure **3.9**b). Lastly, for the 7.25 W cm^{-2} dataset we select a temperature threshold of 57 °C which corresponds to a predicted optimal composition of 0.42 volume fraction of metal (equation 3.26,

Figure **3.9**c). In all cases tested, our optimization methodology is able to select the volume fraction within the given sample range that maintains sub-threshold temperatures for the longest amount of time. Notably, we do not observe a decrease in accuracy with increasing levels of thermal loading, which increases our confidence in the quasi-steady

state assumption used in our optimization methodology within a reasonable range of power levels.

3.5.4. Trends in optimums

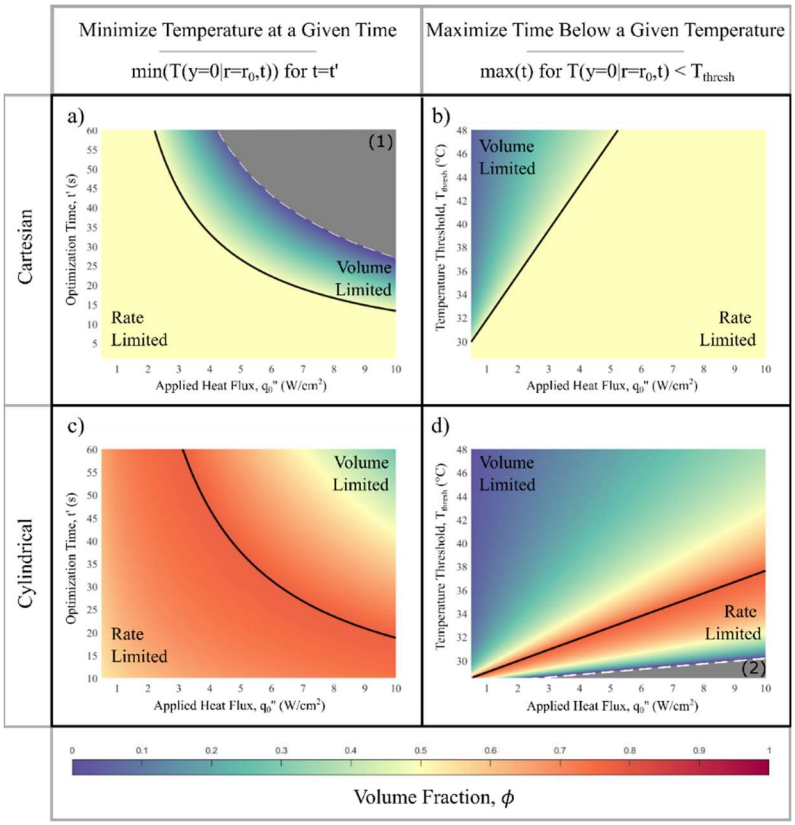

Figure 3.10. Example maps of optimal volume fraction with varying thermal inputs for a,b) Cartesian systems and c,d) cylindrical systems with a,c) the goal of minimizing the temperature at different times ($\boldsymbol{min}\ \left(\boldsymbol{T}(\boldsymbol{y}=\boldsymbol{0}|\ \boldsymbol{r}=\boldsymbol{r_o},\boldsymbol{t})\right)$ for $\boldsymbol{t}=\boldsymbol{t}'$) and b,d) the goal of maximizing the time the system's heated boundary can remain below a range of threshold temperatures (max(t) for $\boldsymbol{T}(\boldsymbol{y}=\boldsymbol{0}|\ \boldsymbol{r}=\boldsymbol{r_o},\boldsymbol{t})<\boldsymbol{T_{thresh}}$), for varying thermal loads. Black solid lines indicate the divide between the rate limited regime and the volume limited regime. Dashed white lines indicate the border of the region where optimization is bounded, where (1) the PCM volume is insufficient to manage the thermal load and (2) the problem is ill defined due to extremely short time scales.

To help understand how optimal volume fraction is dependent on application needs we can compare analytically optimized volume fraction selections across varying thermal loads. In Figure 3.10 we map out an optimal composition space with varying parameters of the design problem. The geometric basis of the cylindrical design problem was chosen to mirror our experimental analysis with a 3.6 mm inner radius and outer radius of 19.1 mm, while the dimension associated with the Cartesian problem was chosen as 15.5 mm to match the width of the cylindrical composite layer. Simulated material properties are set as the known properties of octadecane and AlSi12 (Table 3-1).

Analysis of trends within the design space is particularly useful if the application parameters are not ideally set and may vary somewhat in thermal loading or run time. For such cases, an optimal composition can be identified, and knowledge of trends can be used to inform adjustments from said optimum. Figure 3.10 demonstrates that the *rate limited* and *volume limited* regimes have very distinct trends over the analyzed space.

Notably, the optimum for systems with a Cartesian basis the optimal volume fraction in the *rate limited* regime is the same across all applications and design objectives because the solution is solely determined by material properties. Aside from this case, the optimal volume fraction will always decrease farther from the intersection of the two regimes. For cylindrical systems, the optimal volume fraction in the *rate limited* regime increases leading up to the regime intersection. This difference between cylindrical and Cartesian based systems can be attributed to an increase in circumferential thermal

capacitance with increasing melt front propagation radius for cylindrical based systems compared to Cartesian based systems. This varying optimal volume fraction within the rate limited regime for cylindrical systems suggests that while a completely uniform material is the optimal configuration for Cartesian systems, compositionally variant systems present an opportunity for future work in cylindrical systems.

For all cases in the *volume limited* regime, the optimal volume fraction will always decrease with distance from the regime boundary intersection. This can be rationalized as a necessity to increase the time before the completion of melting. This is expected by recalling the completion of melting corresponds to a sharp decrease in performance and the addition of thermal capacitance will delay the onset of this point.

We also identify regimes indicated by the gray regions in Figure 3.10, where the analytical model yields solutions less than zero (Figure 3.10a,d). In this regime having a completely PCM system is the optimal composition, assuming a PCM based solution, but using a PCM is likely not the ideal thermal management approach if all other design problem parameters are fixed. This is because, in these cases, the dynamics of the melting process begin to be dwarfed by the thermal loading making the temperature damping from the phase change process insignificant. There are two explanations for these bounds which are unique to the corresponding framing of the optimization problem. When considering the problem of minimizing the temperature at a given time, the optimization is bounded in the *volume limited* regime in the limits of longer time and applied heat flux (Figure 3.10a, grey region). This can be understood as the conditions under which the system volume is insufficient for the application and even a complete PCM composition cannot

prevent the completion of melting, after which performance rapidly drops off. When considering the problem of maximizing the time the system can remain below a given temperature, a different bound emerges (Figure 3.10d, grey region). This bound can be understood as the region where the problem is ill defined, i.e. in this region the time to reach the threshold temperature is very small (~1 s) and the difference between differing compositions becomes negligible.

3.5.5. Example Optimization Processes

In this section we provide practical examples of the application of this work. We constrain the problem to only consider optimization with aluminum and octadecane with properties defined in Table 3-1. In each example we assume the initial state of the material system is entirely solid and held at a negligible distance from the melting temperature. All edges of the system, aside from the heated boundary, are considered adiabatic. Solutions to thermal problems below are assumed to be in the form of finned heatsinks, representing the upper limit of anisotropic heat transfer away from the heat source [44]. Furthermore, fin spacings are assumed to be sufficiently small to achieve homogeneous composite behavior [35-37].

3.5.5.1. Example Problem 1:

Consider a cylindrical battery producing heat at a rate of $q_o'' = 10\ W cm^{-2}$ nested in a concentric cylindrical thermal storage package with an allowable inner radius of $r_o = 0.5\ cm$ and outer radius of $r_f = 2\ cm$. The goal of this thermal storage package is to keep

the temperature of the battery below 48 ℃ (i.e. 20 ℃ over the melting temperature, $\Delta T_{\text{thresh}} = 20$ ℃) for the longest possible amount of time.

The *rate limited* solution to this problem is solved using equation 3.24 yielding a volume fraction of $\phi = 0.84$. The *volume limited* solution to this problem is solved using equation 3.28 yielding a volume fraction of $\phi = 0.43$. Per our methodology the lower of the two values is the true optimum, which is $\phi = 0.43$, indicating we are in the *volume limited* regime of the design problem.

To support this optimization result and demonstrate the disadvantages of deviating from the optimal composition, we employ our numerical model to simulate various compositions within the design space and asses the timescales associated with each composition for the given temperature threshold (Figure **3.11**). At the optimal volume fraction, the battery surface can remain below the threshold temperature for $\sim 43\, s$ (Figure **3.11**). For this particular design problem, if the system is PCM deficient, i.e. the volume fraction is higher than the optimum, the performance as measured by the time below the threshold temperature decreases linearly by ~12% of the optimum for every increment of 10% of the sample space range ($\phi = 0.1$) (Figure **3.11**b). If the system is PCM rich, i.e. the volume fraction is lower than the optimum, the performance decreases more rapidly than the PCM deficient side of the problem. Within the first volume fraction increment of 10% ($\phi = \phi_{OPT} - 0.1$) the performance drops by ~40% and further steps drop quadratically with the fourth step corresponding to a performance drop of ~97% (Figure **3.11**b).

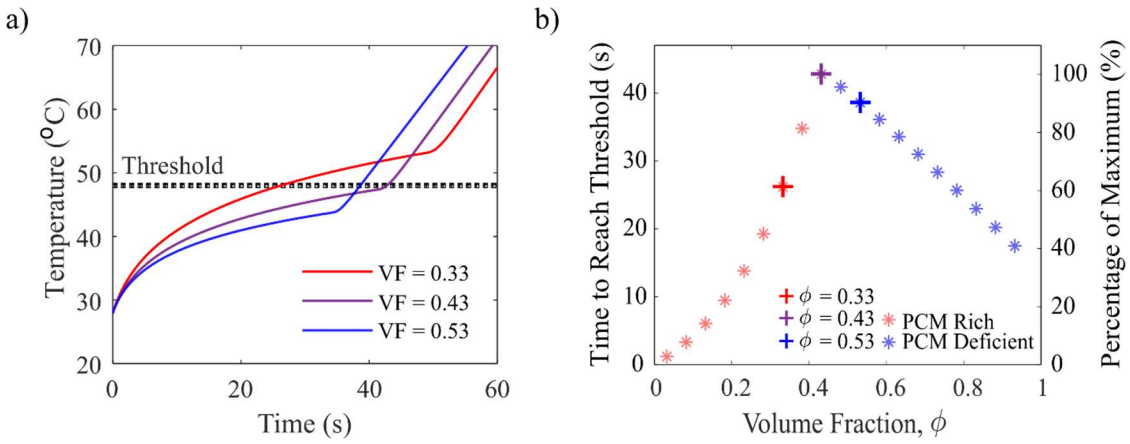

Figure 3.11. a) Numerical results for the temperature of the battery surface boundary for the optimized thermal storage package $\boldsymbol{\phi = 0.43}$ and with a deviation from this optimum by 10% of the sample space range ($\boldsymbol{\phi = 0.33}$/ $\boldsymbol{\phi = 0.53}$). Temperature threshold given by the design problem indicated with dotted line, $\Delta \boldsymbol{T_{thresh}} = \boldsymbol{20}$ ℃. b) Comparison of the performance, measured in time to reach the temperature threshold and as a percentage of the maximum time.

3.5.5.2. Example Problem 2:

As another example, consider an electronics chip producing heat at a level of $q_o'' = 1\, W cm^{-2}$ attached to a rectangular thermal storage package with a maximum height given as $y_f = 1.5\, cm$. The design objective of the thermal storage package is to

minimize the temperature of the chip over the time the chip is active, given as $t' = 120\ s$.

The *rate limited* solution to this problem is solved using equation 3.17 yielding a volume fraction of $\phi = 0.50$. The *volume limited* solution to this problem is solved using equation 3.19 yielding a volume fraction of $\phi = 0.54$. Per our methodology the lower of the two values is the true optimum, which is $\phi = 0.50$, indicating we are in the *rate limited* regime of the design problem.

To support this optimization result and demonstrate the disadvantages of deviating from the optimal composition, we employ our numerical model to simulate various compositions within the design space and assess temperature associated with each composition at the optimization time (Figure **3**.**12**). At the optimal volume fraction, the chip surface at the optimization time reaches a temperature of 31 °C (Figure **3**.**12**a). For this particular design problem, if the system is PCM deficient, i.e. the volume fraction is higher than the optimum, the chip's surface temperature increases linearly by ~20% of the optimum for every increment of 10% of the sample space range ($\phi = 0.1$) (Figure **3**.**12**b). If the system is PCM rich, i.e. the volume fraction is lower than the optimum, the chip temperature is lower than the PCM deficient side of the problem. Within the first volume fraction increment of 5% ($\phi = \phi_{OPT} - 0.05$) the temperature deviates from the optimum by ~2% and further steps of the same increment approximately double with the furthest deviation from the optimum corresponding to a ~39% increase in temperature (Figure **3**.**12**b).

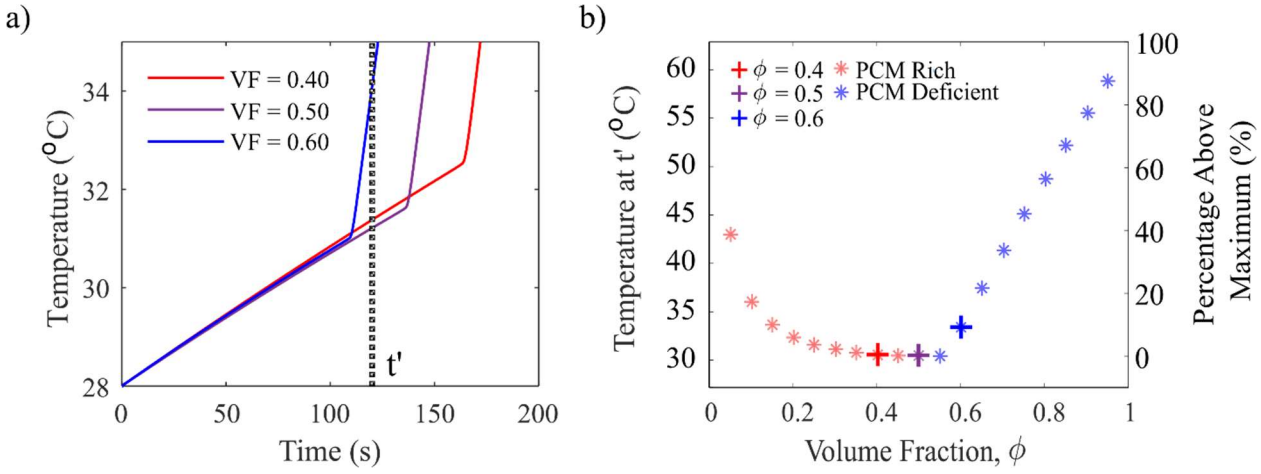

Figure 3.12. a) Numerical results for the temperature of the battery surface boundary for the optimized thermal storage package $\boldsymbol{\phi = 0.5}$ and with a deviation from this optimum by 10% of the sample space range ($\boldsymbol{\phi = 0.4}$/ $\boldsymbol{\phi = 0.6}$). Optimization time given by the design problem indicated with dotted line, $\boldsymbol{t' = 120\ s}$. b) Comparison of the performance, measured in the temperature at the optimization time and as a percentage increase over the minimum temperature rise.

3.5.5.3. Lessons from Examples

Working through specific examples allows us to identify common characteristics that are true of most practical cases, even if it is not a rule over the whole sample space. It has been observed over many test problems that when *rate limited* solutions are identified as the appropriate choice, especially when the *volume limited* optimum deviates from the

rate limited optimum significantly, there is usually a large range of volume fractions with similar performances and deviating from the optimum often causes minimal decrease in thermal buffering capacity. This can be partially seen in Figure 3.11 b where deviating from the optimum by $\phi = 0.05$ yields negligible changes in performance, though deviating farther causes melting to complete on the PCM deficient side. This is expected because the calculated *volume limited* solution is very close to the *rate limited* solution.

Within the *volume limited* regime, for the objective of maximizing thermal buffering at a given time, it is most commonly observed that, for equivalent deviations in volume fraction from the optimum, the PCM rich side of the design space decreases in performance at a lower rate than the PCM deficient side. In this regime, the complementary objective of maximizing the time to achieve a given minimum thermal buffering capacity usually exhibits a sharper peak in performance in the volume fraction space and any deviation from this optimum will cause significant decreases in performance without a strong preference for PCM deficiency or excess.

3.6. Conclusions

Phase change material based heat sink design is an area of intense interest in thermal management applications, wherein the composition of constituent elements remains the most critical design inquiry. In this manuscript, we establish a comprehensive analytical optimization framework for determining the compositions of constituent thermally conductive and capacitive components in composite phase change material layers for Cartesian and Cylindrical based systems. Within the design space, we describe two regimes where performance is limited by rate of heat absorption (*rate limited)* or total

thermal capacitance (*volume limited)*, for which corresponding expressions are derived using the quasi-steady state approximation for melting problems. This design framework spans all permutations of 1) two coordinate bases 2) two boundary condition types and 3) two design objectives to allow for this work to be broadly applicable and practical to apply.

Through a comparison to exhaustive simulation-based optimization, we confirm the accuracy and usefulness of the developed analytical models, demonstrating consistent coefficients of determination of $R^2 \approx 1$ within the *rate limited* regime and an average of $R^2 \approx 0.93$ within the *volume limited* regime. When optimizing thermal buffering capacity in terms heat transfer through the system boundary, it is observed that analytical optimization models are most valid at lower power and shorter time scales as expected from the approximate models we use. We also demonstrate the practical applicability of this work through direct comparison to original experimental results as well as experimental and numerical results from the existing literature. The convergence between these high-fidelity simulations and experiments, and the approximate analytical framework outlined in this manuscript is remarkable and demonstrates the utility of this approach in generating high performing provisional designs of composite PCM structures. Example problems are used to demonstrate the application of this work, where we show an average of 14.6 % decrease in performance when deviating by only 10% of the composition range. In summary, his work provides an unprecedented degree of design control by providing practical and objective oriented guidelines for PCM composite design.

3.7. References

[1] D. Hale, M. Hoover, and M. O'neill, "Phase change materials handbook," *National Aeronautics and Space Admnistration,* 1971.

[2] A. Sharma, V. V. Tyagi, C. Chen, and D. Buddhi, "Review on thermal energy storage with phase change materials and applications," *Renewable and Sustainable energy reviews,* vol. 13, no. 2, pp. 318-345, 2009.

[3] J. Stefan, "Über die Theorie der Eisbildung, insbesondere über die Eisbildung im Polarmeere," *Annalen der Physik und Chemie,* vol. 278, no. 2, pp. 269-286, 1891.

[4] J. C. Jaeger and H. S. Carslaw, *Conduction of heat in solids*. Clarendon Press, 1959.

[5] J. Crank, *Free and moving boundary problems*. Oxford University Press, USA, 1984.

[6] Y. A. Cengel and H. Pérez, *Heat transfer: a practical approach.*, 2 ed. McGraw-Hill, 2002.

[7] D. Q. Kern and A. D. Kraus, "Extended surface heat transfer," 1972.

[8] P. J. Brennan and E. J. Kroliczek, "Heat Pipe Design Handbook: Volume II," *National Aeronautics and Space Admnistration,* 1979.

[9] E. Skrabek, "Heat pipe design handbook, part 1," *National Aeronautics and Space Admnistration,* 1972.

[10] D. Reay, R. McGlen, and P. Kew, *Heat pipes: theory, design and applications*. Butterworth-Heinemann, 2013.

[11] K. Thulukkanam, *Heat exchanger design handbook*. CRC press, 2013.

[12] K. Yazawa, P. J. Shamberger, and T. S. Fisher, "Ragone Relations for Thermal Energy Storage Technologies," *Frontiers in Mechanical Engineering,* vol. 5, 29, 2019.

[13] M. T. Barako, S. Lingamneni, J. S. Katz, T. Liu, K. E. Goodson, and J. Tice, "Optimizing the design of composite phase change materials for high thermal power density," *Journal of Applied Physics,* vol. 124, no. 14, p. 145103, 2018.

[14] P. J. Shamberger and T. S. Fisher, "Cooling power and characteristic times of composite heatsinks and insulants," *International Journal of Heat and Mass Transfer,* vol. 117, pp. 1205-1215, 2018.

[15] J. Woods, A. Mahvi, A. Goyal, E. Kozubal, A. Odukomaiya, and R. Jackson, "Rate capability and Ragone plots for phase change thermal energy storage," *Nature Energy,* vol. 6, no. 3, pp. 295-302, 2021.

[16] T. Christen, "Ragone plots and discharge efficiency-power relations of electric and thermal energy storage devices," *Journal of Energy Storage,* vol. 27, p. 101084, 2020.

[17] J. M. Khodadadi, L. Fan, and H. Babaei, "Thermal conductivity enhancement of nanostructure-based colloidal suspensions utilized as phase change materials for thermal energy storage: A review," *Renewable and Sustainable Energy Reviews,* vol. 24, pp. 418-444, 2013.

[18] J. M. Khodadadi and S. F. Hosseinizadeh, "Nanoparticle-enhanced phase change materials (NEPCM) with great potential for improved thermal energy storage," *Int Commun Heat Mass,* vol. 34, no. 5, pp. 534-543, 2007.

[19] C. J. Ho and J. Y. Gao, "Preparation and thermophysical properties of nanoparticle-in-paraffin emulsion as phase change material," *Int Commun Heat Mass,* vol. 36, no. 5, pp. 467-470, 2009.

[20] M. A. Kibria, M. R. Anisur, M. H. Mahfuz, R. Saidur, and I. H. S. C. Metselaar, "A review on thermophysical properties of nanoparticle dispersed phase change materials," *Energ Convers Manage,* vol. 95, pp. 69-89, 2015.

[21] Y. Guo *et al.*, "Thermal performance of a 3D printed lattice-structure heat sink packaging phase change material," *Chinese Journal of Aeronautics,* vol. 34, no. 5, pp. 373-385, 2021.

[22] G. Righetti, G. Savio, R. Meneghello, L. Doretti, and S. Mancin, "Experimental study of phase change material (PCM) embedded in 3D periodic structures realized via additive manufacturing," *International Journal of Thermal Sciences,* vol. 153, p. 106376, 2020.

[23] W. Li, Z. Qu, Y. He, and W. Tao, "Experimental and numerical studies on melting phase change heat transfer in open-cell metallic foams filled with paraffin," *Applied Thermal Engineering,* vol. 37, pp. 1-9, 2012.

[24] M. Iasiello, M. Mameli, S. Filippeschi, and N. Bianco, "Simulations of paraffine melting inside metal foams at different gravity levels with preliminary experimental validation," in *Journal of Physics: Conference Series*, 2020, vol. 1599, no. 1, p. 012008.

[25] A. Ghahremannezhad, H. Xu, M. R. Salimpour, P. Wang, and K. Vafai, "Thermal performance analysis of phase change materials (PCMs) embedded in gradient porous metal foams," *Applied Thermal Engineering,* vol. 179, p. 115731, 2020.

[26] P. P. Levin, A. Shitzer, and G. Hetsroni, "Numerical optimization of a PCM-based heat sink with internal fins," *International Journal of Heat and Mass Transfer,* vol. 61, pp. 638-645, 2013.

[27] V. Shatikian, G. Ziskind, and R. Letan, "Numerical investigation of a PCM-based heat sink with internal fins," *International Journal of Heat and Mass Transfer,* vol. 48, no. 17, pp. 3689-3706, 2005.

[28] S. Mahmoud, A. Tang, C. Toh, R. Al-Dadah, and S. L. Soo, "Experimental investigation of inserts configurations and PCM type on the thermal performance of PCM based heat sinks," *Applied Energy,* vol. 112, pp. 1349-1356, 2013.

[29] Y. Huang, Q. Sun, F. Yao, and C. Zhang, "Experimental study on the thermal performance of a finned metal foam heat sink with phase change material," *Heat Transfer Engineering,* vol. 42, no. 7, pp. 579-591, 2021.

[30] N. Bianco, S. Busiello, M. Iasiello, and G. M. Mauro, "Finned heat sinks with phase change materials and metal foams: Pareto optimization to address cost and operation time," *Applied Thermal Engineering,* vol. 197, p. 117436, 2021.

[31] Z. A. Qureshi, E. Elnajjar, O. Al-Ketan, R. A. Al-Rub, and S. B. Al-Omari, "Heat transfer performance of a finned metal foam-phase change material (FMF-PCM) system incorporating triply periodic minimal surfaces (TPMS)," *International Journal of Heat and Mass Transfer,* vol. 170, p. 121001, 2021.

[32] J. M. Mahdi and E. C. Nsofor, "Solidification enhancement of PCM in a triplex-tube thermal energy storage system with nanoparticles and fins," *Applied Energy,* vol. 211, pp. 975-986, 2018.

[33] I. Sarani, S. Payan, S. Nada, and A. Payan, "Numerical investigation of an innovative discontinuous distribution of fins for solidification rate enhancement in PCM with and without nanoparticles," *Applied Thermal Engineering,* vol. 176, p. 115017, 2020.

[34] B. Kok, "Examining effects of special heat transfer fins designed for the melting process of PCM and Nano-PCM," *Applied Thermal Engineering,* vol. 170, p. 114989, 2020.

[35] A. Hoe, M. Deckard, A. Tamraparni, A. Elwany, J. R. Felts, and P. J. Shamberger, "Conductive heat transfer in lamellar phase change material composites," *Applied Thermal Engineering,* vol. 178, p. 115553, 2020.

[36] A. Tamraparni *et al.*, "Design and Optimization of Lamellar Phase Change Composites for Thermal Energy Storage," *Advanced Engineering Materials,* vol. 23, no. 1, p. 2001052, 2021.

[37] T. Bauer, "Approximate analytical solutions for the solidification of PCMs in fin geometries using effective thermophysical properties," *International Journal of Heat and Mass Transfer,* vol. 54, no. 23-24, pp. 4923-4930, 2011.

[38] J. Vogel, M. Keller, and M. Johnson, "Numerical modeling of large-scale finned tube latent thermal energy storage systems," *Journal of Energy Storage,* vol. 29, p. 101389, 2020.

[39] C. Beckermann and R. Viskanta, "Natural convection solid/liquid phase change in porous media," *International journal of heat and mass transfer,* vol. 31, no. 1, pp. 35-46, 1988.

[40] A. Sharma, M. Trivedi, K. Agarwal, and N. Nirmalkar, "Thermal energy storage in a confined cylindrical heat source filled with phase change materials," *International Journal of Heat and Mass Transfer,* vol. 178, p. 121603, 2021.

[41] R. Pakrouh, M. J. Hosseini, and A. A. Ranjbar, "A parametric investigation of a PCM-based pin fin heat sink," *Mech. Sci.,* vol. 6, no. 1, pp. 65-73, 2015.

[42] M. Kibria, M. Anisur, M. Mahfuz, R. Saidur, and I. Metselaar, "A review on thermophysical properties of nanoparticle dispersed phase change materials," *Energ Convers Manage,* vol. 95, pp. 69-89, 2015.

[43] C. Zhang *et al.*, "Design for laser powder bed additive manufacturing of AlSi12 periodic mesoscale lattice structures," *The International Journal of Advanced Manufacturing Technology,* vol. 113, no. 11, pp. 3599-3612, 2021.

[44] W. Voigt, "Ueber die Beziehung zwischen den beiden Elasticitätsconstanten isotroper Körper," *Annalen der Physik,* vol. 274, no. 12, pp. 573-587, 1889.

[45] B. Debich, A. El Hami, A. Yaich, W. Gafsi, L. Walha, and M. Haddar, "Design optimization of PCM-based finned heat sinks for mechatronic components: A numerical investigation and parametric study," *Journal of Energy Storage,* vol. 32, p. 101960, 2020.

[46] S. F. Hosseinizadeh, F. L. Tan, and S. M. Moosania, "Experimental and numerical studies on performance of PCM-based heat sink with different configurations of

internal fins," *Applied Thermal Engineering,* vol. 31, no. 17-18, pp. 3827-3838, 2011.

[47] R. Pakrouh, M. J. Hosseini, A. A. Ranjbar, and R. Bahrampoury, "A numerical method for PCM-based pin fin heat sinks optimization," *Energ Convers Manage,* vol. 103, pp. 542-552, 2015.

[48] P. J. Shamberger, "Cooling Capacity Figure of Merit for Phase Change Materials," *Journal of Heat Transfer,* vol. 138, no. 2, 2016.

[49] L. Shao *et al.*, "Figure-of-merit for phase-change materials used in thermal management," *International Journal of Heat and Mass Transfer,* vol. 101, pp. 764-771, 2016.

[50] T. J. Lu, "Thermal management of high power electronics with phase change cooling," *International Journal of Heat and Mass Transfer,* vol. 43, no. 13, pp. 2245-2256, 2000.

[51] J. Bransier, "Stockage periodique par chaleur latente aspects fondamentaux liés a la cinétique des transferts," *International Journal of Heat and Mass Transfer,* vol. 22, no. 6, pp. 875-883, 1979.

[52] M. E. Deckard, J. Felts, and P. J. Shamberger, "Cooling Power and Thermal Buffering in Composite Heatsinks," in *17th IEEE Intersociety Conference on Thermal and Thermomechanical Phenomena in Electronic Systems (ITherm)*, 2018: IEEE, pp. 109-116.

[53] A. Tamraparni *et al.*, "Design and optimization of composite phase change material for cylindrical thermal energy storage," *In Preparation,* 2022.

[54] R. Waser *et al.*, "Fast and experimentally validated model of a latent thermal energy storage device for system level simulations," *Applied Energy,* vol. 231, pp. 116-126, 2018.

[55] D. R. Askeland, P. Fulay, and W. Wright, "The science and engineering of materials 6th edition," *Cengage Learning Inc,* p. 889, 2010.

[56] A. Jayalath, L. Aye, T. Ngo, and P. Mendis, "Multi-scale analysis on thermal properties of cement-based materials containing micro-encapsulated phase change materials," *Construction and Building Materials,* vol. 254, p. 119221, 2020.

[57] Z. Hashin and S. Shtrikman, "A variational approach to the theory of the elastic behaviour of multiphase materials," *Journal of the Mechanics and Physics of Solids,* vol. 11, no. 2, pp. 127-140, 1963.

[58] A. Reuß, "Berechnung der fließgrenze von mischkristallen auf grund der plastizitätsbedingung für einkristalle," *ZAMM-Journal of Applied Mathematics and Mechanics/Zeitschrift für Angewandte Mathematik und Mechanik,* vol. 9, no. 1, pp. 49-58, 1929.

[59] H. Zhou, S. Zhang, and M. Yang, "The effect of heat-transfer passages on the effective thermal conductivity of high filler loading composite materials," *Composites Science and Technology,* vol. 67, no. 6, pp. 1035-1040, 2007.

[60] D. Li, N. Dai, Y. Tang, G. Dong, and Y. F. Zhao, "Design and optimization of graded cellular structures with triply periodic level surface-based topological shapes," *Journal of Mechanical Design,* vol. 141, no. 7, 2019.

[61] J. M. Hill, *One-dimensional Stefan problems: an introduction*. Longman Sc & Tech, 1987.

[62] V. Alexiades, *Mathematical modeling of melting and freezing processes*. CRC Press, 1992.

[63] L. M. Jiji, "Conduction with Phase Change: Moving Boundary Problems," in *Heat Conduction*: Springer Berlin Heidelberg, 2009, ch. 6, pp. 184-214.

[64] L. M. Jiji and S. Gaye, "Analysis of solidification and melting of PCM with energy generation," *Applied Thermal Engineering,* vol. 26, no. 5-6, pp. 568-575, 2006.

[65] J. Crepeau and A. Siahpush, "Approximate solutions to the Stefan problem with internal heat generation," *Heat and mass transfer,* vol. 44, no. 7, pp. 787-794, 2008.

[66] L. S. Yao and W. Cherney, "Transient phase-change around a horizontal cylinder," *International Journal of Heat and Mass Transfer,* vol. 24, no. 12, pp. 1971-1981, 1981.

4. DESIGN OF RADIALLY VARIANT PHASE CHANGE MATERIAL COMPOSITES

4.1. Nomenclature

A	Area, (m^2)
a	Fitting parameter, (unitless)
b	Fitting parameter, (unitless)
c	Fitting parameter, (unitless)
C	Integration constant, (unitless)
C_v^{eff}	Effective volumetric heat capacity, $(J\ m^{-2}\ K^{-1})$
C_m^{eff}	Effective heat capacity, $(J\ kg^{-1}\ K^{-1})$
F	Integration component
G	Integration component
H	Integration component
k	Thermal Conductivity, $(W\ m^{-1}\ K^{-1})$
L_v	Latent heat, $(J\ kg^{-1})$
M	Mass, (kg)
q_o''	Heat flux, $(W\ m^{-2})$
r	Radius, (m)
t	Time, (s)
T	Temperature, (C)
δ	Ratio of metal and PCM conductivities, (unitless)
ρ	Density, $(\mathrm{k}g\ m^{-3})$

ϕ Volume fraction of metal, (unitless)

γ Ratio of metal and PCM densities, (unitless)

Subscripts:

m Metal

p PCM

eff Effective

0 At the inner radius

s At the melt front radius

f At the outer front radius

$melt$ Melting

4.2. Introduction

Phase change material (PCM) composites have been shown to act as highly efficient cooling devices within thermal management systems for the management of transient thermal loads [1-3]. Within such settings, design guidelines relate internal structure to desired performance levels which should be employed to appropriately utilize these materials. To this end, previous work has sought to provide procedures for identifying optimal length scales and internal compositions of constituents [3-9]. While excellent progress is being made on this front, optimization problems are most often considered for a uniformly designed composite, with the field of spatially variant

optimizations leaving significant room for development. This design space presents an opportunity for the design of uniquely high performing systems and incorporation of multiple design objectives that can be tailored for a chosen application. It is currently unknown what advantages may be gained from utilizing increasingly complex designs and where these designs may best be exploited. Due to increased manufacturing complexities, it is especially necessary to understand the benefits of incorporating such designs within thermal management systems.

Within the category of PCM composites, systems usually can be placed into the categories of: composite dispersions [10-13], macro-/micro- porous media [3, 14-18], and finned heat sinks [19-21] or any combination thereof [22-24]. Each category is associated with specific advantages and disadvantages. Finned heatsinks are of especial interest to the thermal management community due to their high manufacturability, tailorability, and access to the entire range of volume fraction space which are not broadly found in the other categories of composites. Furthermore, these heatsinks correspond to the anisotropic upper limit of heat transfer with fin components oriented perpendicular to the heat source [3, 25]. For such finned composite systems, the critical spacing of fins can be determined by identifying the length scale where performance of the macro-scale system corresponds to an effective medium composite of the same composition (Figure 4.1a,b,c) [4, 26]. This can be understood as the length scale below which moving to smaller scale aspects would have no further improvement in performance.

Beyond geometric basis and length scale, the key design variable within these composites is the volume fraction of the constituents within the system. This is most often

studied within the literature using numerical or experimental methods or empirical analyses [7, 21, 27-29]. While these studies are useful for rough characterization of the design space, the usually sparse nature of the datasets involved in comparison to the complete degrees of freedom within the design space, prevents the development of generally applicable design rules. Within an analytical context, figure of merit (FOM) approaches are often employed to select compositions which balance thermal capacitance and thermal conductivity to maximize the rate of heat transfer into the composite from a constant heat source [3, 8, 30]. These approaches are extremely helpful for understanding the principles of heat transfer within PCM composite systems but are limited by their lack of flexibility and limited scope. Within FOM approaches it is especially difficult to account for different performance metrics or design considerations. This is especially relevant to fields such as aerospace or electronics packaging where different performance metrics may be useful or secondary variables, such as mass or volume, may need to be accounted for in the design process. Furthermore, these approaches do not provide direct insight into the relationship between design aspects and specific levels of performance.

Previous work has outlined an approximate analytical methodology relating specific temporal and thermal performance metrics to a corresponding optimal volume fraction [6]. It has been noted that within the performance metrics explored, for Cartesian based effectively infinite systems, the optimal volume fraction is only dependent on material properties, leading to a uniform design space. Whereas for Cylindrical systems, having a radially varying thermal mass leads to a design space of optimal volume fractions dependent on the other known design parameters. This suggests that while Cartesian

systems would not benefit from an internally varying composition, non-uniform designs should be considered for Cylindrical based systems (Figure 4.1d,e).

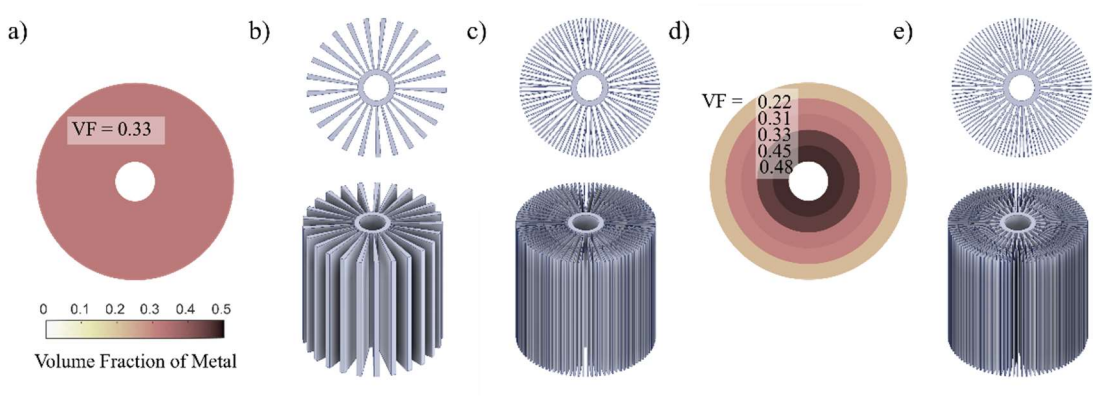

Figure 4.1 a) Schematic representation of the EMA being applied to a constant volume fraction (VF) composite which can be manifested with b) straight fins a constant angle from the center or c) branching fins which allow for closer compliance with the EMA. b) Schematic representation of the EMA being applied to a variant volume fraction composite with discrete levels e) manifested with branching fins with radially varying volume fractions.

Radially variant cylindrical PCM heatsinks have been studied through two primary avenues based in either empirical or numerical methods. Empirical studies generate PCM

composite designs through the select a local maximum from suite of proposed designs [31-33]. While, these studies can lead to some limited conclusions, they are unlikely to generate true optimums or uncover concrete underlying relationships between structure and performance. This can be attributed to the sparseness of the gathered datasets in relationship to the overall design space. The complementary numerical studies most commonly utilize topology optimization to generate spatially varying fins through the maximization of a performance response function [34, 35]. These methods are useful for the generation of true optimum designs, which can give insight into the general form of desired designs. However, the systems created are uniquely applicable for the optimization conditions that they are created for and represent significant computational expense.

In this work, we seek to expand upon the current guidelines for optimal compositional design of cylindrical composite systems through the intentional design of radially varying composition within a composite system. Furthermore, these radially variant composites are explored using considerations for different performance metrics individually, and in combination, to provide highly flexible, application based, optimization approaches. This is accomplished analytically by assuming a general form of the volume fraction profile and using an approximate performance calculation to optimize for the parameters of the profile shape. Analytical optimization is made possible through the utilization of the effective medium approximation. The use of this approximation has been established as a valid approximation in finned PCM composites in the limit of small length scales (Figure 4.1a,d) where the associated Rayleigh numbers become relatively small, corresponding to negligible levels of convective heat transfer

[36]. For these conditions geometric confinement and fluid viscosity dampen the buoyant forces and heat transfer becomes dominated by conduction [20, 29, 37]. Convergence with this approximation is achieved using a critical spacing bifurcation scheme (Figure 4.1b,c). The validity of the analytical optimization is verified using a numerical technique employing Bayesian optimization [38] and finite element modelling [4, 39] to optimize a discrete step profile (Figure 4.1d,e).

Performance is assessed herein in terms of temperature levels, effective heat capacity and effective volumetric heat capacity to allow for the broad application of this work and account for mass and volume in the design considerations, where it is often overlooked. These performance metrics are used to compare the optimized radially variant composites (Figure 4.1d,e) with optimized constant volume fraction composites (Figure 4.1a,c) to assess the advantages of this design approach. Lastly, we utilize multi-objective optimization to design composites that prioritize a given metric while still yielding high performance in a secondary objective. These designs are additively manufactured and experimentally tested to demonstrate how this approach affects the thermal response on each performance level (Figure 4.1b,c,e). The guidelines provided in this work to generate radially variant PCM composites are highly versatile to allow this work to have widespread applicability and the supporting analytical, numerical and experimental results demonstrate high levels of performance which compare favorably against other optimization methods.

4.3. Methods

4.3.1. Problem Statement

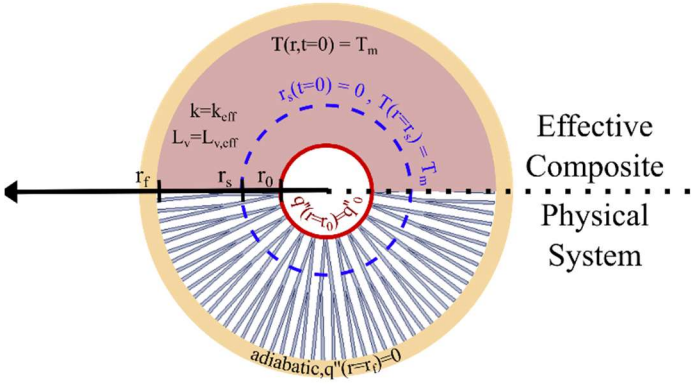

Figure 4.2 Visual depiction of the problem statement in which the physical system is expressed as an effective composite. Red line indicates the heated boundary and blue dashed line indicates the melt front location.

The optimization pursued herein follows the case of a finned cylindrical PCM based heatsink exposed to a constant heat flux thermal load at the inner radius (Figure 4.2). This configuration may represent an electronics component, such as a battery, which outputs a given level of power needing to be dissipated. For such thermal management problems, the primary goal is minimization of the temperature of the powered component, while other factors such as mass or volume may also be accounted for within the design problem.

Within the heatsink, heat transfer is limited to conductive pathways due to the role of PCM confinement between fins effectively eliminating convection, which is valid at low Rayleigh numbers [36, 37]. The materials chosen for this study are octadecane [40,

41] and aluminum alloy AlSi12 which were chosen for their desirable material properties, latent heat and thermal conductivity respectively, and accessibility of application (Table 4-1). To allow for the possibility of tractable analytical optimization, the system is initialized in the solid state at the melting temperature in accordance with the classical Stefan problem [42-44]. A constant heat flux boundary condition is applied at the inner radius of the cylindrical composite. For analytical optimization, the radial design space is considered to be infinite, allowing for free expansion and no interaction with external boundaries. For numerical optimization, the finite system generated is considered to be adiabatic, emulating a perfect insulation.

Table 4-1 Material properties used in original numerical simulations and analytical modelling.

	Units	AlSi12 alloy	Octadecane
k	$W\ m^{-1}\ K^{-1}$	80	0.15
L_v	J m^{-3}	-	1.74 x10^8
ρ	$kg\ m^{-3}$	2700	712
C_p	$J\ kg^{-1}\ K^{-1}$	900	2200
T_m	C	-	28

4.3.2. Single Objective Analytical Optimization

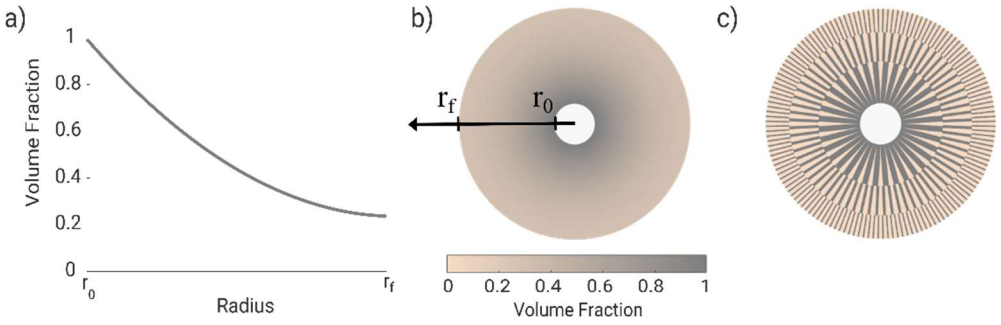

Figure 4.3 a) Continuous volume fraction curve determined by a second order polynomial. Representation of the continuous volume fraction distribution as a radially-varying b) effective medium system and c) a physical manifestation consisting of a branching composite design.

Here we develop analytical solutions for the description of thermal behavior within lamellar PCM composite thermal energy storage systems in cylindrical coordinates for a non-constant metal volume fraction along the radial coordinate axis (Figure 4.3). The properties of the composite are given according to the effective medium approximation for lamella oriented parallel to the direction of heat flow.

$$k_{eff} = k_m\phi + k_p(1-\phi) \tag{4.1}$$

$$\rho_{eff} = \rho_m\phi + \rho_p(1-\phi) \tag{4.2}$$

$$L_{eff} = L_v(1-\phi) \tag{4.3}$$

Where k represents thermal conductivity, ρ represents density, and L_v represents the volumetric heat of fusion for the PCM and the subscripts m, p and eff refer to the metal, PCM and effective properties, respectively [25, 45]. The variable ϕ represents the volume fraction of metal within the composite, and here is given as a quadratic function of radius:

$$\phi = ar^2 + br + c \tag{4.4}$$

where $a, b,$ and c are fitting parameters (Figure 4.3).

The most standard optimization metric for thermal management systems is the minimization of temperature rise of a heated surface or volume. To this end, the temperature profile is determined by solving the 1D heat diffusion equation in cylindrical coordinates [46] given by the equation:

$$\frac{1}{r}\frac{d}{dr}\left([\delta\phi + (1-\phi)]r\frac{dT}{dr}\right) = 0 \tag{4.5}$$

where $\delta = k_m/k_p$ is the ratio of the thermal conductivities of the metal and PCM. The general solution to the temperature profile upon integration is given by equations 4.6-4.9 below:

$$T(r) = -\frac{C_1}{2c(\delta-1)+2}[H(r) + G(r)] + C_2 \tag{4.6}$$

$$H(r) = 2bF\tan^{-1}\left(F(2ar+b)\right) \tag{4.7}$$

$$F = \frac{\sqrt{\delta-1}}{\sqrt{4a(c(\delta-1)+1)-b^2(\delta-1)}} \tag{4.8}$$

$$G(r) = \ln(a(\delta-1)r^2 + b(\delta-1)r + c(\delta-1)+1) - 2\ln r \tag{4.9}$$

Evaluating the temperature at the inner radius r_o of the composite cylinder and the moving melt front r_s results in a temperature profile given by:

$$T(r) = -\frac{([H(r)+G(r)]+[H(r_s)-G(r_s)])}{H(r_o)-H(r_s)+G(r_o)-G(r_s)}\Delta T + T_{melt} \tag{4.10}$$

where ΔT is the temperature difference between the temperature at the inner radius, T_o, and the melting temperature of the PCM, T_{melt}. The heat flow through the system defined at the internal radius r_o of the composite is given by Fourier's Law [46], yielding:

$$q_o'' = -\frac{2k_p[c(\delta-1)+1]\Delta T}{r_o\left(H(r_o)-H(r_s)+G(r_o)-G(r_s)\right)} \tag{4.11}$$

where q_o'' is the heat flux at the inner radius of the composite. The temperature difference between the inner radius and the melt front is then given by the equation:

$$\Delta T = \frac{q_o'' r_o\left(H(r_s)-H(r_o)+G(r_s)-G(r_o)\right)}{2k_p[c(\delta-1)+1]} \tag{4.12}$$

which represents the first optimization metric of interest within this work. From this equation parameters $a, b,$ and c can be fit for the minimization of ΔT to yield the optimal profile for this metric.

As an expansion of the temperature minimization optimization, we define two additional performance metrics, effective volumetric heat capacity, C_v^{eff}, and effective heat capacity, C_m^{eff}. We are defining these variables using the traditional definitions of volumetric heat capacity and heat capacity as a guideline while taking some strong differentiating steps. Firstly, we use the dynamic temperature rise of the heated surface as the variable of interest, which includes the effects of melting, rather than an equilibrated temperature of a given volume. Additionally, calculations are performed in terms of a unit length due to the 2D nature of the heat transfer problem. Lastly, due to the semi-infinite nature of the analytical optimization described here, mass and volume are dynamic characteristics that must be calculated as such for the given optimization time.

For the second optimization metric of interest in this work we evaluate effective volumetric heat capacity defined analytically as [47]:

$$C_v^{eff} = \frac{2\pi r_o q_o'' t}{A\Delta T} \tag{4.13}$$

where A represents the cross-sectional area of the composite as determined by the propagation of the melt front into the semi-infinite design space. The location of the melt front is determined by setting the energy absorbed by the solid over a small time, dt, equal to the volume of material melted and integrating:

$$2\pi q_o'' r_o \int_0^t dt = 2\pi L_v \int_{r_o}^{r_s} r_s(1-\phi) dr_s \tag{4.14}$$

For the case of a quadratically varying volume fraction, the integral yields:

$$6(1-c)(r_s^2 - r_o^2) - 4b(r_s^3 - r_o^3) - 3a(r_s^4 - r_o^4) = \frac{12 q_o'' r_o t}{L_v} \tag{4.15}$$

allowing for the calculation of the melt front location which can be combined with equation 4.13 to relate back to effective volumetric heat capacity and fit the parameters $a, b,$ and c to complete the optimization for this metric.

Lastly, we evaluate the optimization metric of effective heat capacity given analytically as [47, 48]:

$$C_m^{eff} = \frac{2\pi r_o q_o'' t}{M\Delta T} \tag{4.16}$$

where M represents the mass of the composite accounting for the metal and PCM contained within. From equation 4.15 describing the melt front location, the mass of the composite cylinder can be calculated by integrating the density over the volume as:

$$M = \frac{\pi \rho_p}{6}\left[(\gamma - 1)\left(3a(r_s^4 - r_o^4) + 4b(r_s^3 - r_o^3) + 6c(r_s^2 - r_o^2)\right) + 6(r_s^2 - r_o^2)\right] \tag{4.17}$$

where $\gamma = \rho_m/\rho_p$ is the ratio of the densities of the metal and PCM. This equation allows for the calculation of the mass from the melt front location, which can be combined with equation 16 to relate back to effective specific heat capacity. From there the parameters $a, b,$ and c can be fit to maximize effective specific heat capacity to yield the optimal profile for this metric.

4.3.3. Multi-Objective Analytical Optimization

Within the space of optimizing for a single performance metric and allowing for semi-infinite expansion, it has been observed that there is often a large selection of profiles that will yield similar performance levels [49]. This suggests that high levels of performance can be accomplished in terms of a given optimization objective while also selecting for profiles that meet a secondary need, such as decreased mass or volume. We approach this hybrid design problem by selecting one of the three optimization metrics defined above and selecting a given design variable as the secondary metric that can be simultaneously optimized.

For the first step in this process, optimization with the first metric is carried out as a constant volume fraction optimization. This can be accomplished as described in the previous section allowing fitting parameters a and b to become zero. The performance of this system is calculated using the chosen metric and set as a constraint for the secondary design problem. Within this work, the secondary objective is chosen as a minimization of the system's mass. This is distinct from the maximization of the effective heat capacity, C_m^{eff}, through the decoupling of temperature and mass allowing for the prioritization of one metric, temperature, over the other, mass. The final design is created by setting the

value of the primary performance metric equal to the result of the constant volume fraction optimization and iterating different through different composition profiles to find a mass minimizing configuration. This approach is used to demonstrate a possible multi-objective design methodology and the unique advantages of utilizing variable volume fraction profiles over single volume fraction profiles.

4.3.4. Numerical Optimization

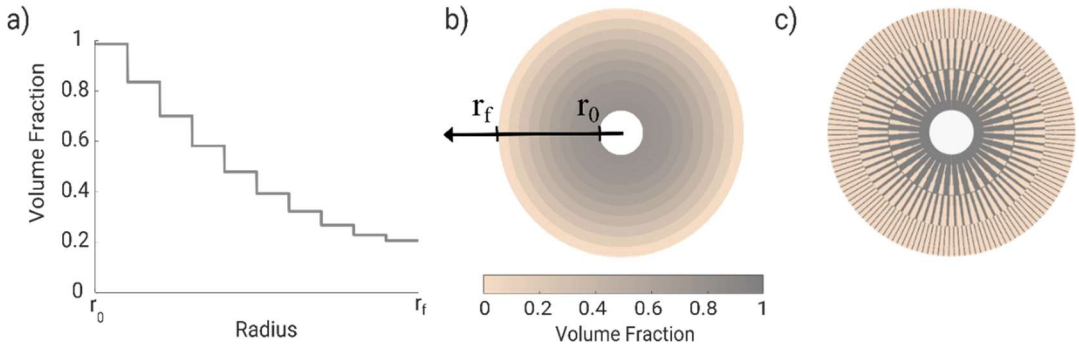

Figure 4.4 a) Discrete volume fraction distribution determined by a numerical array. Representation of the discrete volume fraction distribution as a b) effective medium system and c) a branching composite design.

To verify the form and product of our analytical results we compare against a numerical optimization strategy. This strategy combines the use of Bayesian optimization techniques with finite element simulations to predict high performing compositional configurations.

The finite difference model used herein has been established in previous work as a method of accurately modeling heat transfer in PCM composite systems [4, 39]. In this model we approximate our 3D system as 1D to significantly decrease computational expense and which will be accurate for sufficiently small length scales [4, 26]. The FDA includes the geometric constraints of the inner radius, outer radius, and base height as inputs as well as the applied thermal load and volume fraction values. Using the applied thermal load input, a boundary condition of constant heat flux is applied at the inner radius, and all other boundaries are considered to be adiabatic. Each node within the range of the simulated space is assigned effective properties calculated from the volume fraction distribution input using effective medium theory (as demonstrated in equations 1-3). For each timestep a backwards Euler method is used to calculate heat transfer between and absorbed by each node. Internal calculations execute until the time at which the system is being optimized is reached and the chosen performance metric is given as the output of the simulation.

Within our simulation, we discretize the spatially distributed volume fractions to 20 values, where finite element nodes are grouped and assigned the corresponding volume fraction (Figure 4.4). Initial radial volume fractions are selected using a Latin hypercube sampling scheme. Existing literature results [34, 35] and original preliminary data indicated that a monotonically decreasing profile, with a high-volume fraction of metal closest to the base, will allow heat to be rapidly transferred away from the boundary while still allowing for a high thermal capacity throughout the system. Therefore, in the process of sampling, selected volume fractions are constrained to decrease as radius increases,

narrowing down the design space and decreasing computational expense. The data gathering based on Latin hypercube selection is repeated 20 times to generate an initial dataset, as established by previous work [50].

Once the sample space has been initially gathered it can now be used to fit a response surface using a Gaussian Process Repressor (GPR) to approximate the surface morphology and predict performance in unsampled spaces. From there an acquisition function is employed to select for the next point in the space with the high expected performance. This selected volume fraction distribution point is then run on the FDA to get the corresponding performance metric, which is added to the larger dataset. Each iteration of selection and simulation adds to the fit of the GPR, making further predictions more accurate and driving the performance higher. The optimizer is run for 30 iterations, which is chosen based on the data sufficiency previously explored. This process results in an optimized discrete profile of volume fractions which can be directly compared with the analytically generated profiles.

4.3.5. Experimental Testing

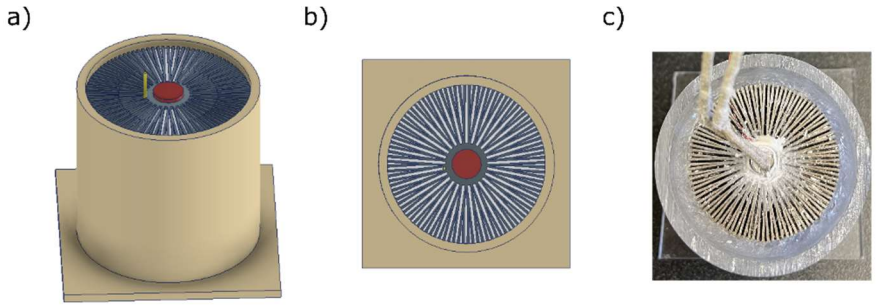

Figure 4.5 Schematic a) front facing and b) overhead view with c) realized image of the experimental basis used to measure temperature rise within a PCM composite system under a constant heat flux thermal load.

The metal basis of the composite structures is fabricated from Aluminum alloy, AlSi12, originally in the powder state obtained from 3D Systems, PS2585-18. Laser powder bed fusion is utilized to precisely manufacture complex structures (beam spot diameter: 80 μm) with low porosity (< 1 vol.%). Longitudinally uniform fin structures bifurcate when spacing between fins exceeds 1 mm to satisfy the EMA to the best of our ability. Fin width along a given circumference is determined by the number of bifurcations and the volume fraction of a chosen section. These structures are infiltrated octadecane and refrigerated to solidify before testing occurs. All testing takes place within an insulating layer of silicone foam to minimize heat loss and mimic an adiabatic environment as closely as possible. The cylindrical composites are initial initially held isothermally at 22 °C where all the PCM is in the solid state. During each test a cartridge

heater is used to apply a constant thermal load of 10 W cm^{-2} and thermistors attached to the inner wall of the cylinder record the temperature rise (Figure 4.5).

4.4. Results and Discussion

4.4.1. Numerical and Analytical Comparison

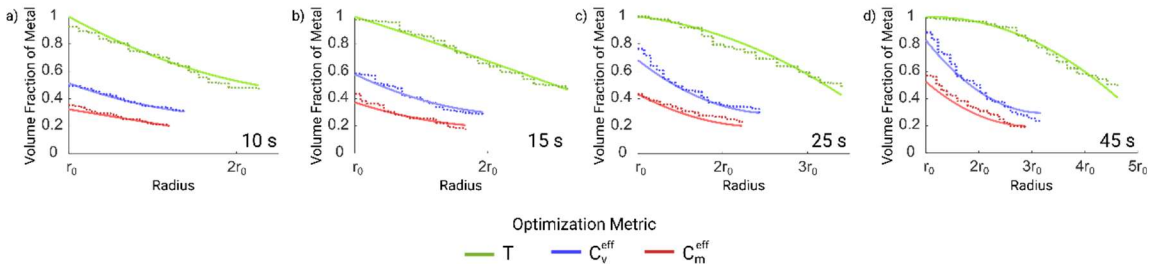

Figure 4.6 For a heat flux of 5 W cm^{-2} optimal profiles for a cylindrical PCM composite with an inner radius of 5mm are generated numerically (dotted lines) and analytically (solid liens) for the times of a) 10 s, b) 15 s, c) 25 s, and d) 45 s and the optimization metrics of temperature (green), effective volumetric heat capacity (blue) and effective specific heat capacity (red).

Both numerical and analytical results confirm the advantage and optimality of radially variant composites across the three performance metrics used here (

Figure 4.6). One of the fundamental assumptions in our analytical model is that the optimal profile can be appropriately fit with a quadratic profile. To justify this assumption, we employ the previously discussed numerical optimization technique which divides a volume into discrete sections and optimizes the profile with the volume fraction of each section used as the optimization variables (§*Numerical Optimization*). A direct comparison of our numerical comparisons with analytical models shows strong agreement, confirming sharp drops or less well-behaved profiles are not necessary to consider and quadratic fitting is sufficient to achieve optimal performance (
Figure 4.6).

Deviations between numerical and analytical results are to be expected, firstly, due to the uniformity of the performance space in relation to the large degrees of freedom making optimization problems generally challenging. To confirm that we are converging on the global optimum, simulations of discrete and continuous profiles yield equivalent levels of performance or favor the continuous profile. Furthermore, alignment between numerical and analytical results tends to be stronger at shorter time scales and lower thermal loading values because a smaller radius of melt front propagation allows for finer discretization spacing which will more closely mimic a continuous profile in thermal response.

4.4.2. Trends in Optimality

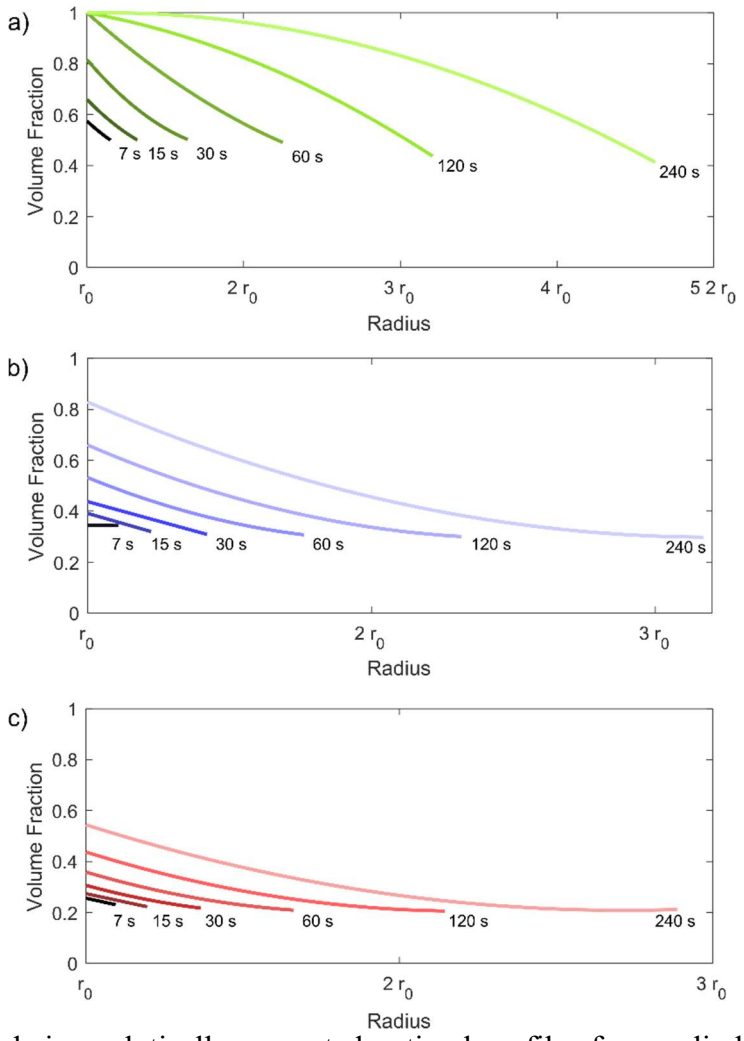

Figure 4.7 Trends in analytically generated optimal profiles for a cylindrical composite with an inner radius of 5 mm under a constant heat flux load of 1 W cm^{-2} when optimizing for a) temperature minimization, b) effective volumetric heat capacity maximization, and c) effective specific heat capacity maximization.

As observed in numerous previous work, the optimality of a composite's composition is specific to a set of constraints and loadings that are given by the design problem (Figure 4.7) [3, 6, 51]. This is confirmed here where the optimization time is shown to directly determine the morphology of the optimal profile and emphasizes the necessity of tailoring design to the needs of the chosen application. At very low temperature rises, i.e. at short times and/or low heat fluxes, the generated optimized radial profiles are highly linear. As time scales and thermal loads increase in magnitude, the concavity of the optimize profiles changes mostly depending on the chosen optimization metric. Within the range analyzed here, analytical optimization yields consistently radially decreasing profiles for metal volume fractions. This is to be expected because, as previously discussed, at smaller radii a higher proportion of metal is necessary to rapidly transfer heat away from its source which can later be absorbed by the larger proportion of PCM at larger radii. Furthermore, we observe that the lower bound of the optimized profiles remains relatively constant across the optimization scenarios. The value of this limit roughly coincides with the optimal volume fraction calculated for Cartesian based systems: 0.50 volume fraction for temperature minimization, 0.23 volume fraction for effective heat capacity maximization and, 0.33 volume fraction for effective volumetric heat capacity maximization (Figure 4.7). Conceptually this can be reasoned by considering any individual circumferential section of the cylinder. In the limit of decreasing radial width of these sections the inner and outer radius values converge, corresponding with the Cartesian limit. Therefore, decreasing the metal volume fraction below the limiting Cartesian value will not be favorable to the system.

Figure 4.7a demonstrates that for the optimization metric of temperature minimization there are two distinct behavioral trends. At lower and moderate time scales, the volume fraction of the inner radius increases with time, until an upper limit of complete metal is reached. After this upper limit has been reached, the optimized profiles decrease in concavity. This is explained by the fact that when temperature minimization is the primary objective the higher conductivity of the metal provides the highest rate of heat transfer away from the source, keeping temperatures low. This results in optimal profiles that require a large volume of space corresponding to a larger outer radius compared to the other optimization metrics.

For the optimization metrics of effective heat capacity and effective volumetric heat capacity concavity increases with time scales, tending toward a higher composition of PCM. This is explained by the weighting of mass and volume as a part of the performance metric that should be decreased, allowing for higher thermal capacity to decrease the overall system's outer radius. In these cases, it is still necessary to have high metal volume fractions nearest to the heat source for rapid heat transfer into the heatsink which is balanced with low metal volume fractions to slow the propagation of the melt front. In the cases of very large thermal loads and long times the inner composition does get pinned at a completely metal composition, but the concavity never reverses as seen in the temperature optimization trends. This can lead to the non-monotonic results where the volume fraction has a local minima within the range of the utilized area near the outer edge of the cylinder where the outer radius has an increased proportion of metal. This

effect is caused by a need to rapidly increase the proportion of metal to delay the propagation of the thermal front.

4.4.3. Single vs Variable Volume Fraction

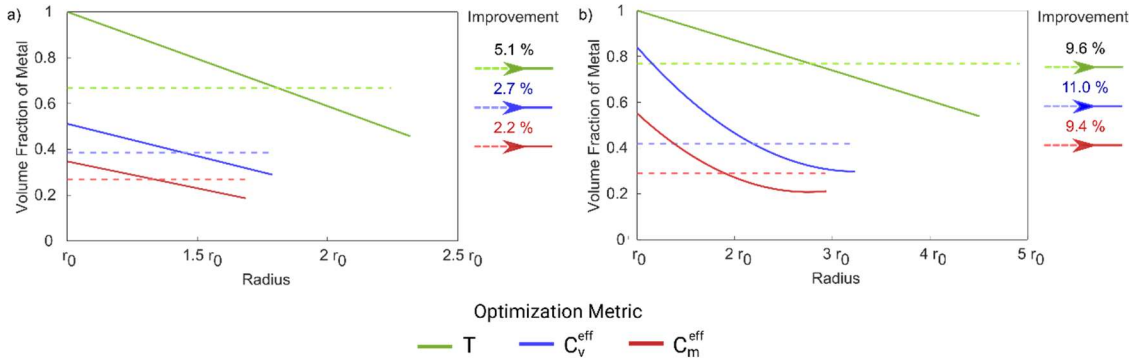

Figure 4.8 Analytically generated optimal profiles for constant volume fraction (dashed lines) and variant volume fraction (solid lines) cylindrical composite with an inner radius of 5 mm, with the thermal loadings of a) 2.5 W cm^{-2} for 25 s and b) 5 W cm^{-2} for 50 s for the optimization metrics of temperature (green), effective volumetric heat capacity (blue) and effective specific heat capacity (red).

To assess the value of pursuing this optimization methodology, incorporating compositionally variant profiles, it is useful to compare against the simpler optimization for a single invariant volume fraction system. Figure 4.8 directly compares optimized

profiles for single (dashed lines) and radially variant (solid lines) profiles for two individual cases of a given time and heat flux. In all cases, the variant profile range will cross through the value of the constant optimized profile. Furthermore, for the example optimizations shown, the variant profile always outperforms the constant profile designs. We observe the magnitude of this improvement is highly dependent on geometry, thermal load, time scale and performance metric. It is, therefore, crucial to understand the effects of these factors on the relative improvement in performance to justify the implementation of more complex design and manufacturing processes. Subsequent analysis follows this same approach of analytically generating optimal profiles for constant and variant volume fraction profiles and recording the improvement of the variant profile over it's constant counterpart.

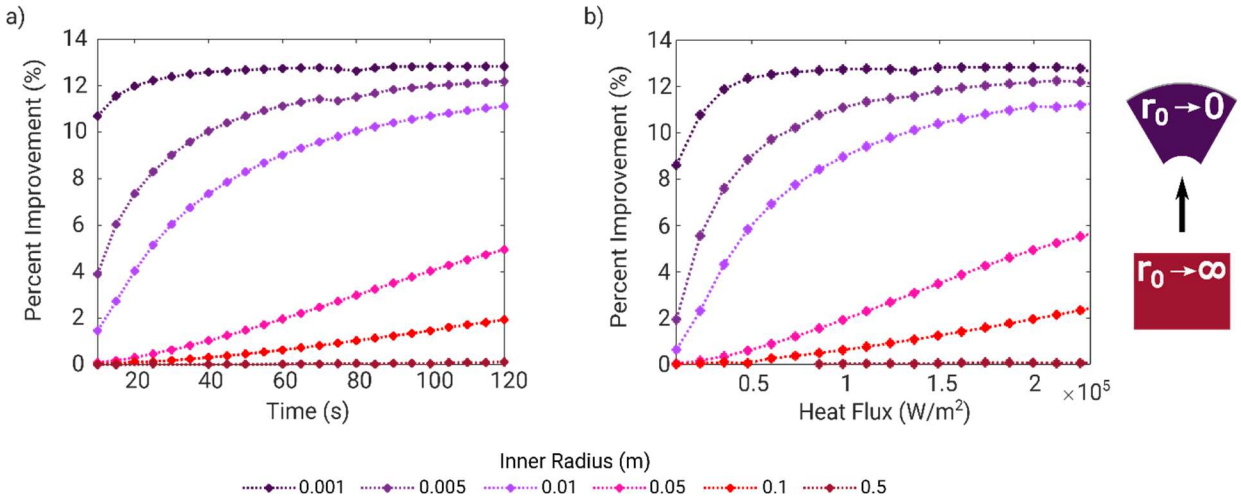

Figure 4.9 Improvement of variant volume fraction designs over constant volume designs as it trends with a) time for a constant thermal load of 5 W cm^{-2} and with b) heat flux at a constant optimization time of 30s compared across differing values of internal radii for the optimization metric of temperature minimization.

It was previously predicted that for the design of Cartesian based systems, compositionally variant profiles would provide no advantage because in the rate limited regime the design space is constant and uniform [6]. We confirm this prediction by varying the inner radius of the cylindrical composite in the optimization problem. This is shown in

Figure 4.9 for the optimization metric of temperature minimization. As expected, as the inner radius is increased and we approach the Cartesian limit, $r_0 \approx r_f$, the improvement

of the variant optimization over an invariant optimization decreases rapidly. For the thermal configurations tested here, an inner radius of 0.5 m represents convergence with the Cartesian limit and shows no improvement to incorporating a radially variant volume fraction design. This effect also explains the lower improvement values at lower magnitudes of heat flux and optimization times because the melt front propagation is less advanced, more closely resembling a Cartesian configuration.

As the inner radius is decreased at the outset of our design process, we are able to achieve a larger advantage for incorporating radially variant design up to an observed limit (

Figure 4.9). This represents the cylindrical limit where $r_0 \ll r_f$ and is directly contrasted against the Cartesian limit. Longer time scales and higher heat flux loads allow for the system to approach this upper limit due to the advanced propagation of the melt front. This limit is achieved more quickly when the system design specifies a small inner radius in the design. For the thermal configurations here, we observe an upper limit of approximately 12.5 % which will largely be dependent on the properties of the chosen constituent materials.

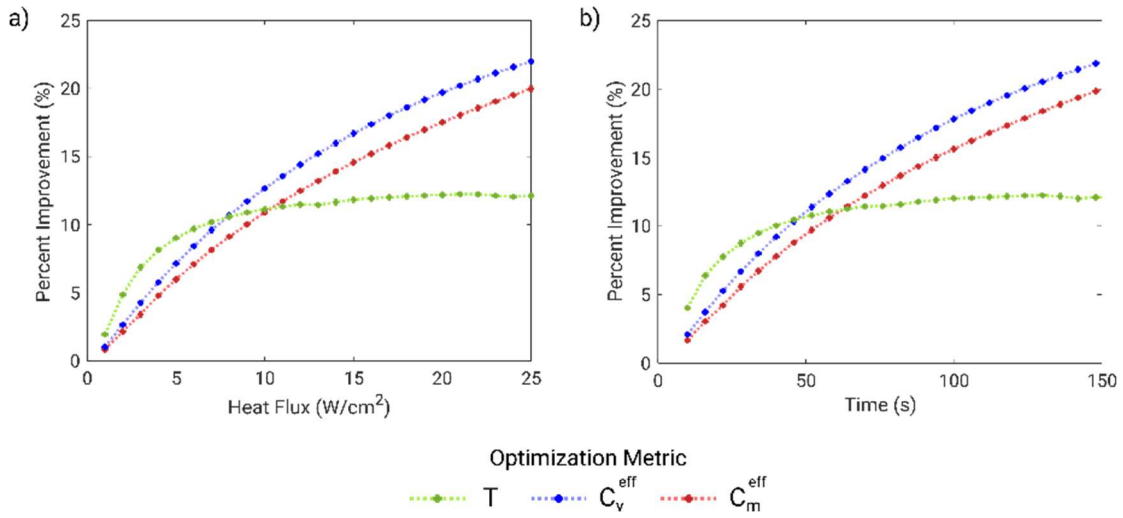

Figure 4.10 Improvement of variant volume fraction designs over constant volume designs as it trends with a) time for a constant thermal load of 5 Wcm^{-2} and with b) heat flux at a constant optimization time of 30s with an inner radius of 5 mm compared across different optimization metrics of temperature (green), effective volumetric heat capacity (blue) and effective specific heat capacity (red).

Unlike the performance metric of temperature minimization, the maximization of effective heat capacity and effective volumetric heat capacity is not bounded by an upper limit (Figure 4.10). This is an effect caused by the allowance for a semi-infinite optimization. At longer times and higher heat fluxes the melt front of the single volume fraction optimization can reach extremely large propagation radii. For the corresponding variant volume fraction optimization, the performance metrics of effective heat capacity

and effective volumetric heat capacity strongly bias the design toward high thermal capacity yielding low melt front propagation radii. This bias is also balanced by a higher volume fraction of metal closer to the base preventing large temperature rises, which would negatively affect both measures of heat capacity. Therefore, allowing for an infinite space leads to an unbounded potential for improvement from a hypothetical standpoint that can be partially accessed within the confines of a real applied system design.

4.4.4. Hybrid Design Objectives

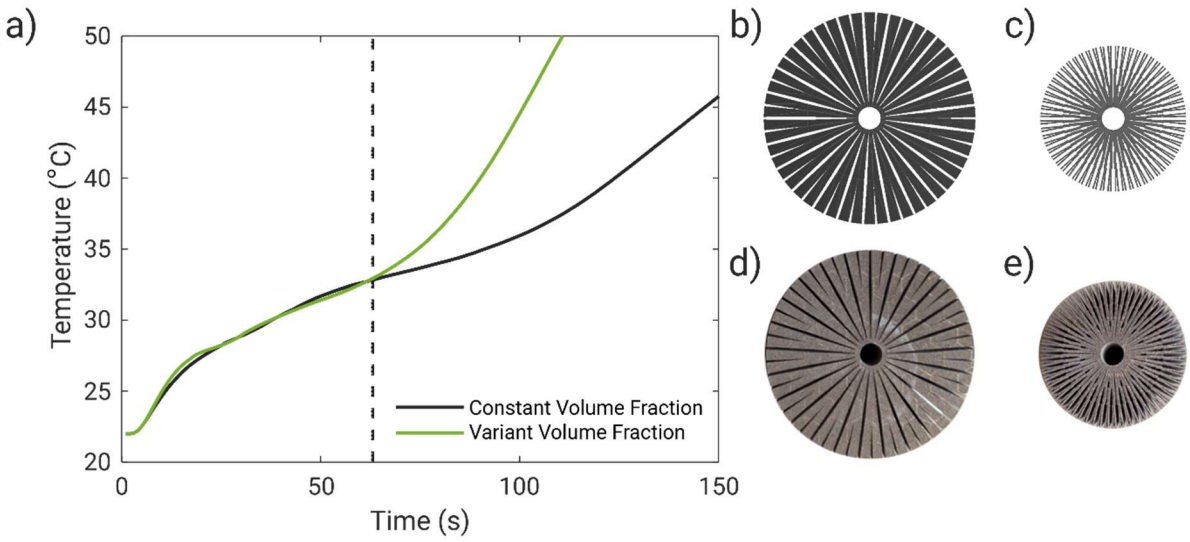

Figure 4.11 Hybrid temperature opimization a) experimental results for thermal loading of 10 Wcm^{-2} for the constant volume fraction optimized system (solid black) as compared to the variant volume fraction optimized system (solid green) designed for the optimization time of 40 s after the onset of melting (dashed). b,c) Generated designs and d,e) manufactured systems for b,d) constant and c,e) variant volume fraction optimizations.

As discussed in section 2.3, many applications motivate the incorporation of a hybrid objective for optimal design. To demonstrate one possible execution of this methodology we consider a cylindrical system with an internal radius 0.5 cm is optimized under a heat load of 10 W cm^{-2} at an optimization time of 40 s. The primary objective of the design process is to dampen the temperature rise at the inner radius with the secondary

objective of creating a lightweight design. To execute the design for this hybrid objective, the system is first designed for the objective of minimizing the temperature at the optimization time for a constant volume fraction, resulting in a constant 80 % metal composition profile. The expected temperature rise for this design is analytically determined to be 11.8 ℃. Setting this value as the design constraint for the variable volume fraction optimization with the goal of minimizing mass resulting variable volume fraction profile decreases within the range (0.99 VF to 0.35 VF).

The effectiveness of this methodology can be demonstrated through experimental testing of the single optimization system in comparison to the hybrid objective optimization system (

Figure 4.11). The measured experimental temperature rise at the optimization time is observed as 4.82 ℃ for the case of the single optimization system and 4.78 ℃ for the hybrid objective optimization system. While this is significantly lower than the predicted value, the matching of the temperature values within 1% leads us to believe that discrepancies can be primarily attributed to a thermal lag and spatial inconsistencies within the heater, and we are successful in the application of our optimization technique.

Critically, between the constant and variable volume fraction designs we are able to decrease the total mass of the composite system by over 280 %, from 322.0 g to 113.7 g respectively. This results in an increase of specific heat capacity from 3.08 kJ $kg^{-1}K^{-1}$ to 8.79 kJ $kg^{-1}K^{-1}$ as well as a 32% decrease in the total volume of the composite. This level of improvement emphasizes the usefulness of this methodology for application where competing factors can be balanced within the design problem.

4.5. Conclusions

Utilizing design techniques for the creation of radially variant cylindrical PCM composites gives a high degree of flexibility in terms of individual and combined performance metrics. In this work we describe analytical techniques for the generation of optimal composition profiles along the radial axis which are supported through comparable numerical optimization results. The utility of this approach is demonstrated by comparing optimized designs of the radially variant systems with radially constant systems, where we consistently see improvement from the cylindrical variant design structures. This improvement is found to have a high geometric dependance where the cylindrical limit represents the upper bound of performance and is contrasted with the Cartesian limit where no improvement is produced from variant optimization. Single objective variant optimization is explored for three performance metrics herein 1) temperature minimization, 2) effective volumetric heat capacity, and 3) effective heat capacity. Across all performance metrics it is observed that a larger improvement in variant design performance over constant design performance occurs at longer time scales and larger magnitude thermal loads. However, improvement in temperature minimization is found to have an upper limit that is achieved more rapidly in the cylindrical limit. This is not observed for the other performance metrics due to the effects of the semi-infinite basis of the optimization problem and competing factors within the performance metrics. Lastly, we demonstrate the application of a hybrid design methodology where a primary performance metric is selected for the optimization while a secondary variable is also accounted for, catering for applications where it is necessary to consider multiple

objectives. In this work, the variety of approaches to the analytical design of radially variant PCM composites, using individual and combined performance objectives, allow for the highly versatile tailoring systems to the specific needs of a given application.

4.6. References

[1] D. Hale, M. Hoover, and M. O'neill, "Phase change materials handbook," *National Aeronautics and Space Admnistration,* 1971.

[2] A. Sharma, V. V. Tyagi, C. Chen, and D. Buddhi, "Review on thermal energy storage with phase change materials and applications," *Renewable and Sustainable energy reviews,* vol. 13, no. 2, pp. 318-345, 2009.

[3] M. T. Barako, S. Lingamneni, J. S. Katz, T. Liu, K. E. Goodson, and J. Tice, "Optimizing the design of composite phase change materials for high thermal power density," *Journal of Applied Physics,* vol. 124, no. 14, p. 145103, 2018.

[4] A. Hoe, M. Deckard, A. Tamraparni, A. Elwany, J. R. Felts, and P. J. Shamberger, "Conductive heat transfer in lamellar phase change material composites," *Applied Thermal Engineering,* vol. 178, p. 115553, 2020.

[5] A. Tamraparni *et al.*, "Design and Optimization of Lamellar Phase Change Composites for Thermal Energy Storage," *Advanced Engineering Materials,* vol. 23, no. 1, p. 2001052, 2021.

[6] A. Hoe *et al.*, "Objective Oriented Phase Change Material Composite Heat Sink Design ", (In Review).

[7] R. Pakrouh, M. J. Hosseini, A. A. Ranjbar, and R. Bahrampoury, "A numerical method for PCM-based pin fin heat sinks optimization," *Energ Convers Manage,* vol. 103, pp. 542-552, 2015.

[8] P. J. Shamberger, "Cooling Capacity Figure of Merit for Phase Change Materials," *Journal of Heat Transfer,* vol. 138, no. 2, 2016.

[9] J. Y. Ho, Y. S. See, K. C. Leong, and T. N. Wong, "An experimental investigation of a PCM-based heat sink enhanced with a topology-optimized tree-like structure," *Energ Convers Manage,* vol. 245, p. 114608, 2021.

[10] J. M. Khodadadi, L. Fan, and H. Babaei, "Thermal conductivity enhancement of nanostructure-based colloidal suspensions utilized as phase change materials for thermal energy storage: A review," *Renewable and Sustainable Energy Reviews,* vol. 24, pp. 418-444, 2013.

[11] J. M. Khodadadi and S. F. Hosseinizadeh, "Nanoparticle-enhanced phase change materials (NEPCM) with great potential for improved thermal energy storage," *Int Commun Heat Mass,* vol. 34, no. 5, pp. 534-543, 2007.

[12] C. J. Ho and J. Y. Gao, "Preparation and thermophysical properties of nanoparticle-in-paraffin emulsion as phase change material," *Int Commun Heat Mass,* vol. 36, no. 5, pp. 467-470, 2009.

[13] M. A. Kibria, M. R. Anisur, M. H. Mahfuz, R. Saidur, and I. H. S. C. Metselaar, "A review on thermophysical properties of nanoparticle dispersed phase change materials," *Energ Convers Manage,* vol. 95, pp. 69-89, 2015.

[14] Y. Guo *et al.*, "Thermal performance of a 3D printed lattice-structure heat sink packaging phase change material," *Chinese Journal of Aeronautics,* vol. 34, no. 5, pp. 373-385, 2021.

[15] G. Righetti, G. Savio, R. Meneghello, L. Doretti, and S. Mancin, "Experimental study of phase change material (PCM) embedded in 3D periodic structures realized via additive manufacturing," *International Journal of Thermal Sciences,* vol. 153, p. 106376, 2020.

[16] W. Li, Z. Qu, Y. He, and W. Tao, "Experimental and numerical studies on melting phase change heat transfer in open-cell metallic foams filled with paraffin," *Applied Thermal Engineering,* vol. 37, pp. 1-9, 2012.

[17] M. Iasiello, M. Mameli, S. Filippeschi, and N. Bianco, "Simulations of paraffine melting inside metal foams at different gravity levels with preliminary experimental validation," in *Journal of Physics: Conference Series*, 2020, vol. 1599, no. 1, p. 012008.

[18] A. Ghahremannezhad, H. Xu, M. R. Salimpour, P. Wang, and K. Vafai, "Thermal performance analysis of phase change materials (PCMs) embedded in gradient porous metal foams," *Applied Thermal Engineering,* vol. 179, p. 115731, 2020.

[19] P. P. Levin, A. Shitzer, and G. Hetsroni, "Numerical optimization of a PCM-based heat sink with internal fins," *International Journal of Heat and Mass Transfer,* vol. 61, pp. 638-645, 2013.

[20] V. Shatikian, G. Ziskind, and R. Letan, "Numerical investigation of a PCM-based heat sink with internal fins," *International Journal of Heat and Mass Transfer,* vol. 48, no. 17, pp. 3689-3706, 2005.

[21] S. Mahmoud, A. Tang, C. Toh, R. Al-Dadah, and S. L. Soo, "Experimental investigation of inserts configurations and PCM type on the thermal performance of PCM based heat sinks," *Applied Energy,* vol. 112, pp. 1349-1356, 2013.

[22] Y. Huang, Q. Sun, F. Yao, and C. Zhang, "Experimental study on the thermal performance of a finned metal foam heat sink with phase change material," *Heat Transfer Engineering,* vol. 42, no. 7, pp. 579-591, 2021.

[23] Z. A. Qureshi, E. Elnajjar, O. Al-Ketan, R. A. Al-Rub, and S. B. Al-Omari, "Heat transfer performance of a finned metal foam-phase change material (FMF-PCM) system incorporating triply periodic minimal surfaces (TPMS)," *International Journal of Heat and Mass Transfer,* vol. 170, p. 121001, 2021.

[24] J. M. Mahdi and E. C. Nsofor, "Solidification enhancement of PCM in a triplex-tube thermal energy storage system with nanoparticles and fins," *Applied Energy,* vol. 211, pp. 975-986, 2018.

[25] W. Voigt, "Ueber die Beziehung zwischen den beiden Elasticitätsconstanten isotroper Körper," *Annalen der Physik,* vol. 274, no. 12, pp. 573-587, 1889.

[26] T. Bauer, "Approximate analytical solutions for the solidification of PCMs in fin geometries using effective thermophysical properties," *International Journal of Heat and Mass Transfer,* vol. 54, no. 23-24, pp. 4923-4930, 2011.

[27] B. Debich, A. El Hami, A. Yaich, W. Gafsi, L. Walha, and M. Haddar, "Design optimization of PCM-based finned heat sinks for mechatronic components: A numerical investigation and parametric study," *Journal of Energy Storage,* vol. 32, p. 101960, 2020.

[28] S. F. Hosseinizadeh, F. L. Tan, and S. M. Moosania, "Experimental and numerical studies on performance of PCM-based heat sink with different configurations of internal fins," *Applied Thermal Engineering,* vol. 31, no. 17-18, pp. 3827-3838, 2011.

[29] R. Pakrouh, M. J. Hosseini, and A. A. Ranjbar, "A parametric investigation of a PCM-based pin fin heat sink," *Mech. Sci.,* vol. 6, no. 1, pp. 65-73, 2015.

[30] L. Shao *et al.*, "Figure-of-merit for phase-change materials used in thermal management," *International Journal of Heat and Mass Transfer,* vol. 101, pp. 764-771, 2016.

[31] J. Weng, Y. He, D. Ouyang, X. Yang, G. Zhang, and J. Wang, "Thermal performance of PCM and branch-structured fins for cylindrical power battery in a high-temperature environment," *Energ Convers Manage,* vol. 200, p. 112106, 2019.

[32] S. Liu, H. Peng, Z. Hu, X. Ling, and J. Huang, "Solidification performance of a latent heat storage unit with innovative longitudinal triangular fins," *International Journal of Heat and Mass Transfer,* vol. 138, pp. 667-676, 2019.

[33] Y. Huang, L. Song, S. Wu, and X. Liu, "Investigation on the thermal performance of a multi-tube finned latent heat thermal storage pool," *Applied Thermal Engineering,* vol. 200, p. 117658, 2022.

[34] A. Pizzolato, A. Sharma, K. Maute, A. Sciacovelli, and V. Verda, "Design of effective fins for fast PCM melting and solidification in shell-and-tube latent heat thermal energy storage through topology optimization," *Applied Energy,* vol. 208, pp. 210-227, 2017.

[35] A. Pizzolato, A. Sharma, K. Maute, A. Sciacovelli, and V. Verda, "Topology optimization for heat transfer enhancement in latent heat thermal energy storage," *International Journal of Heat and Mass Transfer,* vol. 113, pp. 875-888, 2017.

[36] C. Beckermann and R. Viskanta, "Natural convection solid/liquid phase change in porous media," *International journal of heat and mass transfer,* vol. 31, no. 1, pp. 35-46, 1988.

[37] A. Sharma, M. Trivedi, K. Agarwal, and N. Nirmalkar, "Thermal energy storage in a confined cylindrical heat source filled with phase change materials," *International Journal of Heat and Mass Transfer,* vol. 178, p. 121603, 2021.

[38] J. Mockus, *Bayesian approach to global optimization: theory and applications*. Springer Science & Business Media, 2012.

[39] M. E. Deckard, J. Felts, and P. J. Shamberger, "Cooling Power and Thermal Buffering in Composite Heatsinks," in *17th IEEE Intersociety Conference on Thermal and Thermomechanical Phenomena in Electronic Systems (ITherm)*, 2018: IEEE, pp. 109-116.

[40] C. Vélez, M. Khayet, and J. O. De Zárate, "Temperature-dependent thermal properties of solid/liquid phase change even-numbered n-alkanes: n-Hexadecane, n-octadecane and n-eicosane," *Applied Energy,* vol. 143, pp. 383-394, 2015.

[41] A. Abdi, M. Ignatowicz, S. N. Gunasekara, J. N. W. Chiu, and V. Martin, "Experimental investigation of thermo-physical properties of n-octadecane and n-eicosane," *International Journal of Heat and Mass Transfer,* vol. 161, p. 120285, 2020.

[42] V. Alexiades, *Mathematical modeling of melting and freezing processes*. CRC Press, 1992.

[43] J. Stefan, "Über die Theorie der Eisbildung, insbesondere über die Eisbildung im Polarmeere," *Annalen der Physik und Chemie,* vol. 278, no. 2, pp. 269-286, 1891.

[44] T. Jonsson, "On the one dimensional Stefan problem: with some numerical analysis," ed, 2013.

[45] D. R. Askeland, P. Fulay, and W. Wright, "The science and engineering of materials 6th edition," *Cengage Learning Inc,* p. 889, 2010.

[46] Y. A. Cengel and H. Pérez, *Heat transfer: a practical approach.*, 2 ed. McGraw-Hill, 2002.

[47] M. F. Ashby, H. Shercliff, and D. Cebon, *Materials: engineering, science, processing and design*. Butterworth-Heinemann, 2018.

[48] M. M. Rathore, *Thermal engineering*. Tata McGraw-Hill Education, 2010.

[49] A. Hoe, J. Felts, and P. J. Shamberger, "Numerical Evaluation of Thermal Energy Storage Rate in Planar and Cylindrical Phase Change Material Composites," *(In Review)*.

[50] A. Hoe, A. Easley, M. Deckard, J. Felts, and P. J. Shamberger, "Forward Selection Methodology for Phase Change Material Composite Optimization," in *2020 19th IEEE Intersociety Conference on Thermal and Thermomechanical Phenomena in Electronic Systems (ITherm)*, 2020: IEEE, pp. 674-680.

[51] A. Sciacovelli, F. Gagliardi, and V. Verda, "Maximization of performance of a PCM latent heat storage system with innovative fins," *Applied Energy,* vol. 137, pp. 707-715, 2015.

5. DYNAMIC CHARACTERIZATION OF PHASE CHANGE MATERIAL COMPOSITESS UNDER HARMONIC HEATING*

5.1. Nomenclature

A	Cross sectional area, (m^2)
h	Heat transfer coefficient, ($W\ m^{-2}\ K^{-1}$))
k	Thermal conductivity, ($W\ m^{-1}\ K^{-1}$)
P	Power, (W)
R	Thermal resistance, (K W^{-1})
T	Temperature, (T)
θ	Phase Lag, (°)
x	Height, (m)

Subscripts:

hot	Heated Side
$cold$	Cooled Side
$ambient$	Ambient
sys	System
$sample$	Sample

5.2. Introduction

Phase change materials (PCMs) serve to increase the effective thermal capacitance of an electronic package or component, thereby reducing the transient temperature rise during periods of high-power dissipation. The bulk of current literature on PCM-based component analysis focuses on the response of a component to a step change in thermal boundary conditions, whereas actual components and devices that are best suited for PCM application are often subjected to pulsed or other non-steady boundary conditions. Such boundary conditions are of particular interest as they include information about the combination dynamics of both melting and solidifying processes. However, non-steady boundary conditions add significant complexity to the non-steady phase change problem, which already has limited solutions in the simplest cases. Among non-steady boundary conditions, harmonic heating involves several distinct advantages from an experimental perspective, especially the ability to identify a phase lag of the response temperature signal in comparison to the input power signal.

While the transient response to harmonic heating in a thermal conductor has been studied extensively in the literature and has known analytical solutions [1, 2], there is a lack of equivalent focus and depth in the PCM literature. There has been some effort to study the effects of non-steady heat loads on PCM slabs however there are many different configurations and boundary conditions that may be considered, each with their own challenges and solutions. Non-steady heating conditions can take many forms including pulsed [3], exponential [4], harmonic [5], and linearly varying loads [6].

Within the scope of this work, we focus on harmonic heating of a slab of phase change material with a constant temperature cooling component on the opposing side, equivalent to convective boundary with a large heat transfer coefficient (Figure 5.1). This configuration is chosen because it can be directly related to electronic components that produce heat periodically.

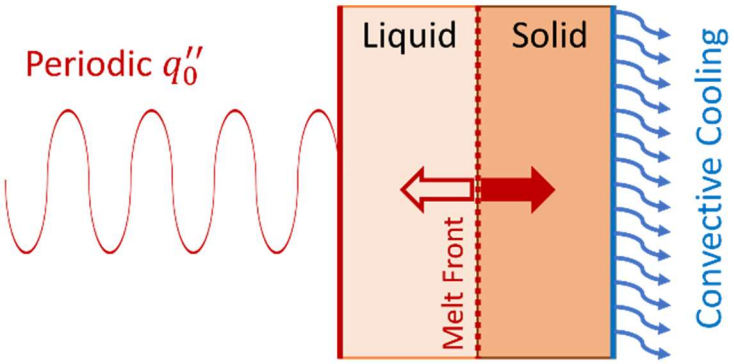

Figure 5.1 Schematic representation of the primary system under investigation consisting of a PCM slab with a periodic thermal load (q_0'') applied to one side and a convective cooling condition on the opposite side.

Previous numerical work corresponding to this configuration successfully identified trends in amplitude of the output temperature signal as well as the phase lag between input power and temperature response [5, 7]. Most significantly, it was observed

that the phase change process damped thermal oscillations in a specific region when compared to non-melting materials. This proved to be useful for identifying a zone where the operating parameters correspond to the activation of melting without remaining entirely liquid within the quasi-steady convergent behavior.

In the pursuit of this goal, we establish a methodology for measuring the transient response of a PCM under harmonic thermal loads. The measurement of the PCM's temperature at the heated boundary contains two important measurable quantities, phase lag and temperature amplitude, which can then be related to their associated power inputs to assess how the varying factors of power offset, amplitude and frequency affect the responsiveness of the material. By monitoring trends in input power and response variables we can confirm the existence of and characterize the previously modeled operating zones. Most notably, we can identify where the PCM slab meaningfully dampens the temperature of the cooled surface. In addition, comparing the results of differing materials allows for an understating of how various material properties effect the thermal response of the material. Furthermore, contrasting the response of melting and non-melting materials provides a means of directly analyzing the effect of the melting process. Beyond the immediate results shown in this Chapter, this study lays the groundwork for future exploration through the identification of areas of improvement for the experimental setup and procedures.

5.3. Methods

5.3.1. Sample Selection

Investigated samples include stainless steel as a conventional metallic solid and octadecane as a common PCM. These materials were selected to assess their differing responsiveness under varying harmonic loads based on their widely contrasting thermal diffusivities as well as presence or absence of a compatible melt process. A 0.95 cm thick sample of T-304 annealed stainless steel was chosen for testing and sanded down to increase uniformity.

Octadecane was chosen as the PCM under investigation because it is of particular interest for near room temperature thermal management. All samples under investigation were 2.54 cm in length and 2.54 cm in width to match the dimensions of the heater, approximating a 1D heat transfer condition.

5.3.2. Sample Mounting

The harmonic boundary conditions are accomplished using a thick film heater printed on polyimide film, and cold plate in series with the material under investigation. The harmonic power of the thick film heater is driven by a Keysight B2961A power supply. The cooling boundary condition on the opposite side is achieved using a cold plate that connects to a circulating water chiller held at 20 ºC to attain approximately isothermal conditions.

Four K type thermocouples are used to gather temperature data: two on the heated side and two on the cooled side, roughly equally diagonally from the center to the corners. Minimal amounts of polyimide tape were used to fix thermocouples in place while adding as little additional thermal resistance as possible. The thermocouples are calibrated prior to mounting to ensure accuracy and repeatability of results. For analysis of the solid metal

samples thermal paste is added on the sample surface using the paste dots deposited in a quincunx pattern and spread thinly to fill in any gaps between the material and thick film heater (Figure 5.2a). For analysis of PCMs an insulating vessel is used to contain liquid materials through melting. The thick film heater is affixed to the inside wall of the vessel which is filled with liquid PCM and allowed to completely solidify before testing begins (Figure 5.2b). An insulating foam is added on the outermost boundaries of the system to help limit parasitic heat loss. The entire system is kept in place using a large vice to clamp all components together and maintain good contact between all constituents.

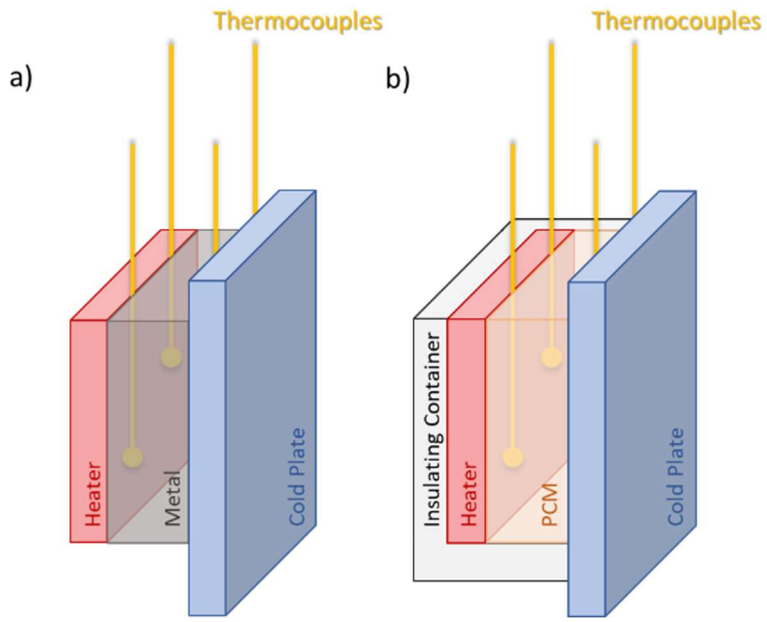

Figure 5.2 Configuration of the experimental rig highlighting the heat source and cooling boundary as well as the location of thermocouples in reference to the a) metallic material or b) PCM under investigation.

5.3.3. Data Gathering and Processing

A LabVIEW program is used to control the power source and record temperature outputs from the power supply as well as the temperature data. In each run, the heater applies a sinusoidal thermal input, depending on the choice frequency, DC offset, and amplitude of the incident heat flux determined by the program. The sampling rate for each run was set to 10 Hz and each run was set to execute for 30-60 minutes depending on the

responsiveness of the material under investigation to achieve a quasi-steady response that is consistent over multiple periods.

With an assembled rig and completed program, data is first gathered for octadecane with varying thermal loads defined by the three control variables. The convective cooling boundary was found to remain relatively isothermal ($\Delta T < 0.1$ ºC) under all thermal loads applied in this work and therefore is treated as an isothermal boundary condition in this study. Thus, the temperature of the heated boundary is singularly used in further analysis.

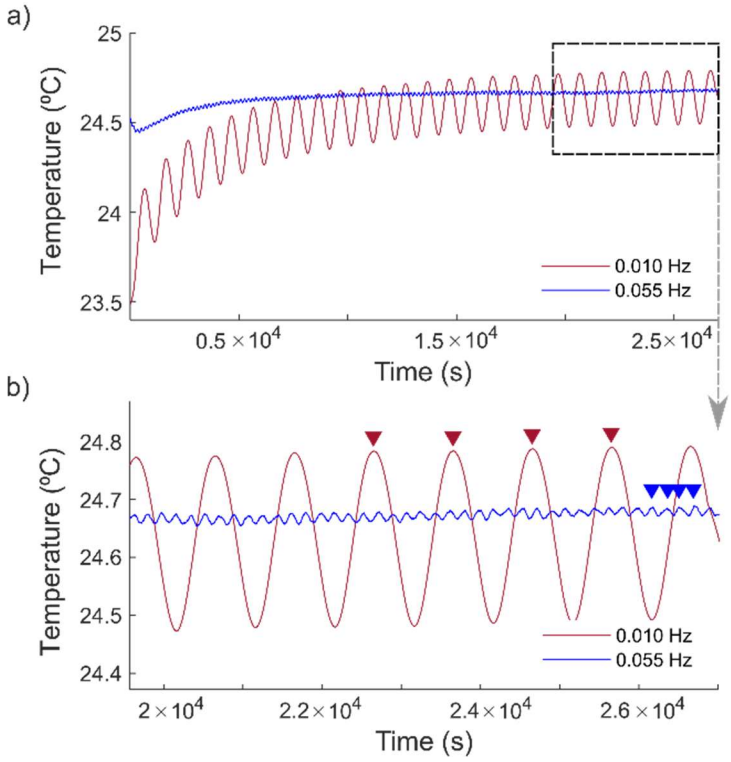

Figure 5.3 Output temperature signals over the a) entire run time and b) end convergent cycles for a 18.1 $mW \cdot cm^{-2}$ power offset and amplitude. Black box in (a) indicates the range associated with (b) and red and blue indicators correspond to the output peaks used in analysis of the 0.01 Hz and 0.055 Hz data.

After all data is gathered, the heated boundary temperature data is then processed using a moving average filter with the filter range dependent on the input frequency (Figure 5.3). After the filter is applied it is necessary to isolate the convergent end behavior which corresponds to the steady state material response to the given thermal load. The

very last period of the run is rejected to normalize the phase of the output signals analyzed. Then the preceding four periods are isolated as the output behavior used in further analysis.

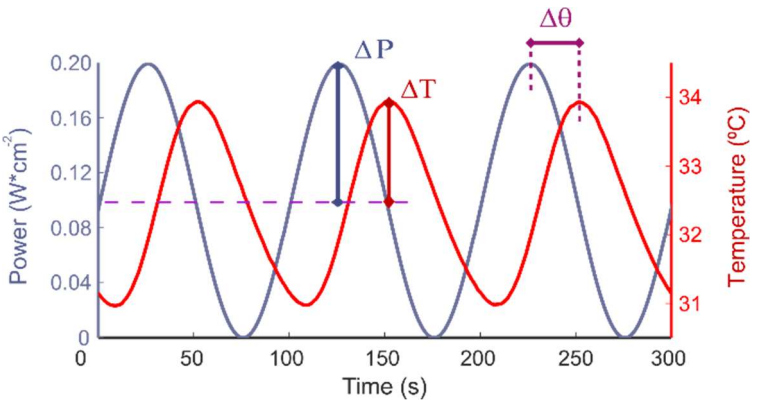

Figure 5.4 Comparison of power and heated boundary temperate data demonstrating the meaning behind the power amplitude of the input signal (ΔP) and temperature amplitude of the output signal (ΔT) as well as the phase lag between the two signals (Δθ).

It is worth noting that due to the low levels of heating within the context of this work even small fluctuations of the environment can cause deviation between tests. These low temperature rises are significantly lower than expected values, indicating high levels of heat loss to the environment, and containing system. The work presented as suites of data is taken in immediate series to ensure consistency across data that is directly compared.

From the data gathered there are many useful metrics and measures that can be extracted (Figure 5.4). For both voltage input and temperature output we extract an amplitude (ΔT), which is defined as the maximum deviance from the average value and half the total range. Phase lag ($\Delta\theta$) is a description of the offset between the input and output signals. These values can all be used as a measure of a materials thermal response that is highly influenced by material properties.

5.4. Results and Discussion

5.4.1. PCM Characteristic Response

As discussed in the previous section one of the useful metrics that can be used to characterize a material is the temperature amplitude of the heated boundary when a harmonic heating load is applied. For conventional materials it is understood that the amplitude of the output temperature signal will increase linearly with greater magnitude of the power input signal as well as more complexly with a decreased frequency [5]. In this work we isolate frequency (Figure 5.5a), power amplitude (Figure 5.5b) and voltage offset (Figure 5.5c) of the loads imposed on the heater, which is used to test the materials. The effect of decreasing the frequency gives the material more time to both heat and cool over the set period which leads to larger temperature swings (Figure 5.5a). It is observed for octadecane in this specific configuration that extremely low frequencies (on the order of 0.01 Hz) were most suitable for testing due the improved signal to noise ratio and increased utilization of the range of melting temperatures.

Increasing both voltage offset, and voltage amplitude increases the output temperature amplitude as well as the temperature offset (Figure 5.5b,c). In the context of

applications, for a given frequency the input voltage variables should be chosen such that the temperature swings fall within the range of melting temperatures and can contribute to the cooling of the heated boundary.

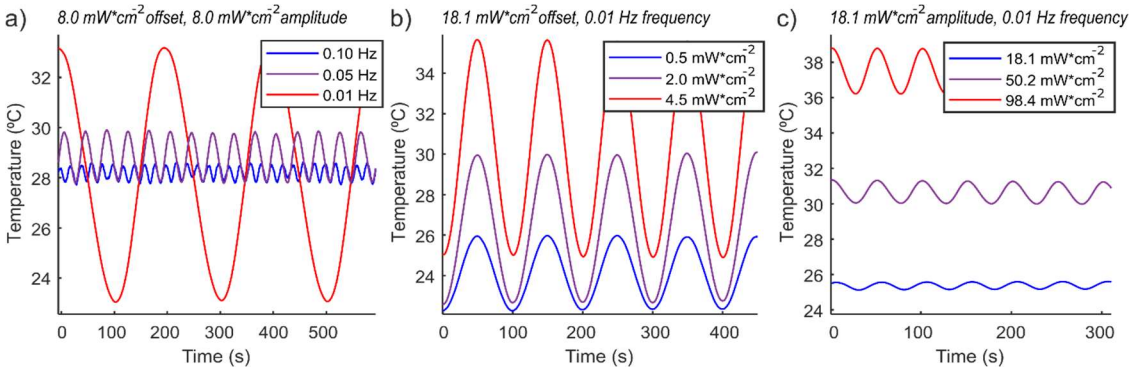

Figure 5.5 Temperature output data for heated octadecane while varying the a) frequency b) power amplitude and c) voltage offset of the input signal while keeping the remaining two control variables constant as labeled above their respective plots.

5.4.2. Phase Lag Analysis

The phase lag is observed to be only dependent on frequency and not be affected by magnitude of the power input within the range tested in this body of work. Lower frequencies correspond to lower phase lag between the input voltage and output temperature signals. This is because longer periods give the material adequate time to

adapt to changing thermal loads and approach an adjusted steady state (Figure 5.6b). For higher frequencies, the thermal loads fluctuate too rapidly for the material to absorb in time with the loading (Figure 5.6c). It is conceivable that this can be used as a measure of thermal diffusivity upon future development. For further testing on PCMs a 0.01 Hz frequency was chosen to allow for clear signals from the temperature fluctuations.

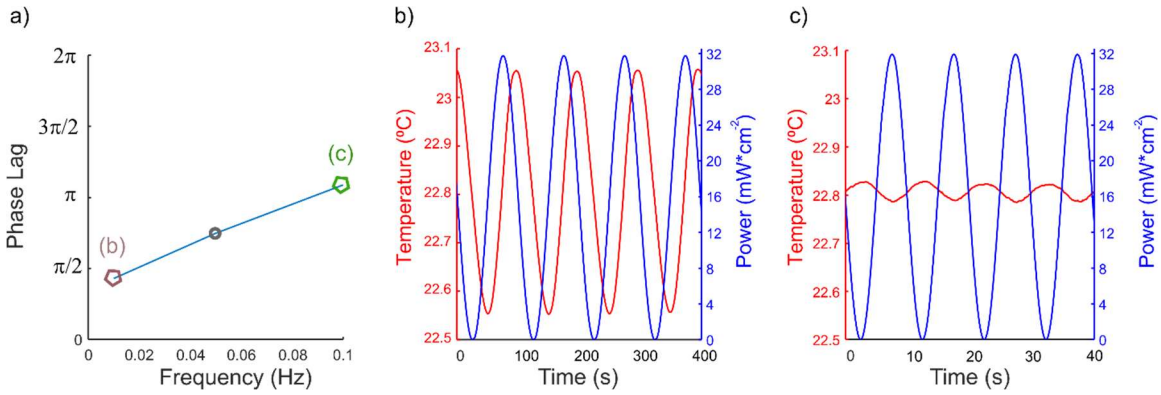

Figure 5.6 a) Trends in phase lag between input voltage and temperature output signal dependent on frequency of the input signal for a slab of octadecane. b) Low frequency example, 0.01 Hz, corresponding to a relatively low phase lag and c) higher frequency example, 0.1 Hz, corresponding to a relatively high phase lag.

5.4.3. Amplitude Analysis

Taking a particular subset of these control variables, offset and amplitude voltages, we can observe the specific subset of the sample space where the offset and amplitude are equal. This portion of the sample space has the advantage of spanning a large range of temperature outputs, preventing the complications of negative voltages, and the existence of a known analytical solution for non-melting materials that can be used for comparison. Taking a suite of data with increasing voltage amplitude/offset and identifying the temperature amplitude of the output signal allows for the identification of behaviors unique to PCMs.

The output temperature amplitude for each of the input power values can be compared against known analytical solutions for this specific configuration for non-melting materials [5]. Comparing the experimental data with these analytical predictions demonstrates that analytical estimates we predict higher temperatures than those experimentally observed (Figure 5.7a,b). This is to be somewhat expected due to the additional thermal mass of the surrounding system that is not accounted for and parasitic heat loss. However, at the magnitude observed, future work is necessary to further limit and account for heat losses within the system. The inclusion of a scaling factor allows for the shifting of predicted values to better assess the overall trends in amplitude (Figure 5.7a,b). We show that the analytical predictions line up well with experimental results in the low and high power limits with a deviation region for a given region of the power sample space. While standard non-melting materials have a straightforward monotonically increasing relationship between input voltage amplitude and output temperature

amplitude, for PCMs we observe a dampening of the temperature amplitude over a finite range (Figure 5.7a,b). This region corresponds to power inputs that lead to temperatures within the melting range of the material (Figure 5.7c).

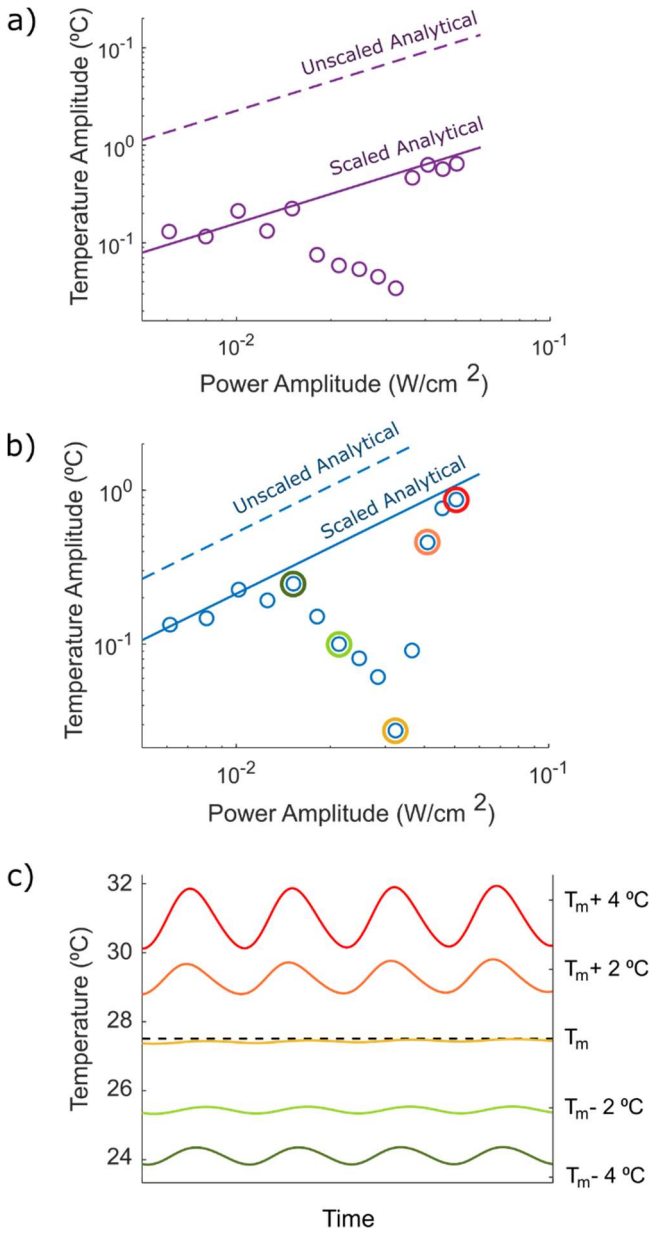

Figure 5.7 a) 0.055Hz and b) 0.01 Hz results comparing the power input signal with equal offset and amplitude with the corresponding output temperature amplitude. Temperature predicted analytically (dashed lines) then scaled to account for additional internal thermal resistances (solid lines). c) Demonstration of the damping of output temperature amplitudes about the melt temperature.

Octadecane, like other paraffin waxes, is known to melt over a large range of temperature values which was also observed in this work as demonstrated by the range of power amplitudes which experience damping. The maximum damping point for the 0.01 Hz dataset corresponds to 27.5 $mW \cdot cm^{-2}$ (Figure 5.7b) and furthermore the approximate average temperature of 27.4 ºC (Figure 5.7c). This melting point was confirmed by DSC yielding an average melting point of 27.5 ºC across multiple samples. In other PCMs with a narrower range of melting the temperature dampening effect is expected to occur over a much narrower range of voltage/power inputs.

The identification of this range is crucial for understanding the use of these materials. If the thermal load is too large or small so that the convergent response is either fully melted or fully solid at all times with no activation of the melting process, then there is no advantage to the inclusion of the PCM as a thermal management component. This means for our specific configuration, including thickness and cooling temperature, the acceptable thermal loads where the phase change process meaningfully cools the heated boundary occurs approximately in the region of 18.1 $mW \cdot cm^{-2}$ (input power range: 0 – 72.3 $mW \cdot cm^{-2}$) to 32.1 $mW \cdot cm^{-2}$ (input power range: 0 – 128.5 $mW \cdot cm^{-2}$) for a signal with equal power offset and amplitude.

5.4.4. Material Comparison

When comparing different materials there are several key factors to consider that explain the difference between observed responses. By comparing differing materials under equivalent thermal loads, it becomes clear how material properties dictate the thermal response of the material. In Figure 5.8 the thermal results of octadecane and

stainless steel are directly compared for equivalent thermal loads. It is observed that octadecane leads to higher quasi-steady temperatures than the stainless-steel specimen. Additionally, octadecane demonstrates significantly lower temperature amplitudes than the stainless-steel counterpart, i.e. smaller swings in temperature. This can be explained by the fact that octadecane has a much lower thermal conductivity than the highly conductive stainless steel.

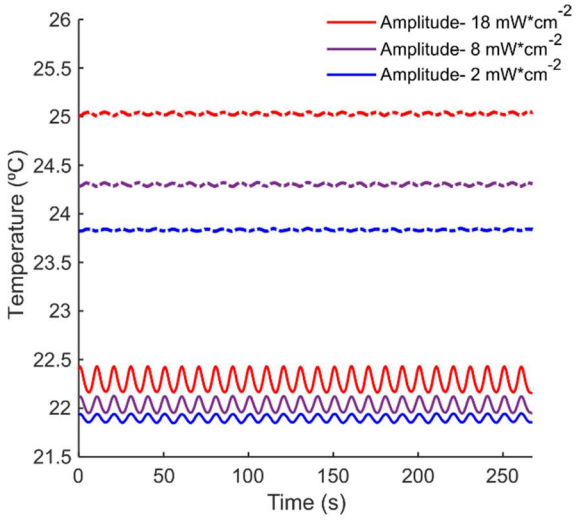

Figure 5.8 Characteristic temperature response of octadecane (dashed lines) and stainless steel (solid lines) under thermal loads with varying voltage amplitude. The frequency is held constant at 0.1 Hz and the power offset is set as 18.1 $mW \cdot cm^{-2}$.

5.5. Initial Conclusions

In this study we experimentally investigate the thermal response of a PCM slab subjected to harmonic heating and convective cooling on opposing boundaries through the assembly of an experimental setup which allows for the recording of temperature measurements at the boundaries of the material under investigation. By varying the properties of frequency, power offset and power amplitude we probe the effects of the input thermal loading signal on the output temperature response. This allows for the identification of the effects of the melting process as well as characteristic material properties on the thermal response.

We present a fundamental comparison of experimental results to analytical predictions which may be greatly expanded upon in future work. Through an increased understanding of the influence of the material characteristics on their response to imposed thermal loads we anticipate the future development of a characterization methodology for determining material properties using the approach detailed in this work.

5.6. Ongoing Continuation

The above discussion lays strong groundwork for further exploration into experimental harmonic analysis, using the observations we made from the above study. Further exploration is primarily motivated by strong deviations from expected values in the study. In section 5.3.3 above we implement the use of a scaling factor to analyze trends for our amplitude analysis. This is accomplished by scaling the analytical solution for harmonic heating of a non-melting material and fitting to the linear portion of the experimental data with thermal loads of equal offset and amplitude. This is effective for

demonstrating how deviations from this line are the result of dampening from the effects of PCM melting. However, we were unable to address specifically the source or magnitudes of the contributions to this factor. This prevents any possibility of analytically predicting the location of the anti-resonance zone within the thermal configuration space. Furthermore, an analytical description of the location or morphology of this zone could provide higher levels of insight into the application and design of PCM based thermal components.

Throughout the above work we observe temperature rises that are much lower than expected. This could be attributed to a number of factors including, convective forces, heat loss, PCM migration and internal resistances. To combat these factors, we have implemented a redesign of the experimental setup. The largest difference between iterations of the experimental rig is the orientation, where the new setup follows a horizontal orientation (Figure 5.9a). Within this setup the sample under investigation is heated from the top and is placed above the cold plate with a thermal interface material (TIM) aiding with contact between the cold plate and sample. This effectively eliminates convective forces due to the directional heating from the top of the sample. Furthermore, in the previous experimental setup PCM migration caused the rejection of many datasets which is alleviated by this setup. The experimental rig has also been modified to prevent heat loss through the utilization of a vacuum insulation panel on the heated side of the sample lifted off the heater from an insulated foam. These changes make a purely PCM investigation not possible due to the melting of the PCM causing an unstable mounting point for the Kapton film paper but has many advantages in the study of PCM composites.

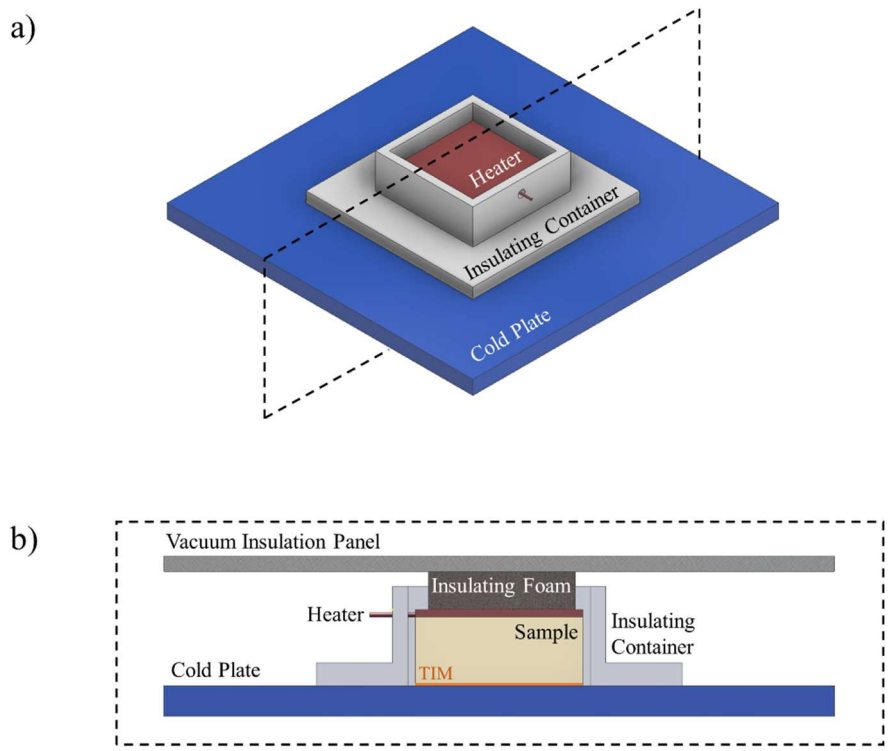

Figure 5.9 a) Schematic view of the modified horizontal experimental setup and b) cross sectional view, with components labeled.

The experimental results presented in this chapter represent purely metal or PCM samples, which provide a foundation for analysis establishment and a baseline for observable thermal response. We seek to expand upon the analysis by expanding into the space of composite analysis, in accordance with the other Chapters of this dissertation. For the initial exploration into the space of composite analysis we obtain samples of 1) copper foam and 2) polyurethane foam. We characterizer these foams under steady and

harmonic power thermal loads and with and without the infiltration of PCM into the foams. A direct comparison of the foams with and without the addition of PCM allows for the direct observation into the cooling effects of PCM inclusion. More interestingly, we can also compare the copper and polyurethane foams. Within these tests, for the copper foam composite the copper serves as the primary conductive pathway and for the polyurethane composite the PCM serves as the primary conductive pathway. Therefore, a direct comparison of these two systems provides insight into the role conductive elements play in determining the characteristic response of a composite.

To further our analytical pursuits, we have also developed a calibration methodology to account for any heat loss that may inevitably still occur. For the application of this methodology, the applied voltage is stepped up in even increments and for each step the temperature is allowed to equilibrate. Temperature measurements are taken from the heated boundary (T_{hot}), cold plate (T_{cold}), and the ambient temperature ($T_{ambient}$). From the relationship between power applied and observed temperature rises, Fourier's law can be modified to account for losses. This is accomplished through the determination of the resistance attributed from the system (R_{sys}), separated from the resistance of the sample under investigation, and a heat transfer coefficient (h) to account for loss to the environment as:

$$(T_{hot} - T_{cold}) = (P - h\,A(T_{hot} - T_{ambient}))(R_{sys} + \frac{dx}{k_{sample}A}) \quad (5.1)$$

where A, k_{sample} and dx represent the area cross-sectional area, thermal conductivity and height of the sample. Once this characterization is accomplished it should be applied to

further testing by predicting more complex material responses and furthermore be used in the prediction of the anti-resonance zone.

Preliminary data for stainless steel is used to determine the effectiveness of the steps we have taken. A 1 in thick sample is chosen and heated under equal conditions, increasing the voltage applied through the heater from 1 V to 20 V in steps of 1 V (Figure **5.10**). Initial observations show much larger temperature rises than observed in the previous setup. When comparing experimentally measured results to a simple calculation from Fourier's law, assuming a conductivity of 14.4 W/mK, we show extremely high agreement which is very encouraging for future use of this experimental rig [8]. For further confidence we will gather more data across different metal samples begore moving to PCM composites especially being mindful to sample across different magnitudes of power inputs.

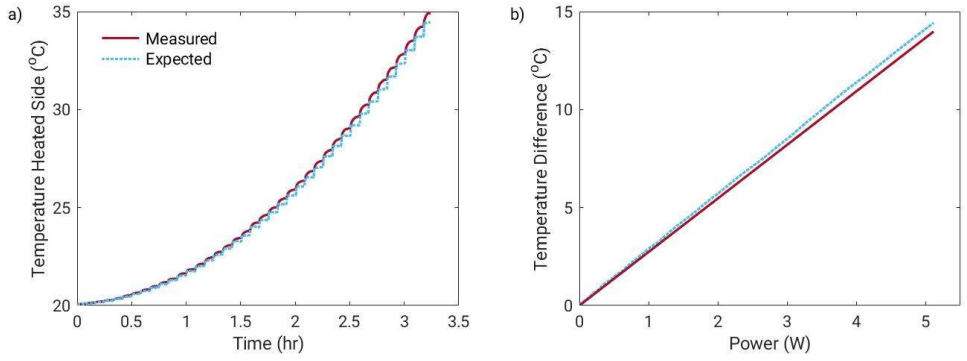

Figure 5.10 a) Temperature data gathered as a 1 in sample of stainless steel is heated and b) the relationship between temperature difference across the sample with power, comparing measured and expected values.

In addition to the experimental work described within this section numerical simulations should also be run in parallel using the finite element model established in Chapter 2 of this dissertation. This has been done to an extent in work by Shamberger et. al through the simulation of harmonic boundary conditions with opposing convective cooling [9]. However, this study did not branch into composite exploration and development. A comparison of experimental and numerical results can provide through the identification of discrepancies. The type and circumstances of occurrence related to these differences may reveal key considerations for the real-world application of these materials and provide insight into key factors necessary for further analytical consideration.

5.7. References

[1] H. S. Carslaw and J. C. Jaeger, *Conduction of heat in solids*, 2 ed. Clarendon Press, 1959.

[2] L. S. Yao and J. Prusa, "Melting and Freezing," *Advances in Heat Transfer,* vol. 19, pp. 1-95, 1989.

[3] A. Rakotondrandisa, Danaila, I., Danaila, L., "Numerical modelling of a melting-solidification cycle of a phase-change material with complete or partial melting," *International Journal of Heat and Fluid Flow,* vol. 76, pp. 57-71, 2019.

[4] R. Furzeland, "A comparative study of numerical methods for moving boundary problems," *IMA Journal of Applied Mathematics,* vol. 26, no. 4, pp. 411-429, 1980.

[5] P. Shamberger, A. Hoe, M. Deckard, and M. Barako, "Dynamics of melting in a slab under harmonic heating and convective cooling boundary conditions," *Journal of Applied Physics,* vol. 128, no. 10, p. 105102, 2020.

[6] J. Mennig and M. N. Özişik, "Coupled integral equation approach for solving melting or solidification," *International Journal of Heat and Mass Transfer,* vol. 28, no. 8, pp. 1481-1485, 1985.

[7] P. Shamberger, A. Hoe, M. Deckard, and M. Barako, "Effects of Boundary Conditions on the Dynamic Response of a Phase Change Material," in *2020 19th IEEE Intersociety Conference on Thermal and Thermomechanical Phenomena in Electronic Systems (ITherm)*, 2020: IEEE, pp. 985-992.

[8] R. Graves, T. Kollie, D. McElroy, and K. Gilchrist, "The thermal conductivity of AISI 304L stainless steel," *International journal of thermophysics,* vol. 12, no. 2, pp. 409-415, 1991.

[9] P. J. Shamberger, A. Hoe, M. Deckard, and M. T. Barako, "Dynamics of melting in a slab under harmonic heating and convective cooling boundary conditions," *Journal of Applied Physics,* vol. 128, no. 10, p. 105102, 2020.

6. CONCLUSIONS & FUTURE DIRECTIONS

6.1. Summary

This dissertation examines the relationship between phase change material (PCM) composite structure and characteristic response to thermal loading. This is accomplished through the characterization of fundamental heat transfer principles within these composites. The consequential established principles are then translated into design principles, allowing for the optimization of PCM composite systems, and response analysis, creating and understanding for the appropriate application of these materials.

Chapter 2 of this dissertation serves to establish the tools of our investigation into the thermal behavior of PCM composite materials. This is accomplished, firstly through the development of a finite element model allowing for the direct simulation and investigation of PCM composites under various thermal loads. Simulation of PCMs and PCM composites is used to identify characteristic regimes and the associated critical times. Furthermore, numerical models are used to analyze the accuracy and limitations of two approximate analytical models, 1) the effective medium approximation and 2) the fin approximation in describing thermal transport in PCM composites. From this study, it is established the finite element model and effective medium approximation may be used for future exploration when considerations for the limitations these methods are accounted for. Furthermore, an analysis of optimal length scales within lamellar composites is established.

Utilizing the finite element model and effective medium approximation established in Chapter 2, Chapters 3 and 4 translate the previously established fundamental

heat transfer observations into methodologies for optimal PCM composite design. The effective medium approximation is utilized to increase the tractability of analytical development, yielding solutions for the description of optimal volume fractions corresponding to different configurations of the thermal design problem. This approximation is further applied numerically to allow for the rapid testing of thermal configurations and verification of the validity of the resulting analytical solutions. Optimal design solutions are provided for the basis of compositionally uniform and variant composites, in Chapters 3 and 4 respectively, across a variety of performance metrics. Variant composites were shown to allow for high performance in the cylindrical limit, especially when accounting for secondary design considerations, such as mass or volume.

With concrete design principles in place, the final considerations addressed by this dissertation concern the appropriate application of these PCM composites. Because the nature of PCMs necessitates the utilization of transient thermal loads, in Chapter 5 we experimentally examine the thermal behavior of PCMs under harmonic thermal loads. The result of this is an observation of a regime wherein the melt process of the PCM is effectively exploited to dampen the temperature rise of the heated boundary. The ongoing work in this effort is explained in this section with the aim of further characterizing and predicting this observed regime.

6.2. Possible Future Directions

6.2.1. Expansion on Harmonic Analysis

Chapter 5 details the work we have accomplished in our study of PCMs exposed to harmonic thermal loads. This includes the experimental identification of the numerically predicted regime in which temperature rise is dampened by the melt process of the PCM as well as an initial analysis of the effects of loading different composites under harmonic loads [1]. While this provides useful information on PCM response to non-constant thermal loads, there is also much room for further exploration into this topic. Chapter 5 includes a discussion in section 5.5 a discussion on the immediate next steps for this project. The primary result of this further study should be an ability to predict under what thermal loading conditions a PCM will respond within the characteristic anti-resonance regime.

As a parallel to the analysis, we completed for constant boundary conditions within this dissertation, the harmonic analysis laid out previously can also be extended to the principles of composite design. From a known application with identified harmonic parameters, it would be beneficial to maximize the temperature dampening effects through full utilization of the PCM melt process. This could be accomplished through the intentional design of composites. To achieve this, a study examining the role of composition on the morphology of the anti-resonance zone could be conducted. It may also be possible to create analytical expressions for optimal volume fractions or critical system lengths which should be developed based on the observations from methodologies for predicting the location of the anti-resonance zone and the principles established in Chapter 3 of this dissertation.

6.2.2. Additional Non-Steady Thermal Loading

In addition to the exploration of harmonic thermal loads discussed above, other non-steady thermal loads should be considered. Periodic thermal loads relating to realistic applications can take any number of forms including, but not limited, sine, sawtooth, square or triangle. Each of these signal types will produce a different characteristic response from the PCM system and the intricacies of this difference should be explored to increase our understanding of the responsiveness of these systems. This exploration should be explored numerically and experimentally, which may provide some insight into the role of non-idealities in PCM application. These studies could explain the relationship between material responsiveness to non-steady thermal loading and proper application.

In addition to periodic type loads, more complex and arbitrary loads should also be considered. This is especially pertinent considering real world applications rarely have perfectly well-behaved consistent loads. An approach to this problem could be to analyze the response of PCM systems to a single pulse of a given shape. In parallel with building up a signal from arbitrary thermal pulses, a the thermal response from the PCM may also be able to be calculated from a sum of known individual responses. Both the periodic and arbitrary thermal loading analyses should be carried out for PCMs as well as the composites in which they are contained. Variance of the signal should be analyzed in relation to the performance of the PCM material and especially PCM composites, which may give further insight into how non-steady thermal loading affects the needs of the design problem.

6.2.3. Convection Included Composite Development

For the analyses contained within this dissertation heat transfer is limited to conductive pathways, neglecting the role of convection experienced by many real systems. While this approximation is valid in many cases, as discussed in the text, there are also case where convection may be unavoidable or favorable for the application of PCM composites. Some selections from the literature can suggest that optimal use of PCMs is best achieved when convection is maximized [2, 3]. These systems compare highly individualized optimal systems for a thermal, preventing direct comparisons from generating general conclusions across the entire design space.

Currently, there are no widely-applicable concrete guidelines for the PCM composite design for the maximization of convective forces. Using similar approaches to the ones contained in this work, an optimization scheme for maximizing convective forces through PCM composite design should be developed. This is likely to be very challenging due to the complexities of convective based heat transfer and should first be approached numerically while seeking possible analytical approximate models.

With optimization methodologies for primarily conduction and convection based optimization in place, these methods could be applied to the same optimization problem and the results compared. From these comparisons a thorough analysis should be performed to give concrete limits for the types of problems that are best suited to different optimization approaches in terms of time scales, thermal loading and materials selection.

6.2.4. Cooling Conditions

For the optimization problems and methods presented in this work we consider the non-heated boundaries of a given composite heatsink to be perfectly adiabatic. However,

since PCM applications require a period of recharging after use, a cooling stage must be included in the incorporation of these materials as parts of thermal management systems. The role of cooling conditions is partially addressed in Chapter 5 through the incorporation of a convective cooling boundary. Further consideration should be given to how the magnitude and type of cooling condition affects the utilization of the PCM composite. Such cooling conditions could include convective or constant temperature boundary conditions and could span a large range of magnitudes. On one extreme this could result in the overutilization of the cooling condition which would lead to underutilization of the PCM composite and unnecessary power usage from active cooling systems. On the opposing side the heated boundary could completely overwhelm the cooling side preventing the occurrence of a true recharge state. As such, heating and cooling boundaries must find a balance with relation to the abilities of the PCM composite. Analyses of the relationship between ideal system cooling parameters and PCM performance are necessary for the construction of synergistic thermal management systems.

Beyond idealized conceptualizations of cooling conditions further consideration should be given to the non-idealities of the re-solidification process. Often when employing analytical and numerical methods the re-solidification process is modeled as a perfectly complementary problem to the melting process. However, in reality this is not often the case and factors such as PCM migration, undercooling or non-homogeneous (e.g., bubbles or grain boundaries) solidification could complicate the utilization of these systems. Each of these factors should be considered to conceptually explore their effect on the dynamics of melting/freezing. Further experimental work is also recommended to

explore under what conditions or in what materials these factors are more often observed and the effect they have on the overall system.

6.2.5. Expansion of PCM Selection

For the studies contained herein, analysis is largely limited to PCM selection between three options octadecane, hexadecane and lithium nitrate trihydrate. These materials were selected primarily for their high latent heat, application relevant melting points and ease of incorporation. This is standard but there is an opportunity for a higher level exploitation from materials selection in terms of these factors. From the optimization methods lined out by this paper material properties can directly be linked to given levels of performance. Therefore, if a given level of performance is desired, a function of differing material properties can be created balancing different factors. The utilization of this method should be demonstrated and relationships between individual material properties and performance should be explored.

The study of PCM selection can also be explored through the prediction of the existence of new materials. Through machine learning techniques and thermodynamic principles, new compositions of synthesized materials can be predicted. Predicted new materials can further be explored through direct experimentation or ab initio simulation techniques. If a desired combination of material properties is desirable for a given application, within reasonable physical expectations, it is very possible we could tailor materials design to the application itself.

6.3. References

[1] A. Hoe, J. Felts, and P. J. Shamberger, "Numerical Evaluation of Thermal Energy Storage Rate in Planar and Cylindrical Phase Change Material Composites," *(In Review)*.

[2] J. Xie, K. F. Choo, J. Xiang, and H. M. Lee, "Characterization of natural convection in a PCM-based heat sink with novel conductive structures," *Int Commun Heat Mass,* vol. 108, p. 104306, 2019.

[3] A. Pizzolato, A. Sharma, K. Maute, A. Sciacovelli, and V. Verda, "Design of effective fins for fast PCM melting and solidification in shell-and-tube latent heat thermal energy storage through topology optimization," *Applied Energy,* vol. 208, pp. 210-227, 2017.